Methodologies for non-linear dynamic simulations in product development

ScuDo

Scuola di Dottorato ~ Doctoral School

WHAT YOU ARE, TAKES YOU FAR

Doctoral Dissertation

Doctoral Program in Management, Production and Design Engineering (30^{th}cycle)

Methodologies for non-linear dynamic simulations in product development

By

Matteo Scapolan

******

Supervisor(s):

Prof. Elvio Bonisoli

Doctoral Examination Committee:

Prof. M. Amabili, Referee, McGill University, Montreal, Canada

Prof. F. Pellicano, Referee, Università degli Studi di Modena e Reggio Emilia

Prof. P. P. Valentini, Università di Roma Tor Vergata

Prof. F. Leali, Università degli Studi di Modena e Reggio Emilia

Prof. A. Vigliani, Politecnico di Torino

Politecnico di Torino

2018

Declaration

I hereby declare that, the contents and organization of this dissertation constitute my own original work and does not compromise in any way the rights of third parties, including those relating to the security of personal data.

Matteo Scapolan
2018

* This dissertation is presented in partial fulfillment of the requirements for **Ph.D. degree** in the Graduate School of Politecnico di Torino (ScuDo).

Το Σόφη Λυν *Μινάς*

Abstract

In this thesis the efficient numerical simulation of non-linear dynamic systems is addressed through the use of reduced models. The problem of reducing simulation time with marginal loss of accuracy has been studied for many decades, with the purpose of accelerating the design phase and allowing the use of more accurate virtual prototypes. The process of transforming an original model and describing a complex physical system into a less computational demanding one, is generically defined as *model order reduction* or *model reduction*. The resulting model is therefore known as *reduced model*. Despite decades of attempts and several successfully applied methods, this topic still represents an open point, especially for what concerns complex non-linear systems.

The aim of this thesis is to develop methodologies which exploit the linear modal analysis as a reliable and consolidated tool in reducing the computational cost of non-linear systems. Formulations which retains the non-linear behaviour while exploiting well established linear analyses are sought.

Non-linearities in non-linear systems can then be retained or linearised around linearisation points. After a review of the literature, in Chapter 2, both approaches are examined. First, a reduced model which redefines the non-linearities in a cubic form is implemented (Chapter 3). Then, a novel reduction method based on the linearisation in the configurations space is proposed in Chapter 4 and 5.

Chapter 4 discusses the linearisation procedure, with the use of a specific base for each linearisation point, so that the non-linear system is globally approximated by a piecewise linear system, described through a set of linear ones. Interactions between them are then used to retain the non-linear properties, with the local linearised systems named *subsystems*.

The reduction of the model is discussed in Chapter 5, with a focus on the mode selection procedure in generating reduced linear subsystems, while in Chapter 6, after

an application to a simple lumped system, two categories of examples are proposed, defining two possible interaction methods regarding the set of subsystems. In the first category a discrete interaction is used, with a subsystem replacing the previous one, while in the second category a continuous interaction is implemented, with more reduced linear subsystems evolving simultaneously. For each category single and multi-parameters examples are proposed, with an analysis of the performance included.

The method discussed in Chapter 3 is implemented, developing a non-linear beam element and testing the reduction on both numerical and experimental cases. Good agreement in reproducing the reference data is proven for the considered examples. The novel method developed in Chapter 4 and 5 is described, discussed and applied to several numerical examples. This method proves effective in reducing the computational time while maintaining a good approximation. An energy-based mode selection algorithm is introduced and applied, showing positive effects on the model reduction method performance.

Contents

List of Figures

List of Tables

Chapter 1

Introduction

The modern technological world presents unique combinations of new challenges and novel methods and instruments to face them. Traditionally, the approach to science and scientific problems has been split into the two complementary branches of *theory* and *experiments*. These classic disciplines interacted with each other for centuries. Physical experiments and observation of the reality lead to theoretical formulations, that were proved and validated through other physical experiments. This is a strict definition of *scientific method* and still holds.
Contemporary technology allows us to extend the experimental approach to the virtual world, using computer simulations to obtain predictions based on theory. Moreover, virtual simulations constitute the core of a *virtual design environment* that allows designers and engineers to dramatically speed up and facilitate the design and optimization phase of product development. Products, particularly innovative ones, can be designed faster, with improved reliability and at a lower cost.

Figure 1.1 depicts a typical product development cycle, highlighting the *design* and the *prototype* phases.

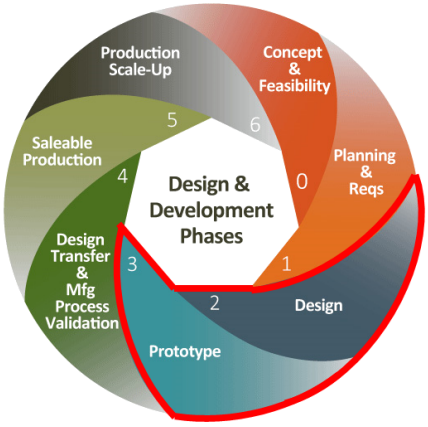

Fig. 1.1 Product development cycle.

Commonly, prototypes are built to validate the previous phase (design), with several iterations occurring to improve the product design. This key part of the cycle influences significantly the *time to market* of the product, which should be as short as possible, in order to provide innovative products. The use of physical prototypes increases the duration of this phase, due to the time necessary to build and test them. Moreover, prototypes are usually expensive, but their use is necessary to have a final product with the intended performance and functionalities. The use of reliable virtual prototypes, implementing a virtual design environment, reduces both the time and the cost of these phases, allowing moreover a more detailed design phase. It is in fact possible to explore more solutions (and to better optimize the product design) if more iterations are made possible by a faster and cheaper prototype phase. The virtual models used to realize the virtual prototypes need however to be reliable, providing accurate results, as close as possible to the real product.

As a consequence, demand for realistic and reliable simulations grows, leading to interesting and stimulating challenges in the field of computational science. Any realistic simulation requires the error of the virtual model with respect to the real system to be small, which in turns lead to more complex and therefore computationally demanding models.

In science two kinds of systems can be identified: if the model can be obtained with a finite number of components, which adequately describe the system, a *discrete* problem is obtained. On the other extreme, if the subdivision continues indefinitely, the problem can only be defined through infinitesimal quantities, leading to differential equations and to a *continuous* problem.
Computer are incredibly useful in performing large amounts of simple calculations; moreover, "*The limitations of human mind are such that it cannot grasp the behaviour of its complex surroundings and creations in one operation. Thus, the process of subdividing all systems into their individual components or 'elements', whose behaviour is readily understood, and then rebuilding the original system from such components to study its behaviour is a natural way in which the engineer, the scientist, or even the economist proceeds.*", as [2] states. These two factors have led the engineering community to formulate and develop the finite element method [3, 2]. This method is based on the discretization, with the consequent approximation, of continuous problems. Improvements have been made, from the first models in the 1960s to today's finite element tools, but the base idea holds. More realistic models involve more complex descriptions, which translate into large and/or more complex models. It is not always a guarantee that the discretization of the problem will maintain an adequate level of accuracy: even the smallest problems may require an appropriate complex description of each of their parts, significantly increasing the computational burden.

The numerical simulation of predictive models is therefore a fundamental tool in the design of complex systems. The models considered that can generally be described as dynamical models. They are usually of high order, which means that they are described by a large number of Ordinary Differential Equations (ODEs). The high order of complexity of these models is due to the inherent complexity of the system described or to the discretization of the original partial differential equations.

A procedure that allows us to reduce the order and computational cost, while still retaining accuracy has been sought and pursued for decades (see Section 2). In this thesis this topic is analysed; a model order reduction (or simply *model reduction*) method is implemented and tested. A new method is formulated, implemented and finally validated. These two methods present significantly different approaches. The first, focused on the use of a linear base to obtain non-linear equations of motion. In the latter, linear and uncoupled equations of motion are obtained, through the use of a non-linear (or better, varying) base.

In this thesis a review of the model reduction methods available is presented in Chapter 2, highlighting those best fitting the problem considered and describing in more detail those used as starting point for the novel method proposed here. In Chapter 3 a method previously proposed is implemented and tested with numerical and experimental examples. Lastly, in Chapter 4, 5 and 6, a novel method is introduced, discussed and applied to numerical examples.

Chapter 2

Literature Review

Model Order Reduction (MOR) methods have been used and developed in several fields. This is logical as many scientific problems can benefit from reduced computational cost while maintaining a reasonable accuracy. Only engineering fields are discussed here, with particular focus on structural dynamics. Methods developed in other engineering areas are briefly examined and discussed, since contaminations between methods originating in different fields always enrich and serve as starting point for new ideas.

In order to be solved, complex continuous physical systems need to be described through the use of models. Each physical system can be described by means of several kinds of models, depending on the necessary level of fidelity. Models can be, e.g., continuous or discrete, as well as non-linear or linear. It is important to note that increasing the fidelity of a model generically increases the difficulty in finding the solution. Continuous models are usually more precise than discrete ones, but they require analytical solutions, which are not always easy to find or existent. Analogously, non-linear models are more accurate than linear ones. Several properties of linear systems (such as the superposition principle) cannot be used in non-linear models, making obtaining the numerical solution require significantly increased computational costs.

Once the model is defined, it is possible to further reduce its computational cost maintaining a comparable level of accuracy through MOR procedures. Discretization-based methods, such as the Finite Elements Method (FEM), can already be considered MOR methods, since they construct piece-wise approximation polynomials over

the spatial domain, solving for the unknown variables at specific locations (nodes). In this thesis however, FE models are considered as the reference, full-size model and are therefore used as starting point for MOR procedures.

The nature of the model reduction method varies depending on the original problem and on the model used to describe it. In the following, a brief chronological overview of a selection of the proposed methods is presented, while in Subsections 2.3 and 2.4, some of the methods hereafter introduced are discussed in detail, highlighting the most relevant to the method proposed in this thesis.

MOR methods can be classified by the starting model considered: a first main distinction can be obtained by dividing linear and non-linear models. Linear model reduction methods (introduced in Subsection 2.1) are based on linear systems and therefore characterized by linear equations of motion, in which the superposition principle is applicable.

Non-linear model order reduction methods (introduced in Subsection 2.2) are based on non-linear models, which are able to reproduce the original system with greater accuracy. Depending on the reduction procedure, the reduced model can be based on non-linear equations (as is the full-size model) or on linear ones, if a linearisation procedure is introduced.

Regardless the field of origin, all MOR method can be divided into two main categories:

- Data-based methods (Subsection 2.3)
- Model-based methods (Subsection 2.4)

The main difference between these two classes is that data-based methods are built using previous simulations of the full system, while model-based methods only take into account system characteristics.

2.1 Linear Model Order Reduction - Overview

Linear model order reduction methods have been extensively studied and so, well established and consolidated procedures readily are available. Given the purpose and the applications of this thesis, they are not extensively described and analysed, but they are taken into account as starting point.

For linear systems linear modal analysis is widely used, since it allows for the uncoupling of the system's equations of motion, so that the truncation of the selection of only a subset of the identified modes results practical and effective. Mode superposition methods, in the form of the mode displacement reduction method and its extensions ([4, 5]) use this idea. Component Mode Synthesis (CMS) can be considered an extension of the mode superposition method, in which the structure is divided into smaller substructures and then linear modes are applied.

2.2 Non-linear Model Order Reduction - Overview

Non-linear procedures still constitute an open point, even if several approaches have been studied and proposed. In the following, some historical mention of non-linear model order reduction methods is provided. Later in this chapter, the most relevant method for this work are more deeply analysed.

In 1980, [6] a reduced basis technique was proposed, with an associated computational algorithm, for predicting the non-linear static response of structures. The structure studied was described through a total Lagrangian formulation and discretized by using displacements finite elements. A nodal displacement vector was then expressed as a linear combination of a limited number of basis vectors and a Rayleigh-Ritz technique was used to approximate the finite element equations by a reduced system of non-linear equations. Basis vectors selection was highlighted, providing criteria to be followed. The same author provided, in [7], a survey on the non-linear MOR methods available at the time (1981).

Three model order reduction procedures for non-linear dynamical systems applied to geometrically non-linear structures were studied and compared by [8], which used a discretization by means of finite elements. The methods analysed used *Tangent modes*, *Modal derivatives* or *Static modes*. Additionally, three ways to calculate

modal derivatives were proposed. The focus of this paper was on the selection of the basis vectors, a theme which is often analysed and proposed. Several authors have this identified as one of the key points of any MOR technique. In [8] modes are gathered from the initial state of the structure and were then updated or incremented: optimization of the selection of the basis vectors for a specific time instant was considered.

Semi-discrete models, with linear quadratic non-linearities have also been studied using, e.g., a condensation method ([9]). In this paper, an interesting definition of model reduction was proposed: "*model reduction is the mathematical synthesis of a reduced, practicable mathematical model from a known-but-intricate, complex mathematical model so that the essential physics of the original model of the physical system is preserved*". Models governed by linear time-varying differential-algebraic equations were considered in [10], which proposed an automatic extraction procedure for non-linear RF blocks. Such systems exhibit a nearly-linear signal path, but with potentially highly non-linear time-varying components. The proposed reduction procedure was based on a multipoint rational approximation algorithm, formed by an orthogonal projection of the original time-varying linear system into an appropriate Krylov subspace. The use of multipoint approximation entails that the transfer function and some of its derivatives are matched at several points in the complex plane.

Proper Orthogonal Decomposition (POD) methods, discussed in more detail in Subsection 2.3.1, were largely used for model order reduction, as in [11], which considered frictionally excited systems and used POD to obtain an optimal modal reduction. Chaotic dynamics were used in obtaining the basis to represent the system's dynamics. Such basis was used in a Galerkin's approximation to reduce the order of the system. The ROM was then evaluated and the effectiveness of using POD instead of the natural linear modes of the system was proved. Additionally, interesting guidelines for setting the reduction threshold were proposed.
The aerospace industry largely uses reduction methods, especially when several physical phenomena are involved. Aircraft panels, subjected to combined thermal and acoustic effects strong enough to induce a severe geometrically non-linear behaviour were considered by [12]. A reduced order modelling strategy was proposed, assessing several possible modal bases. The importance of in-plane displacements modes was highlighted and a novel basis was introduced, with separate representations of the transverse displacements and their induced in-plan counterparts. The same example

was used by [13], which formulated and validated a reduced order model for the prediction of the response, in terms of displacements, stresses and fatigue life. In this work, standard finite element software was used, developing a method that produces a set of cubic non-linear differential equations in terms of modal coordinates. Once again, particular attention was posed on the basis used, which includes transverse deflection modes of the linear panel and some associated in-plane mode (dual modes).

Geometrically non-linear vibrations of thin structures were used by [14], which proposed a normal form procedure, computed for non-linear oscillators with quadratic and cubic non-linearities. In this paper, all the linear modal damping terms were gathered together "*in order to define a precise decay of energy onto the invariant manifolds, also defined as non-linear normal modes (NNMs)*". Proposed examples were for a 2-DoFs simple system and a continuous circular cylindrical shell with external resonant forcing. The aim of the paper was to propose a systematic asymptotic method including the damping effects in the reduction process.

Model uncertainties and stochastic parameters were considered by [15], in which general methods for reduced order models of a geometrically non-linear dynamical system were proposed. Polynomial chaos expansion was used and cubic stiffness in modal coordinates was considered. Parametric Reduced Order Models (ROMs) were widely used and studied. Interpolation about reduced-order matrices as a means to obtain parametrized ROMs was proposed by [16], with spline element-wise interpolation of the system's matrices. Interpolation was performed in the tangent space and results are mapped back to the original space.

In the last years one of the main directions of the research about reduce models is the selection of appropriate bases for the reduction. A Static Modes Switching (SMS) methodology was proposed in [17]: a body flexibility mode set was selected at each time instant in the integration, including only those modes that significantly contribute to the solution. Flexible modes were obtained through Component Mode Synthesis (CMS), showing how several model reduction procedures can be used and combined. Other papers based on the same methodology were [18] and [19].
Model order reduction procedures were used recently for model parameters identification purposes, in [20]. Noisy measurements were considered and transient PDF-based models were used, with unknown parameters corresponding to physical properties. A POD procedure was used, with each ROM seen as point on a certain Riemannian manifold, tracked and interpolated during the sampling process.

Another data-based approach was proposed by [21], with a dimensional reduction of discrete, high-fidelity, non-linear, finite element structural dynamics models. Specifically, this method consisted in an energy-conserving sampling and weighting (ECSW) hyper reduction method for discrete (or semi-discrete), non-linear, finite element structural dynamics models.

Localized non-linearities result particularly attractive for model order reduction procedure: [22] used in fact a harmonic balance solution to determine non-linear response of structures with localized non-linearities. The solution was simplified through an exact dynamic reduction along with the modal expansion technique, providing a tool applicable and tested on discrete and continuous systems that converts the system equations of motion in each harmonic to a small set of non-linear algebraic equations. This method can be used to predict periodic steady state response. Multi-body models and specifically compliant mechanisms were analysed by [23], which proposed a model order reduction technique, in the form of Krylov subspace reduction. This method was applied as second step in the modelling of compliant mechanism, where the first step consisted in splitting the whole structure into deformable hinges and rigid links, at which lumped masses, representing inertia properties are associated. Continuous-time linear systems, solved by employing Linear Matrix Inequalities (LMIs) were used by [24], which solved a finite frequency H_∞ model reduction problem. Non-linear vibrations of structures and structural components were taken into account by [25], with a two-step natural mode discretization. Firstly, a linear analysis on the full system was performed, then a discretization of the non-linear problem was obtained. One of the key point was the study of a recipe to select natural modes to be retained, in order to effectively study non-linear vibrations of an angle-ply laminated circular cylindrical shell.

An interesting survey and comparison was proposed by several authors [26–30], while [31] proposed a comprehensive introduction to the subject. In particular, [27] showed a comparison between methods originated in different field, namely structural dynamics, numerical mathematics and systems and control, [26] was focused on geometrically non-linear structures and in the use of commercial non-linear finite element software, [29] considered a circuit high order model of a capacitor, [28] took into account a non-linear transmission line and studied both model and data-based method, while [30] was focused on parametric reduced order models.

Model order reduction methods appeared at first in the structural dynamics field and they were used for the identification of eigenfrequencies or the computation of Frequency Response Functions (FRFs). Mode displacements reduction methods have been deeply studied, developed and improved [5, 32], while another important family of methods developed in this field is based on the Component Mode Synthesis (CMS) [33, 32, 34].
Systems and control field is mainly focused on the analysis of dynamic systems and the design of feedback controllers; in this area, methods based on balanced truncation ([35–37]) or on Hankel norm approximation [38, 31, 36]

2.3 Data-based methods

Data-based model order reduction methods use experimental data or previous simulations of the full order system to build the reduced model. Splitting the whole simulation process into off-line and on-line phases, the off-line phase is the one in which the reduced model is built, while the on-line phase is the one in which the reduced model is used in simulation. In data-based methods the off-line phase is the more computationally expensive and it can require a significant amount of time, but it needs to be performed only once. This class of approaches is more profitable when the simulation of the reduced model needs to be performed a large number of times, e.g. in parametric analyses or optimization. Typically, in fact, data-based methods allow to build a particularly efficient reduced model, significantly faster to simulate than the original one. Moreover, it is possible, for certain methods, to use experimental data in the generation of the reduced model, allowing for system identification techniques ([28]).

One of the most studied and developed method is the Proper Orthogonal Decomposition, discussed in the following, while several other methods have been proposed. As an example, a projection based non-linear model reduction approach was recently proposed by [21], which considered discrete, high-fidelity, non-linear, finite element structural dynamics models and their reduction. In this work, an Energy-Conserving Sampling and Weighting (ECSW) hyper reduction method for discrete (or semi-discrete), non-linear, finite element structural dynamics models was used.

2.3.1 Proper Orthogonal Decomposition

Proper Orthogonal Decomposition (POD) method can be defined as "*multi-variate statistical method that aims at obtaining a compact representation of the data.*" ([39]). Considering a set of data, obtained experimentally or from simulations of the full model, POD method projects the original data onto a subspace, defined through the eigenvectors of the sample covariance matrix. By retaining only the eigenvectors associated with the largest eigenvalues, the model is reduced. An interesting property of this approach and one of the reasons of its success, is its optimality, since it minimizes the average squared distance between the reduced representation of a signal and the original one.
Since it uses linear eigenvectors, POD method is a linear approach and its optimality property is true for linear approximation of the non-linear system. Despite that, it is largely used in non-linear model reduction since, as stated by [40], POD represents "*a safe haven in the intimidating world of non-linearity; although this may not do the physical violence of linearisation methods*".

Before illustrating in more detail the POD method, a brief historical overview is provided in the following.
The POD method was proposed independently by several authors, including [41], [42], [43], [44] and [45]. Several developments, variations and modification were proposed in the last 60 years; other methods, developed independently, can be considered as special application of the POD method, such as the Principal Component Analysis (PCA), discussed in the following. For what concerns the equivalence and relationships between all these methods and other, [46], [47] and [48] proposed a detailed discussion about the equivalence of the POD, PCA and KLD (refer also to [49]), and their connection with the Singular Value Decomposition (SVD).
The use of POD for extracting coherent structures from turbulent flows was proposed by [40], which identified "*organized spatial features which repeatedly appear and undergo a characteristic temporal life cycle*". The same topic was further elaborated by the same authors, in [50].
Similarities between Proper Orthogonal Modes (POMs) and linear natural modes was discussed by [51], which showed their equivalence when the system is linear o weakly non-linear.
An application on a variation of the Jeffcot rotor, modelled as a continuous rotor, including gyroscopic effects, was proposed by [52], which tried to overcome

the lumped non-linear model used in the field at the time. The "assumed modes method" is used to discretize and partially decoupling the Partial Derivatives Equations (PDEs), in order to solve them numerically. A focus is place on the selection of suitable modes for decoupling the system and the different numerical issues are described and discussed, providing moreover a comparison between numerical and experimental results.

A comparison of linear (POD) and non-linear Galerkin methods was proposed by [53], with application on the reduction of infinite dimensional systems PDEs to low dimensional systems Ordinary Differential Equations (ODEs). In this work, questions about the choice of the modeshapes and the choice of the number of modes to be used are addressed. In particular, since the focus was on system's stability, only unstable or close to instability modes are considered.
A summary and analysis of 3 POD methods (KLD, PCA and SVD) was proposed by [54]. Derivation of the models and performances are analysed and the equivalence problem is discussed via a theoretical comparison. Equivalence of the matrices, objective functions, optimal base vectors, mean-square errors and asymptotic connections are demonstrated and proved, taking into account the POD of discrete random vectors.
Focusing on Micro-Electro-Mechanical Systems (MEMS), [55] proposed a review of applications of POD methods to model reduction. The focus, in this work, is on noisy data and a neural-network-based method that combines robust PCA neural network model with Galerkin procedure is used.
On larger scale, [56] used the POD method on the non-linear response of perfect and imperfect, simply supported circular cylindrical shells to harmonic excitation. Time-series response was obtained through the conventional Galerkin approach, using normal modes as projection basis, while the POD method was used on these time-series to extract proper orthogonal modes and create a reduced order model.
An interesting analysis of POD methods was proposed by [39], which used the proper orthogonal decomposition in place of the non-linear normal modes to extract modes from a non-linear structure. Modes obtained are used for the dual purpose of model order reduction and feature extraction. Additionally, it contains an historical review of the POD method.
A Bayesian approach to non-linear inverse problems was used by [57], which used Galerking projection on a polynomial chaos basis to build a reduced surrogate inexpensive to evaluate.

More recently, [58] used the Krylov subspaces and the POD methods together, providing moreover a MATLAB code, written for Non-symmetric Band Lanczos algorithm.

Referring to [39], the mathematical formulation of the POD method is obtained by firstly considering a random field $\Theta(x,t)$ on an arbitrary domain Ω. It is then defined $\mu(x)$ as the mean value of $\Theta(x,t)$, so that $\theta(x,t)$ has null mean value, as reported in eq.2.1.

$$\Theta(x,t) = \mu(x) + \theta(x,t) \tag{2.1}$$

Taking into account a generic time instant t^k, the snapshot $\theta^k = \theta(x,t^k)$ is defined. Considering a collection of snapshots, at different time instant, the POD method aims to find their most characteristic structure $\phi(x)$. Mathematically, this is equivalent to obtaining the basis function that maximize the ensemble average of the inner products between θ^k and $\phi(x)$, as expressed by eq.2.2

$$max\left(\left\langle\left|\int_\Omega \theta^k(x)\phi(x)d\Omega\right|^2\right\rangle\right) \tag{2.2}$$

where $\langle\cdot\rangle$ denotes the averaging operation and $|\cdot|$ denotes the modulus. An additional constraint used is that $||\phi||^2 = 1$, which imposes unitary norm for the eigenvectors. In [50] it is shown that the maximum, with reference to eq.2.2, is reached when eq.2.3 is satisfied.

$$\int_\Omega \left\langle \theta^k(x)\,\theta^k\left(x'\right)\right\rangle \phi\left(x'\right)dx' = \lambda\phi(x) \tag{2.3}$$

As a consequence, the solution of eq.2.2 is given by the orthogonal eigenfunctions $\phi_i(x)$, called Proper Orthogonal Modes (POMs), with the corresponding eigenvalues λ_i, called Proper Orthogonal Values (POVs). POMs can be then used as basis for the decomposition of the field $\theta(x,t)$, as proposed by eq.2.4

$$\theta(x,t) = \sum_{i=1}^{\infty} a_i(t)\phi_i(x) \tag{2.4}$$

where the coefficients $a_i(t)$ are determined by $a_i(t) = (\theta(x,t),\phi_i(x,t))$.

An interesting property of POMs is that the first POM is the best single vector to capture the data in input (optimal vector), while the second one is the best one in

a space orthogonal to the first one. In this sense the basis of vector formed by the POMs and obtained through the POD method is the optimal one; however, this is true only for the linear approximation of the system and it is based uniquely on the input data. The energy ε contained in the data is defined as $\varepsilon = \sum_j \lambda_j$ and the energy percentage captured by the generic i^{th} mode is given by $\lambda_i / \sum_j \lambda_j$.

For additional details about the computation of the POD, refer to [39].

2.4 Model-based methods

Model-based reduction techniques use data uniquely from the model of the system considered, which means that no simulations of the complete system are necessary. This is particularly important when the full system is complex to simulate and/or when the number of simulations of the Reduced Order Model (ROM) is limited. The off-line phase is in fact reduced to some simple model analysis and this results particularly beneficial when the on-line phase does not require extended computational time.

Despite being used in different engineering field, in this thesis the focus is on structural dynamics, even if other methods and applications will be illustrated. In the following several model-based reduction methods are briefly illustrated.

2.4.1 Guyan

One of the first and most used and developed method for model order reduction was proposed by [59]. This reduction is based on the elimination of those coordinates at which no force is applied: it is therefore a method acting solely in physical coordinates. This first approach is called *Static Condensation*, since it starts from the static problem. It is possible to rearrange the structural equations as per eq.2.5.

$$\begin{Bmatrix} \boldsymbol{F_m} \\ \boldsymbol{0} \end{Bmatrix} = \begin{bmatrix} \boldsymbol{K}_{mm} & \boldsymbol{K}_{ms} \\ \boldsymbol{K}'_{ms} & \boldsymbol{K}_{ss} \end{bmatrix} \begin{Bmatrix} \boldsymbol{x_m} \\ \boldsymbol{x_s} \end{Bmatrix} \tag{2.5}$$

The two equation resulting from splitting forced and not forced coordinates yields to eq.2.6. All the forced coordinates (or Degrees of Freedom, DoFs) are called *master*,

while the remaining ones are called *slave*.

$$\boldsymbol{F}_m = \left(\boldsymbol{K}_{mm} - \boldsymbol{K}_{ms}\boldsymbol{K}_{ss}^{-1}\boldsymbol{K}'_{ms}\right)\boldsymbol{x}_m \tag{2.6}$$

The transformation matrix $\boldsymbol{T}$, as defined in eq.2.7 is used in $\boldsymbol{x} = \boldsymbol{T}\boldsymbol{x}_m$, to both obtain the full set of equation based on *master* DoFs and to reduce the stiffness matrix.

$$\boldsymbol{T} = \begin{bmatrix} \boldsymbol{I} \\ -\boldsymbol{K}_{ss}^{-1}\boldsymbol{K}'_{ms} \end{bmatrix} \tag{2.7}$$

By using the same transformation for the mass matrix, eq.2.8 is obtained, considering therefore $\boldsymbol{K}_R = \boldsymbol{T}'\boldsymbol{K}\boldsymbol{T}$ and $\boldsymbol{M}_R = \boldsymbol{T}'\boldsymbol{M}\boldsymbol{T}$.

$$\begin{aligned} \boldsymbol{M}_R &= \boldsymbol{M}_{mm} - \boldsymbol{M}_{ms}\boldsymbol{K}_{ss}^{-1}\boldsymbol{K}'_{ms} - \left(\boldsymbol{K}_{ss}^{-1}\boldsymbol{K}'_{ms}\right)'\left(\boldsymbol{M}'_{ms} - \boldsymbol{M}_{ss}\boldsymbol{K}_{ss}^{-1}\boldsymbol{K}'_{ms}\right) \\ \boldsymbol{K}_R &= \boldsymbol{K}_{mm} - \boldsymbol{K}_{ms}\boldsymbol{K}_{ss}^{-1}\boldsymbol{K}'_{ms} \end{aligned} \tag{2.8}$$

In eq.2.8 the mass matrix $\boldsymbol{M}$ is partitioned as reported in eq.2.9.

$$\boldsymbol{M} = \begin{bmatrix} \boldsymbol{M}_{mm} & \boldsymbol{M}_{ms} \\ \boldsymbol{M}'_{ms} & \boldsymbol{M}_{ss} \end{bmatrix} \tag{2.9}$$

Kinetic and potential elastic energy are demonstrate not to vary, as shown in eq.2.10.

$$\begin{aligned} T &= \frac{1}{2}\dot{\boldsymbol{x}}'\boldsymbol{M}\dot{\boldsymbol{x}} = \frac{1}{2}\dot{\boldsymbol{x}}'_m\boldsymbol{T}'\boldsymbol{M}\boldsymbol{T}\dot{\boldsymbol{x}}_m = \frac{1}{2}\dot{\boldsymbol{x}}'_m\boldsymbol{M}_R\dot{\boldsymbol{x}}_m \\ V &= \frac{1}{2}\boldsymbol{x}'\boldsymbol{K}\boldsymbol{x} = \frac{1}{2}\boldsymbol{x}'_m\boldsymbol{T}'\boldsymbol{K}\boldsymbol{T}\boldsymbol{x}_m = \frac{1}{2}\boldsymbol{x}'_m\boldsymbol{K}_R\boldsymbol{x}_m \end{aligned} \tag{2.10}$$

However, being the reduced mass matrix a combination of stiffness and mass elements, the eigenvalue problem is not exactly preserved. Moreover, the choice of the *master* degrees of freedom is particularly critical: the quality of the approximation of the dynamic behaviour of the reduced system depends in fact by the lowest frequency of the full system, with all *master* DoFs fixed ([60]).
In order to correct this issue, several evolution of the original procedure have been proposed, such as the *Dynamic Condensation*, which uses a dynamic condensation matrix that can be defined as ([60]):

- single-mode dependent
- multi-mode dependent

- response dependent

The single-mode matrix is defined as the relation of an eigenvector between *master* and *slave* DoFs and it is therefore defined for each mode separately, as per eq.2.11, leading to separate reduced models.

$$\boldsymbol{T}(\lambda) = -\left(\boldsymbol{K}_{ss} - \lambda \boldsymbol{M}_{ss}\right)^{-1} \left(\boldsymbol{K}_{ms} - \lambda \boldsymbol{M}_{ms}\right) \tag{2.11}$$

The multi-mode matrix is defined as the relations of a multi-eigenvector p, once again between *master* and *slave* DoFs, and it can be obtained as per eq.2.12

$$\boldsymbol{T} = \boldsymbol{\Phi}_{sp} \boldsymbol{\Phi}_{mp}^{+} \tag{2.12}$$

Response-dependent matrix can be considered a data-based reduction technique, since it is defined as the relations of responses between *master* and *slave* DoFs (eq.2.13).

$$\boldsymbol{X}_s(t) = \boldsymbol{T} \boldsymbol{X}_m(t) \tag{2.13}$$

2.4.2 Component Mode Synthesis

The main idea on which this class of methods is based is to consider the structure of interest "*as an assemblage of discrete structural elements*" ([61]). Each substructure can be reduced separately, reducing therefore the order of the full model. Using basic mass and stiffness matrices for each substructure, together with conditions of geometrical compatibility along the boundaries, [61] proposed a method for dealing with the assemblage of the whole system. Two forms of generalized coordinates are used in this method. The first kind is a set of boundary generalized coordinates, which give displacements and rotations of nodes along boundaries between substructures: they are related to the displacement modes of the substructures, known as *constraint modes*. The second kind is a set of normal-mode generalized coordinates, related to the free vibration modes of each substructures, considering the boundaries to be fixed.

Taking into account a generic r^{th} substructure, connected with the substructures $(r-1)$ and $(r+1)$, the first step is to define the substructure of interest considering all boundary conditions as fixed. The stiffness matrix of the r^{th} substructure, which is considered known, is partitioned, splitting interior and boundary nodes. The latter

are always expressed in terms of physical coordinates, while internal nodes can be described by means of any kind of generalized coordinates. Modal coordinates are largely used for this purpose, given their ability of describing most of structure deformation with a limited number of DoFs (modeshapes). [61] defines *constraint modes* "as the mode shapes of the interior freedoms due to successive unit displacement of boundary points, all other boundary points being totally constrained", describing how to obtain them. Complementary, normal modes of the inner structure are defined with all boundary nodes constrained. Only a portion of the normal modes are retained, effectively performing the model order reduction.
After the original version ([61]), in following years several improvements were proposed, using time-domain or frequency-domain methods (see [34] for a review) and this technique is still used nowadays, as proposed by [32], which developed an extension of the Craig-Bampton substructuring technique that included high order static correction modes, in order to improve the representation of the dynamic of the global system. In this work, residual forces appearing as a consequence of the model reduction procedure were drastically decreased. Even more recently, [33] proposed an experimental substructure model, based on a transmission simulator. Fixed interface modes were here used in place of the free ones, combining analytical and experimental based substructure models. The problem analysed was the experimental-analytical analysis of a structure attached to a fixture, where the whole system was modelled together and the model of the sole structure was extracted by subtracting the model of the fixture, obtained through a Craig-Bampton representation.

2.4.3 Balanced Truncation

The Balanced Truncation method has its root in the field of system and control (e.g. [37]) and it is based on the idea of truncating the system considered, at a certain point. In this field the interest typically lies on the input-output relationship, so that a state space transformation, which does not alter the input-output behaviour, is used. Considering the generic linear dynamical system described in eq.2.14 with the classical systems and control notation, eq.2.15 express a generic transformation in

the state space

$$\begin{aligned} \frac{d\boldsymbol{x}}{dt} &= \boldsymbol{A}\boldsymbol{x} + \boldsymbol{B}\boldsymbol{u} \\ \boldsymbol{y} &= \boldsymbol{C}^T\boldsymbol{x} + \boldsymbol{D}\boldsymbol{u} \end{aligned} \tag{2.14}$$

$$\boldsymbol{T}\tilde{\boldsymbol{x}} = \boldsymbol{x} \tag{2.15}$$

If the transformation is performed by using the eigenvalue decomposition of matrix $\boldsymbol{A}$ (eq.2.16), $\boldsymbol{T}^{-1}\boldsymbol{A}\boldsymbol{T}$ is a diagonal matrix, containing all the matrix eigenvalues.

$$\boldsymbol{A}\boldsymbol{T} = \boldsymbol{A}\boldsymbol{\Lambda} \tag{2.16}$$

It is possible to retain, by ordering and truncating, only the dominant ones, restricting T and performing therefore a *modal truncation*. The *Truncated Balanced Realization* (TBR) exploits controllability Gramian and observability Gramian matrices of the linear time invariant system of eq.2.14. By assuming stability for **A**, Lyapunov equations can be obtained for the Gramians: once these matrices are found, a transformation that balances the system is sought. This means having the two matrices equal to each other and corresponding to the diagonal matrix constituted by the Hankel singular values. See [37, 62, 31] for details. After the balancing procedure the truncation is performed, retaining only the largest Hankel single values.
Other uses of this method can be found, as in [36], in which a frequency-weighted model order reduction method, with an a priori error bound, was proposed, yielding to stable models even when both input and output weightings are included. A more recent application can be found in [35]. In this paper the focus was on the model order reduction of time invariant systems with random variable parameters, governed by probabilistic laws. The TBR method was combined with Generalized Polynomial Chaos (GPC) formalism, a tool for uncertainty propagation used for transforming the random LTI system in a balanced form. Such system was then truncated with TBR and the method was applied to a two-degrees of freedom mass-spring system, with uncertain stiffness and damping.

2.4.4 Hankel approximation

The first decisive results on Hankel norm were obtained [63] and [64], while the *modern* Hankel approximation method was introduced in 1984, by [38]. This method is closely related to the Balanced Truncation method and it is based on the Hankel norm to compute an optimal reduction, improving the Balanced Truncation. It was in fact proved that an optimal reduction can be obtained, given a specific norm, called Hankel norm. By considering the single DOF case, eq.2.17 defines the Hankel operator, called $\mathscr{H}$.

$$\mathscr{H} : u \to y = \int_{-\infty}^{0} h(t-\tau)u(\tau) \tag{2.17}$$

In eq.2.17 $h(t)$ is the impulse response in the time domain, defined as per eq.2.18

$$h(t) = Ce^{At}B \tag{2.18}$$

where A, B and C are defined as per eq.2.14 (for the single DOF system), and $t > 0$. The maximal gain of the above defined operator can be calculated as per eq.2.19, which defines the Hankel norm.

$$||\Sigma||_H = \sup_{u \in \mathscr{L}_2(-\infty,0]} \frac{||y||_2}{||u||_2} \tag{2.19}$$

It can be proved that the Hankel norm is the largest Hankel singular value of the system, which is $||\Sigma||_H = \lambda_{max}^{1/2}$.

One of the main limitations of this approach is that ([65]) "*the computation of the Hankel singular values involves the solution of two linear matrix equations, the Lyapunov equations*". Besides that, it also requires the calculation of the eigenvalues of the product of the *reachability* and *observability* grammians matrices, which involves dense computations. This method is therefore successfully applicable only on systems of modest dimension (few hundreds of DOFs).

2.4.5 Krylov

Krylov methods where developed as Lanczos ([66]) and Arnoldi ([67]) methods, firstly used for iterative computation of eigenvalues and modernly used for model order reduction purposes. They are applicable to large complex systems, while main drawbacks are the unavailability of a guaranteed error bounds and the possibility of

not preserving stability properties.
Several improvements and modifications were proposed, including the Padé via Lanczos (PLV) [68–71] (particularly used in model order reduction of circuits) and the multipoint rational interpolation [72].
Krylov methods were also used in combination with SVD-based methods (see [65] for more details and references).

Krylov subspace techniques for reduced order modelling of large scale dynamical systems were considered by [73]. It proposed a Lanczos process based Krylov subspace technique tutorial, for reduced order modelling of linear dynamical systems, providing an overview of several Krylov subspace techniques for dynamical systems. The focus was initially on first-order linear dynamical systems, but second-order and non-linear systems were also addressed.
Based on the notation used by [73], the base idea of Krylov subspace methods is to define a subspace spanned by a sequence of vector, which are generated by using a given matrix **A** and a starting vector **r**. The n^{th} Krylov subspace is named $\mathscr{K}_n(\mathbf{A},\mathbf{r})$ and it is defined by eq.2.20.

$$\mathscr{K}_n(\mathbf{A},\mathbf{r}) = span\left\{\mathbf{r},\mathbf{A}\mathbf{r},\mathbf{A}^2\mathbf{r},...,\mathbf{A}^{n-1}\mathbf{r}\right\} \tag{2.20}$$

In the case of non-symmetry of the matrix **A**, the definition of eq.2.20 refers to *right* Krylov subspace, while eq.2.21 defines the *left* Krylov subspace.

$$\mathscr{K}_n(\mathbf{A}^T,\mathbf{r}) = span\left\{\mathbf{r},\mathbf{A}^T\mathbf{r},\left(\mathbf{A}^T\right)^2\mathbf{r},...,\left(\mathbf{A}^T\right)^{n-1}\mathbf{r}\right\} \tag{2.21}$$

Several authors worked on this field, e.g. [10], with a method for model reduction of linear time-varying differential-algebraic equations. The proposed method was based on the automatic extraction of reduced models for non-linear RF blocks (mixers and filters) that exhibit nearly-linear signal path, but with strongly non-linear time-varying components. In this work the reduction procedure was based on a multi-point rational approximation algorithm, composed by an orthogonal projection of the original time-varying linear system into an appropriate Krylov subspace.
A MATLAB code for Non-symmetric Band Lanczos algorithm was more recently proposed by [58], which used the Krylov subspaces method and Proper Orthogonal Decomposition (POD).

2.4.6 Non-linear Normal Modes

Normal modes are key concept in the theory of linear vibrating systems and it is well know that they allow decoupling of equations of motion and therefore to reduce the linear model by taking into account only a subset of the modes. This key idea is used extensively in several linear model order reduction techniques, as illustrated previously. Two main properties of the Linear Normal Modes (LNMs) are used in this procedure:

1. Invariance: if the motion is limited to a specific LNM, it remains limited to the same LNM for all time
2. Modal superposition: any free and forced oscillation can be expressed as a linear combination of single LNM motions

Non-linear models, however, represent a more accurate description of the real systems and the non-linearities introduced in the model do not allow the use of the two above mentioned properties. As stated by [74], which proposed an interesting overview on the subject, "*any attempt to apply traditional linear analysis to non-linear systems results, at best, in a suboptimal design*".

Defining a non-linear tool analogous to LNMs is a long-lasting challenge that leaded to the definition of Non-linear Normal Modes (NNMs). The first successful attempts where published by Rosenberg, in [75] (NNMs defined for 2-DoFs non-linear system) and in [76, 77]. The first generalization of NNMs to n-DoFs systems was proposed by [78], in which lumped non-linear systems were considered. Normal modes were in this work defined, for non-linear systems, as solution of a maximum-minimum geometrical problem. More specifically, [78] defined them as "*A system of n masses, interconnected by non-linear symmetric springs and having n degrees of freedom is examined. The concept of normal modes is rigorously defined and the problem of finding them is reduced to a geometrical maximum-minimum problem in a n-space of known metric. The solution of the geometrical problem reduces the coupled equations of motion to n uncoupled equations whose natural frequencies can always be found by a single quadrature. An infinite class of systems, o which the linear system is a member, has been isolated for which the frequency amplitude can be found in closed form*".
The same author, in [79], proposed a survey of some geometrical methods, aimed

to study strongly non-linear systems. In this work, NNMs were defined as a way to obtain "*physically interesting solutions*", corresponding to natural free vibrations and steady state forced vibrations in linear systems. More specifically, it was stated "*The concept of normal modes and of eigenvalues is well defined only in linear systems. In fact, the demonstration of the existence of eigenvalues has its roots in the theory of quadratic forms, and its application to vibration problems requires that the potential energy be a quadratic form. The very essence of non-linearity is however that the potential energy is not a quadratic form. Hence, the question of existence of normal mode vibrations cannot be decided in the conventional way of finding eigenvalues, ad of attaching to each an eigenfunction.* [...] *Resonance occurs in the neighbourhood of normal mode vibrations, whether the system is linear or non-linear*".

Nearly rectilinear trajectories of non-linear normal modes, in the form of power series, were proposed by [80, 81], while [82], in the first part of his PhD thesis, considered free and forced oscillations of strongly non-linear, undamped, discrete oscillators. In his work free motions were examined by means of NNMs. Analytical methods for computing similar and non-similar normal modes were presented and mode stability was analysed,as well as normal mode bifurcations. A 2-DoFs system with cubic non-linearity was considered as application: it showed chaotic motions for large energy excitations.

A method for calculating the periodic solutions of non-linear mechanical systems with analytical non-linearities was proposed by [83]. A Jordan normalization procedure was described and generalized to damped harmonically excited oscillators. NNMs for Hamiltonian systems were introduced, showing how to extend the modal synthesis procedure, using a superposition technique based on non-linear modes (obtained from free vibrations) to describe the forced response. Examples provided were one DoF and two DoFs systems with cubic non-linearities.

Non-linear Normal Modes of dynamical systems were explained by means of the theory of invariant manifolds by [84], while [85] used a quasi-linear, plus essentially non-linear, expansions, using Padé approximation to join the two local expansions. In this work quasi-linear systems modes were determined as power series in the amplitude, while homogeneous non-linear modes were defined as power series in the inverse amplitude.

Reduced Order Modelling for geometrically non-linear vibrations of thin structures was considered by [14]. In this work a normal form procedure was computed

for non-linear oscillators with quadratic and cubic non-linearities. As stated by the authors, "*All the linear modal damping terms are gathered together in order to define a precise decay of energy onto the invariant manifolds, also defined as non-linear normal modes (NNMs)*". Proposed examples were a 2-DoFs simple system and a continuous circular cylindrical shell with external resonant forcing.

Despite decades of evolutions and studied, NNMs remain an open research topic since, as stated by [74], "*there is virtually no application of the NNMs to large-scale engineering structures*".

A concise description of the NNM idea was provided by [74], which is considered as main reference in the following brief overview. A generic non-linear system is considered here, in eq.2.22, in its free response.

$$\mathbf{M}\ddot{\mathbf{x}}(t) + \mathbf{K}\mathbf{x}(t) + \mathbf{f}_{nl}\left(\mathbf{x}(t), \dot{\mathbf{x}}(t)\right) = \mathbf{0} \tag{2.22}$$

where $\mathbf{M}$ is the mass matrix, $\mathbf{K}$ is the stiffness matrix, $\mathbf{x}$, $\dot{\mathbf{x}}$ and $\ddot{\mathbf{x}}$ are displacements, velocities and accelerations of each DoF and $\mathbf{f}_{nl}$ is the non-linear restoring force vector. In eq.2.22, moreover, the system is supposed to be already modelled by means of a discrete mechanical model. The first explanatory example proposed by [74] is a simple 2-DoFs system, represented schematically in Figure(2.1), with a cubic stiffness introducing a simple non-linearity.

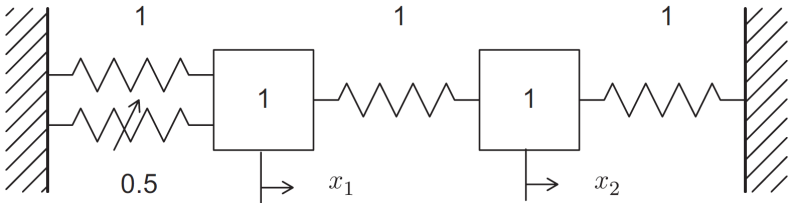

Fig. 2.1 Schematic representation of the 2-DoFs example.

Motion of such system is governed by eq.2.23:

$$\begin{cases} \ddot{x}_1 + (2x_1 - x_2) + 0.5x_1^3 = 0 \\ \ddot{x}_2 + (2x_2 - x_1) = 0 \end{cases} \tag{2.23}$$

Considering the underlying linear system, a first representation of its Linear Normal Modes (LNMs) is obtained and showed in Figure(2.2) through time series.

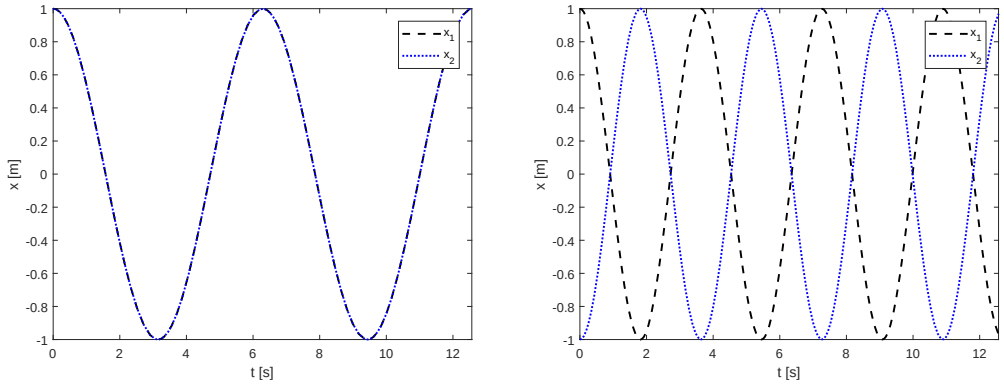

(a) In-phase ($\mathbf{x}(0) = [1,\ 1]$). (b) Out-of-phase ($\mathbf{x}(0) = [1,\ -1]$).

Fig. 2.2 Time series of LNM motions for unitary initial displacements and null initial velocities.

Another way for representing LNM motions is to use the configuration space, as shown in Figure(2.3). As shown, linear modes are corresponding to straight lines in the configuration space.

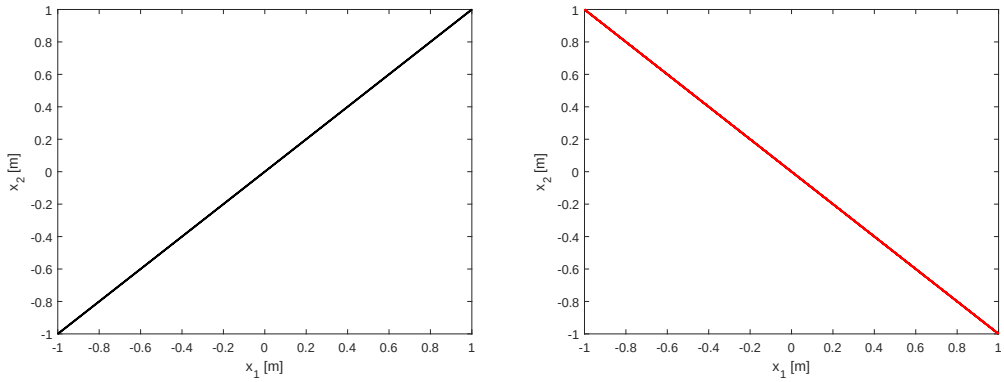

(a) In-phase ($\mathbf{x}(0) = [1,\ 1]$). (b) Out-of-phase ($\mathbf{x}(0) = [1,\ -1]$).

Fig. 2.3 LNM motions in configuration space. Unitary initial displacements and null initial velocities.

Considering the non-linear system, NNMs can be represented by means of the same tools, namely time series and configuration space, as shown in Figure(2.4) and Figure(2.5).

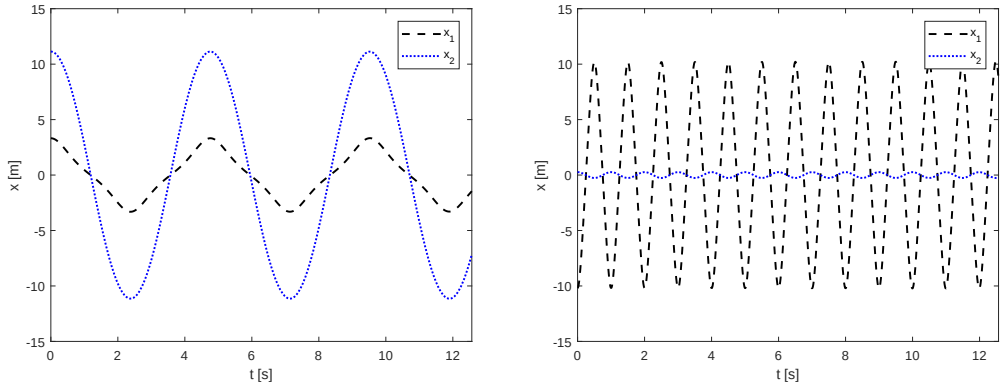

(a) In-phase ($\mathbf{x}(0) = [3.319,\ 11.134]$). (b) Out-of-phase ($\mathbf{x}(0) = [-10.188,\ 0.262]$).

Fig. 2.4 Time series of NNM motions for non-null initial displacements and null initial velocities.

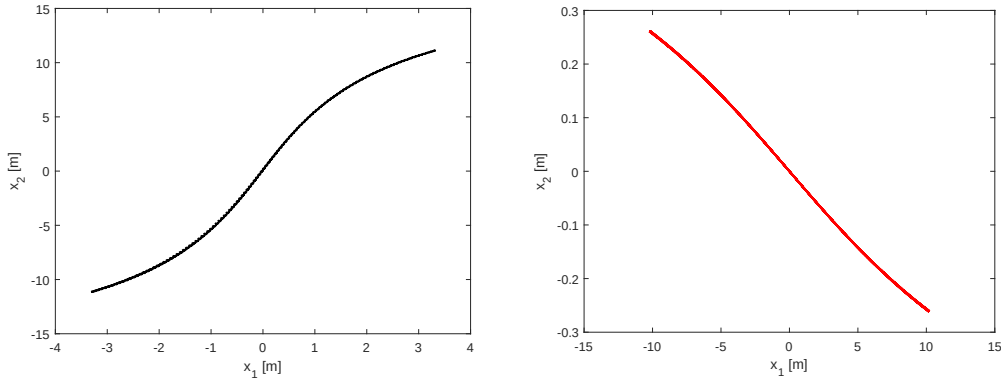

(a) In-phase ($\mathbf{x}(0) = [3.319,\ 11.134]$). (b) Out-of-phase ($\mathbf{x}(0) = [-10.188,\ 0.262]$).

Fig. 2.5 NNM motions in configuration space. Non-null initial displacements and null initial velocities.

It is immediately clear that the NNM motions of the non-linear system do not follow straight lines in the configuration space. They are instead represented by curved lines, resulting from the non-linear relationship between the coordinates during the periodic motion of each mode. Their shape, moreover, depends on the total energy present in the system, complicating even more their definition. Two main definition of Non-linear Normal Mode are proposed in the literature (see [74] for more details):

- Rosenberg: *vibration in unison of the system*
- Shaw & Pierre: *two-dimensional invariant manifold in phase-space*

There are differences between the two definition and the Shaw & Pierre definition can be seen as a generalization: Rosenberg's definition, i.e., cannot easily be extended to non-conservative systems. Moreover, internal resonance as the one shown in Figure(2.6), are not describable as NNM in a strict sense, since the vibration of the system is no longer in unison. It is however possible to *extend* Rosenberg's definition to cover these grey areas.

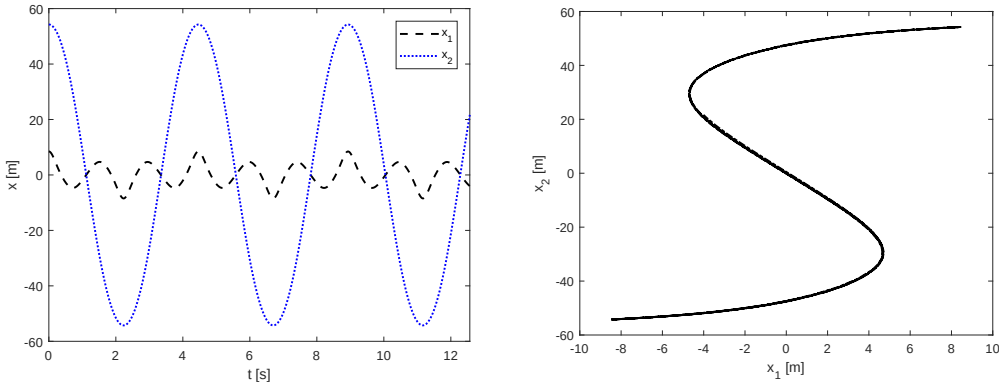

(a) Time series.

(b) Configuration space.

Fig. 2.6 Internally resonant NNM, with 3:1 resonance. $(\mathbf{x}(0) = [8.476,\ 52.263])$.

Non-linear Normal Modes have different properties with respect to Linear Normal Modes:

- *Frequency-energy dependence*: the resonant frequency of NNMs depend on the energy of the system, i.e. the amplitude of the oscillation
- *Modal interaction*: NNMs may interact during a general motion of the system (e.g. internal resonance phenomena)
- *Mode bifurcation*: the number of NNMs of a system may exceed its number of DoFs, due to mode bifurcations
- *Mode stability*: contrary to LNMs, NNMs can be either stable or unstable (small perturbations of initial conditions lead to the elimination of the mode oscillation)

2.4.7 Modal Coefficients

The use of linear modeshapes to reduce non-linear models is used in a method here called Modal Coefficients (MC). In this method the equations of motion of the model remain non-linear, preserving the system non-linearity: a polynomial expansion in terms of modal displacements is used to reproduce the original non-linearity. Details of the method and its implementation are discussed and proposed in the following chapters, while a quick overview of origins and applications is here provided. In this method the equations of motion are written in modal coordinates with non-linear stiffness forces usually expressed as cubic form (second and third order) in modal coordinates. Polynomial coefficients are obtained by prescribing particular displacement fields and solving the related static non-linear problems.

The MC method was proposed by [86] and [87], with the same author continuing developing the method ([88]). In [86] random vibrations of multi-DoFs systems were considered, with the solution obtained via the application of two different versions of a stochastic linearisation methods, based on the energy of the system. The novel approach proposed the determination of non-linear stiffness coefficients, reproducing the geometrical non-linearity. The new approach was used in combination with the equivalent linearisation technique and it was implemented as a computer program, while a commercial non-linear FEM program was used in building the reduced model. In [87] the same author applied the method to geometrically non-linear finite-element models, considering again random vibrations of a multi-DoFs system.

The MC method was used by [89], which applied this approach to model large deflections of beams with response involving multiple vibration modes, with aircraft surface panels as proposed application. The same example was considered by [12], which focused on aircraft panels subjected to combined thermal and acoustic effects, strong enough to induce a severe geometrically non-linear behaviour. In this work several modal bases for reduced order modelling were assessed and the in-plane displacements importance was highlighted, introducing a novel base, with separate representations of the transverse displacements and their induced in-plan counterparts.

Bending-membrane coupling problems were considered by [88], while [13] took into account again the prediction of the response, in terms of displacements, stresses and fatigue life, of aircraft panels subjected to severe thermo-acoustic loading. In

this work a focus was posed on the basis used, which included transverse deflection modes of the linear panel and some associated in-plane mode (commonly known as dual modes). In a review of several methods for reduced order models with stochastic parameter and model uncertainties of a geometrically non-linear dynamical system, [15] considered and reviewed the MC method, applying it to STEP approach.

Non-linear vibrations of piezoelectric layered beams (NEMS) were then considered by [90], which used a custom geometrical non-linear von Karaman beam model. Short circuit normal modes were used for the model reduction, as a basis for the MC method.

2.4.8 Trajectory Piecewise Linear approximation

A method named Trajectory PieceWise Linear (TPWL) approximation was presented by [91]; it was based on the representation of a non-linear system with a piecewise-linear system, reducing each part by means of Krylov projections. The focus was on non-linear circuits and micromachined devices, as the majority of applications of this method, but it can be easily used and adapted for generic non-linear dynamic systems. One should note that in this work, rather than approximating each individual component of the system with a piecewise equivalent, the reduced order model was built through a small set of linearisation points about the state space trajectory, named "*training input*". This key feature is important since the same approach is used in the method proposed in this thesis.

High-level canonical piecewise linear functions were already used by [92] to build a representation basis for target piecewise linear functions. The purpose was the minimization of the number of parameters used and this work provided a useful mathematical tool. A piecewise quadratic cost functions was used by [93], which extended the use of this approach from stability analysis of piecewise linear systems to performance analysis and optimal control. In this work it was possible to find a useful definition and description of piecewise linear systems, which highlights their usefulness: "*[. . .] local linear [. . .] analysis near an equilibrium point of a non-linear system can be improved [...] by splitting the state space into more regions, [...] increasing the flexibility in the non-linear description*". As stated by [93], in fact, any smooth non-linear system can, in principle, be approximated in this way,

up to an arbitrary accuracy, directly addressing the trade-off between precision and computational complexity.

An improved algorithm for the TPWL approximation was proposed by [94]. The proposed extension consisted of applying a more sophisticated projection basis, which merged multiple reduced order bases in Krylov subspaces generated at different linearisation points. A richer aggregated reduced basis was then obtained, enabling to further reduce the order of the model.

The same authors, in [95], focused on micro-machined switches and non-linear circuits, providing an interesting definition of the method: "*The idea is to represent a system as a combination of linear models, generated at different linearisation points in the state space. The key issue in this approach is that we will be considering multiple linearisation about suitably selected states of the system, instead of relying on a single expansion about the initial state. [...] In the regions with multiple non-zero weights, the associated matrix may not be stable, since a convex combination of stable matrices may not be a stable matrix*". In [96] the same approach was used for non-linear dynamical systems; in this work error estimates were given for solutions computed with TPWL reduced order models and problems of preserving stability and passivity were examined.

TPWL approximation method was used in combination with the Truncate Balanced Realization (TBR) by [97] for generating reduced models for a specific class of non-linear dynamical systems. The proposed method was compared to a TBR plus Krylov-based one, showing good accuracy while maintaining a relatively low model extraction cost. Several bases were obtained by using TBR at different states; afterwards, they were all aggregated into a single basis, by using a biorthonormalization algorithm. In [98] the TPWL approximation technique was applied to find approximate models of dynamical systems which are dependent on a number of state variables and parameters and a severely non-linear example was proposed. Applications on circuits and MEMS were proposed by [99], which combined TWPL with Krylov subspaces method.

This method is now illustrated, referring to [95]. In this work the state-space approach is used to describe a large class of non-linear dynamical systems, as

proposed by eq.2.24

$$\begin{cases} \frac{d\mathbf{g}(\mathbf{x}(t))}{dt} = \mathbf{f}(\mathbf{x}(t)) + \mathbf{B}(\mathbf{x}(t))\,\mathbf{u}(t) \\ \mathbf{y}(t) = \mathbf{C}^T\mathbf{x}(t) \end{cases} \tag{2.24}$$

where $\mathbf{x}$ represents the state of the system, $\mathbf{f}$ and $\mathbf{g}$ are non-linear vector-valued functions, $\mathbf{B}$ is a state-dependent input matrix, $\mathbf{u}$ is the input signal, $\mathbf{C}$ is the output matrix and $\mathbf{y}$ is the output signal. The proposed notation is particularly used in circuits and signal, where the dimensions of the output signal can be significantly lower than the system dimensions.

Considering the size of the full model as N and defining $q << N$ as the size of the reduced model, an orthonormal matrix $\mathbf{V}$, of dimensions Nxq, is chosen to represent the projection (as defined in eq.2.25) of the original model into a selected reduced order state-space.

$$\mathbf{x} = \mathbf{V}\mathbf{z} \tag{2.25}$$

In eq.2.25 $\mathbf{z}$ represents the state of the reduced model, i.e. the q^{th} projection of state $\mathbf{x}$ in the reduced order space. By replacing this definition into eq.2.24, eq.2.26

$$\begin{cases} \frac{d}{dt}\left[\mathbf{V}^T\mathbf{g}(\mathbf{V}\mathbf{z}(t))\right] = \mathbf{V}^T\mathbf{f}(\mathbf{V}\mathbf{z}(t)) + \mathbf{V}^T\mathbf{B}(\mathbf{V}\mathbf{z}(t))\,\mathbf{u}(t) \\ \mathbf{y}(t) = \mathbf{C}^T\mathbf{V}\mathbf{z}(t) \end{cases} \tag{2.26}$$

As highlighted by [95], the two main issues of this method are:

- Selecting $\mathbf{V}$ such that the reduced model provides good approximation of the original system
- Finding representations of $\mathbf{V}^T\mathbf{f}(\mathbf{V}\cdot)$ and $\mathbf{V}^T\mathbf{g}(\mathbf{V}\cdot)$ which allow low-cost storage and fast evaluation

The first point can be addressed following several methods, from time-series data, singular vectors from the Hankel operator or using Krylov subspaces, as discussed previously. The second point can be solved by using Taylor's expansion about some initial state $\mathbf{x}_0$, as per eq.2.27.

$$\mathbf{f}(\mathbf{x}) \approx \mathbf{f}(\mathbf{x}_0) + \mathbf{A}_0(\mathbf{x}-\mathbf{x}_0) + \frac{1}{2}\mathbf{W}_0(\mathbf{x}-\mathbf{x}_0)\otimes(\mathbf{x}-\mathbf{x}_0) \tag{2.27}$$

where $\mathbf{A}_0$ is the Jacobian matrix and $\mathbf{W}_0$ the Hessian of $\mathbf{f}(\cdot)$, both evaluated at $\mathbf{x}_0$, while $\otimes$ is the Kronecker product. An analogous linearisation can be performed for $\mathbf{g}(\mathbf{x})$, as reported in eq.2.28.

$$\frac{d\mathbf{g}(\mathbf{x})}{dt} \approx \frac{d}{dt}\left(\mathbf{g}(\mathbf{x}_0) + \mathbf{G}_0\left(\mathbf{x}-\mathbf{x}_0\right)\right) = \mathbf{G}_0\frac{d\mathbf{x}}{dt} \tag{2.28}$$

where $\mathbf{G}_0$ is the Jacobian matrix of $\mathbf{g}$ at $\mathbf{x}_0$.

Considering the linear case, for eq.2.24, the reduced model can be expressed by eq.2.29, while by considering the quadratic model, eq.2.30 define the reduced model.

$$\begin{cases} \mathbf{G}_{0r}\frac{d\overline{\mathbf{z}}}{dt} = \mathbf{V}^T\mathbf{f}(\mathbf{x}_0) + \mathbf{A}_{0r}\overline{\mathbf{z}} + \mathbf{B}_{0r}\mathbf{u} \\ \mathbf{y} = \mathbf{C}_r^T\overline{\mathbf{z}} \end{cases} \tag{2.29}$$

$$\begin{cases} \mathbf{G}_{0r}\frac{d\overline{\mathbf{z}}}{dt} = \mathbf{V}^T\mathbf{f}(\mathbf{x}_0) + \mathbf{A}_{0r}\overline{\mathbf{z}} + \frac{1}{2}\mathbf{W}_{0r}\left(\overline{\mathbf{z}}\otimes\overline{\mathbf{z}}\right) + \mathbf{B}_{0r}\mathbf{u} \\ \mathbf{y} = \mathbf{C}_r^T\overline{\mathbf{z}} \end{cases} \tag{2.30}$$

In the previous two equations the following notation is used:

- $\mathbf{A}_{0r} = \mathbf{V}^T\mathbf{A}_0\mathbf{V}$
- $\mathbf{G}_{0r} = \mathbf{V}^T\mathbf{G}_0\mathbf{V}$
- $\mathbf{B}_{0r} = \mathbf{V}^T\mathbf{B}\left(\mathbf{x}_0\right)\mathbf{V}$
- $\mathbf{C}_r = \mathbf{V}^T\mathbf{C}$
- $\mathbf{W}_{0r} = \mathbf{V}^T\mathbf{W}_0\left(\mathbf{V}\otimes\mathbf{V}\right)$
- $\mathbf{V}\overline{\mathbf{z}} = \mathbf{x}-\mathbf{x}_0$

It has to be note that computing and storing the reduced matrices has a cost of (according to [95]) $O\left(q^2\right)$ in the linear case and $O\left(q^3\right)$ in the quadratic case. Is it therefore practically inefficient to expand the Taylor series to orders higher than 3^{rd}.

The main idea of the TPWL approximation method is to use a set of s linearised systems (referring therefore to eq.2.29), computed at different linearisation points in the state-space: $\mathbf{x}_1,\ldots,\mathbf{x}_s$. Considering a generic i^{th} linearised system, the

corresponding full (not reduced) linear model is described by eq.2.31:

$$\frac{d}{dt}\left(\mathbf{g}\left(\mathbf{x}_i\right)+\mathbf{G}_i\left(\mathbf{x}-\mathbf{x}_i\right)\right)=\mathbf{f}\left(\mathbf{x}_i\right)+\mathbf{A}_i\left(\mathbf{x}-\mathbf{x}_i\right)+\mathbf{B}_i\mathbf{u} \tag{2.31}$$

where all the terms with the i subscript are referred to the i^{th} linear model, with a notation similar to the one used in eq.2.29.

In order to describe the whole piecewise linearised system (i.e. the piecewise linearisation of the original non-linear system), a weighted combination of all the single linear models is considered, as reported in eq.2.32:

$$\frac{d}{dt}\left[\sum_{i=1}^{s}\tilde{w}_i(\mathbf{x})\left(\mathbf{g}\left(\mathbf{x}_i\right)+\mathbf{G}_i\left(\mathbf{x}-\mathbf{x}_i\right)\right)\right]=\sum_{i=1}^{s}\tilde{w}_i(\mathbf{x})\left(\mathbf{f}_i\left(\mathbf{x}_i\right)+\mathbf{A}_i\left(\mathbf{x}-\mathbf{x}_i\right)+\mathbf{B}_i\mathbf{u}\right) \tag{2.32}$$

where all the s terms $\tilde{w}_i\left(\mathbf{x}\right)$ are state-dependent weights, defined so that $\sum_{i=1}^{s}\tilde{w}_i\left(\mathbf{x}\right)=1$.

The reduced order representation of the piecewise linear model is described by eq.2.33:

$$\begin{cases}\frac{d}{dt}\left(\left(\sum_{i=1}^{s}w_i(\mathbf{z})\mathbf{G}_{ir}\right)\mathbf{z}+\delta\cdot\mathbf{w}(\mathbf{z})\right)= \\ \qquad=\left(\sum_{i=1}^{s}w_i(\mathbf{z})\mathbf{A}_{ir}\right)\mathbf{z}+\gamma\cdot\mathbf{w}(\mathbf{z})+\left(\sum_{i=1}^{s}w_i(\mathbf{z})\mathbf{B}_{ir}\mathbf{u}\right) \\ \mathbf{y}=\mathbf{C}_r\mathbf{z}\end{cases} \tag{2.33}$$

where:

- $\mathbf{G}_{ir}=\mathbf{V}^T\mathbf{G}_i\mathbf{V}$
- $\mathbf{A}_{ir}=\mathbf{V}^T\mathbf{A}_i\mathbf{V}$
- $\mathbf{B}_{ir}=\mathbf{V}^T\mathbf{B}_i$
- $\mathbf{C}_r=\mathbf{C}^T\mathbf{V}$
- $\gamma=\left[\mathbf{V}^T\left(\mathbf{f}\left(\mathbf{x}_1\right)-\mathbf{A}_1\mathbf{x}_1\right),\cdots,\mathbf{V}^T\left(\mathbf{f}\left(\mathbf{x}_s\right)-\mathbf{A}_s\mathbf{x}_s\right)\right]$
- $\delta=\left[\mathbf{V}^T\left(\mathbf{g}\left(\mathbf{x}_1\right)-\mathbf{G}_1\mathbf{x}_1\right),\cdots,\mathbf{V}^T\left(\mathbf{g}\left(\mathbf{x}_s\right)-\mathbf{G}_s\mathbf{x}_s\right)\right]$
- $\mathbf{w}(\mathbf{z})=\left[w_1(\mathbf{z}),\cdots,w_s(\mathbf{z})\right]^T$, with $\sum_{i=1}^{s}w_i(\mathbf{z})=1$ for all $\mathbf{z}$

Weighting between the locally linearised models can be computed using information about the distances $||\mathbf{z} - \mathbf{z}_i||$ of every linearisation point from the current state $\mathbf{z}$.

In [95] details about implementation algorithms were provided, together with examples and discussion of issues and results.

Chapter 3

Modal Coefficients Method

In this section the model reduction method proposed by [86] and introduced in Subsection 2.4.7 is implemented. Firstly, in Section 3.1, a non-linear beam element is formulated, based on the von Kármán non-linearity. Such an element is implemented in MATLAB, providing the base for the subsequent model reduction, introduced in Section 3.2. All of the details of the formulation are analysed and developed in this section. Finally, applications of the implemented method are proposed in Section 3.3, providing a comparison with experimental data in Subsection 3.3.2.

It is important to remember that this method uses linear modeshapes to define cubic non-linear equations of motion in modal coordinates.

3.1 Non-linear beam element

In this section a non-linear beam element is developed. A MATLAB environment is used to implement this beam element and calculate the non-linear modal stiffness coefficients. The beam model implemented needs to be able to reproduce the geometrical non-linear behaviour of a beam, this is why a Euler-Bernoulli beam model, with von Kármán non-linearity is considered. For these purposes, combined with traditional Finite Element literature ([3, 2]), [100] and [101] are used as main references, together with [90], which is more focused on the Modal Coefficients topic. In this chapter (and more generically in this thesis) the focus is not to provide a comprehensive discussion about finite element topics, but to introduce all of the main assumptions made in the implementation of a non-linear beam element. The

generic Green-Lagrange strain tensor, expressed in Cartesian coordinate in eq.3.1 is considered,

$$E_{ij} = \frac{1}{2}\left(\frac{\partial u_i}{\partial X_j} + \frac{\partial u_j}{\partial X_i} + \sum_{m=1}^{3} \frac{\partial u_m}{\partial X_i}\frac{\partial u_m}{\partial X_j}\right) \tag{3.1}$$

where X_m represents the generic coordinate axis and u_m the corresponding displacement.

In the case of infinitesimal strain, it is assumed that there is no difference between the reference X_m and the current coordinate system x_m is considered, leading to eq.3.2.

$$\varepsilon_{ij} = \frac{1}{2}\left(\frac{\partial u_i}{\partial x_j} + \frac{\partial u_j}{\partial x_i} + \sum_{m=1}^{3} \frac{\partial u_m}{\partial x_i}\frac{\partial u_m}{\partial x_j}\right) \tag{3.2}$$

In order to simplify the notation, in the following axes directions are all named x while displacements all named u, with the following subscripts used to specify the correspondence with the Cartesian reference system (x, y, z):

- $1 \rightarrow x$
- $2 \rightarrow y$
- $3 \rightarrow z$

Following [101] in the Euler-Bernoulli model and neglecting at this stage the torsion around the axis of the beam, the following assumptions (typical of the Euler-Bernoulli formulation) are made:

- Inextensibility
- Straightness
- Normality of the material lines transverse to the beam axis

Considering then a beam with its main axis along x_1 (i.e. along x), the only non-zero terms of the Green-Lagrange stress tensor are reported in eq.3.3:

$$\varepsilon_{xx} = \frac{\partial u_1}{\partial x} + \frac{1}{2}\left(\frac{\partial u_2}{\partial x}\right)^2 + \frac{1}{2}\left(\frac{\partial u_3}{\partial x}\right)^2 \tag{3.3}$$

The shear stress is in fact neglected, since due to (as per Euler-Bernoulli) torsion only and not being the torsion introduced at this point.

From a kinematic point of view, the above mentioned simplifications lead to eq.3.4,

$$\begin{cases} u_1 = u(x) - yv_{,x}(x) - zw_{,x}(x) \\ u_2 = v(x) \\ u_3 = w(x) \end{cases} \tag{3.4}$$

which derived along the beam axis leads to eq.3.5:

$$\begin{cases} \frac{\partial u_1}{\partial x} = u_{,x}(x) - yv_{,xx}(x) - zw_{,xx}(x) \\ \frac{\partial u_2}{\partial x} = v_{,x}(x) \\ \frac{\partial u_3}{\partial x} = w_{,x}(x) \end{cases} \tag{3.5}$$

In eq.3.4 and eq.3.5 the notation $p_{,k}$ expresses the derivation of p with respect to k. By substituting eq.3.5 into eq.3.3, eq.3.6 is obtained,

$$\varepsilon_{xx} = u_{,x} - yv_{,xx} - zw_{,xx} + \frac{1}{2}v_{,x}v_{,x} + \frac{1}{2}w_{,x}w_{,x} \tag{3.6}$$

with its differential form expressed by eq.3.7:

$$\delta\varepsilon_{xx} = \delta u_{,x} - y\delta v_{,xx} - z\delta w_{,xx} + v_{,x}\delta v_{,x} + w_{,x}\delta w_{,x} \tag{3.7}$$

Finally, the differential form of eq.3.4 is obtained as eq.3.8

$$\begin{cases} \delta u_1 = \delta u(x) - y\delta v_{,x}(x) - z\delta w_{,x}(x) \\ \delta u_2 = \delta v(x) \\ \delta u_3 = \delta w(x) \end{cases} \tag{3.8}$$

The continuous formulation of kinetic (T) and elastic potential (U) energy of the system can be expressed as per eq.3.9.

$$\begin{cases} \delta T = \int_V \rho \left(\ddot{u}_1\delta u_1 + \ddot{u}_3\delta u_3\right) dV \\ \delta U = \int_V E\varepsilon_{xx}\delta\varepsilon_{xx} dV \end{cases} \tag{3.9}$$

Substituting eq.3.4 and its time derivative and expressing the energies in a matrix formulation, eq.3.10 and eq.eq.3.11 are obtained,

$$\delta T = \int_0^l \begin{Bmatrix} \delta u & \delta v & \delta w & -\delta w_{,x} & -\delta v_{,x} \end{Bmatrix} \begin{Bmatrix} I_{00} & 0 & 0 & 0 & 0 \\ 0 & I_{00} & 0 & 0 & 0 \\ 0 & 0 & I_{00} & 0 & 0 \\ 0 & 0 & 0 & I_{02} & 0 \\ 0 & 0 & 0 & 0 & I_{20} \end{Bmatrix} \begin{Bmatrix} \ddot{u} \\ \ddot{v} \\ \ddot{w} \\ -\ddot{w}_{,x} \\ -\ddot{v}_{,x} \end{Bmatrix} dx \quad (3.10)$$

$$\delta U = \int_0^l \begin{Bmatrix} u_{,x} + \frac{1}{2}v_{,x}^2 + \frac{1}{2}w_{,x}^2 & -w_{,xx} & -v_{,xx} \end{Bmatrix} \begin{Bmatrix} A & 0 & 0 \\ 0 & D_z & 0 \\ 0 & 0 & D_y \end{Bmatrix} \begin{Bmatrix} \delta u_{,x} + v_{,x}\delta v_{,x} + w_{,x}\delta w_{,x} \\ -\delta w_{,xx} \\ -\delta v_{,xx} \end{Bmatrix} dx \quad (3.11)$$

where terms in the matrices are calculated as per eq.3.12 and eq.3.13.

$$\begin{aligned} A &= \int_{-\frac{h}{2}}^{\frac{h}{2}} \int_{-\frac{b}{2}}^{\frac{b}{2}} E dy dz = Ebh \\ D_y &= \int_{-\frac{h}{2}}^{\frac{h}{2}} \int_{-\frac{b}{2}}^{\frac{b}{2}} E y^2 dy dz = E\frac{hb^3}{12} \\ D_z &= \int_{-\frac{h}{2}}^{\frac{h}{2}} \int_{-\frac{b}{2}}^{\frac{b}{2}} E z^2 dy dz = E\frac{h^3 b}{12} \end{aligned} \quad (3.12)$$

$$\begin{aligned} I_{00} &= \int_{-\frac{h}{2}}^{\frac{h}{2}} \int_{-\frac{b}{2}}^{\frac{b}{2}} \rho dy dz = \rho bh \\ I_{20} &= \int_{-\frac{h}{2}}^{\frac{h}{2}} \int_{-\frac{b}{2}}^{\frac{b}{2}} \rho y^2 dy dz = \rho\frac{hb^3}{12} \\ I_{02} &= \int_{-\frac{h}{2}}^{\frac{h}{2}} \int_{-\frac{b}{2}}^{\frac{b}{2}} \rho z^2 dy dz = \rho s\frac{h^3 b}{12} \end{aligned} \quad (3.13)$$

In order to obtain the mass and stiffness matrices, discretization by means of finite elements is used. Firstly ε_{xx} is split in two part, as proposed in eq.3.14 ([90]):

$$\varepsilon_{xx} = e + zk \qquad with \begin{cases} e = u_{,x} + \frac{1}{2} w_{,x}^2 \\ k = -w_{,xx} \end{cases} \tag{3.14}$$

Continuous displacements are then discretized by means of interpolation vectors **N**, as reported in eq.3.15. In this equation u^e represents the discretized version of u, which is the continuous displacement, and $\mathbf{u}^e$ is a vector containing displacements at the extremes of the beam element (x_A and x_B).

$$\begin{cases} u^e = \mathbf{N}_u \mathbf{u}^e \\ w^e = \mathbf{N}_w \mathbf{w}^e \end{cases} \qquad with \qquad \mathbf{u}^e = \begin{Bmatrix} u(x = x_A) \\ w(x = x_A) \\ w_{,x}(x = x_A) \\ u(x = x_B) \\ w(x = x_B) \\ w_{,x}(x = x_B) \end{Bmatrix} \tag{3.15}$$

Interpolation vectors **N** are based on the shape functions reported in eq.3.16 and shown in Figure(3.1). These shape functions are of two kinds:

- C^0 functions, for axial displacements
- C^1 functions, for bending displacements

They are defined so that they respect the following boundary conditions at the two nodes of the beam element (x_A and x_B), in order to allow a complete description of the displacements:

- $N_1 \rightarrow x_A = 1 \quad x_B = 0 \quad (C^0)$
- $N_2 \rightarrow x_A = 0 \quad x_B = 1 \quad (C^0)$
- $N_3 \rightarrow x_A = 1 \quad x_B = 0 \quad \dot{x}_A = 0 \quad \dot{x}_B = 0 \quad (C^1)$
- $N_4 \rightarrow x_A = 0 \quad x_B = 0 \quad \dot{x}_A = 1 \quad \dot{x}_B = 0 \quad (C^1)$
- $N_5 \rightarrow x_A = 0 \quad x_B = 1 \quad \dot{x}_A = 0 \quad \dot{x}_B = 0 \quad (C^1)$
- $N_6 \rightarrow x_A = 0 \quad x_B = 0 \quad \dot{x}_A = 0 \quad \dot{x}_B = 1 \quad (C^1)$

$$\begin{cases} N_1 = 1 - \frac{x}{L} \\ N_2 = \frac{x}{L} \\ N_3 = \left(1 - \frac{x}{L}\right)^2 \left(1 + \frac{2x}{L}\right) \\ N_4 = x\left(\frac{x}{L} - 1\right)^2 \\ N_5 = \frac{x^2}{L^2}\left(3 - \frac{2x}{L}\right) \\ N_6 = \frac{x^2}{L}\left(\frac{x}{L} - 1\right) \end{cases} \quad \begin{cases} N_1' = -\frac{x}{L} \\ N_2' = \frac{1}{L} \\ N_3' = -\frac{6x}{L^3}(L - x) \\ N_4' = \left(\frac{x}{L} - 1\right)\left(\frac{3x}{L} - 1\right) \\ N_5' = \frac{6x}{L^3}(L - x) \end{cases} \quad \begin{cases} N_3'' = -\frac{6}{L^3}(L - 2x) \\ N_4'' = \frac{2}{L}\left(\frac{3x}{L} - 2\right) \\ N_5'' = \frac{6}{L^3}(L - 2x) \\ N_6'' = \frac{2}{L}\left(\frac{3x}{L} - 1\right) \end{cases} \tag{3.16}$$

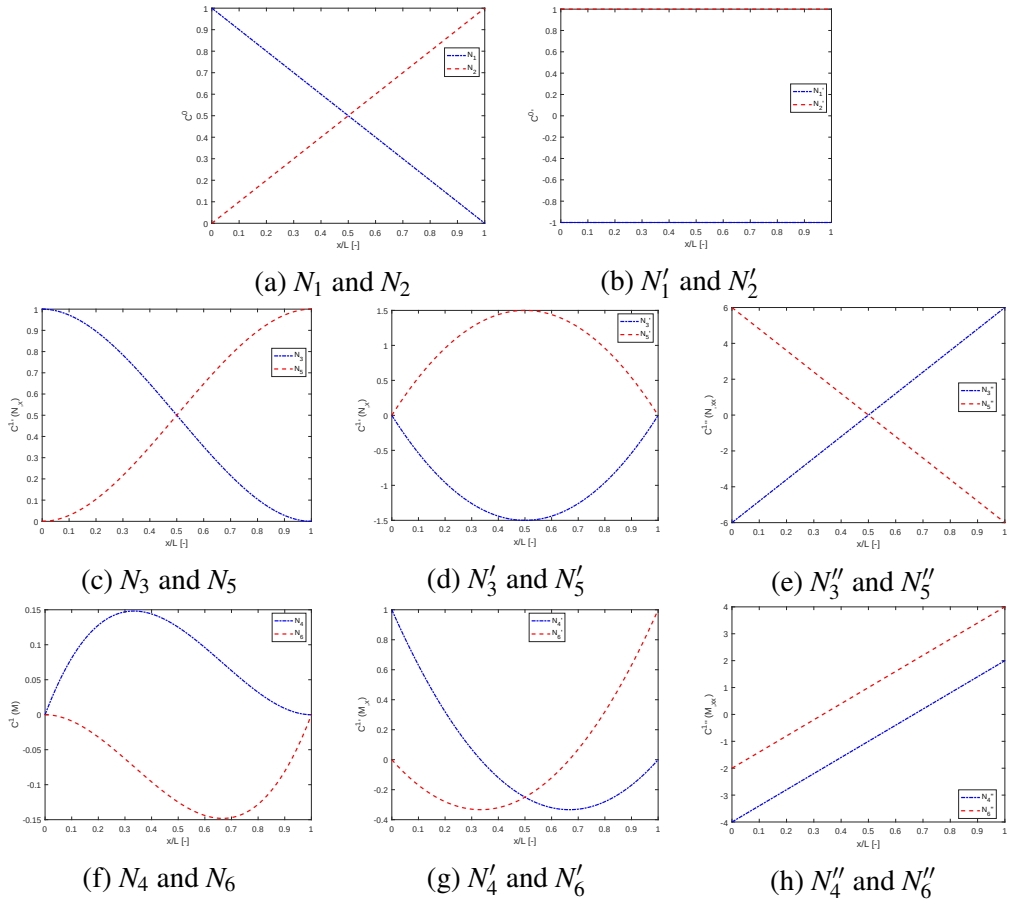

(a) N_1 and N_2 (b) N_1' and N_2'

(c) N_3 and N_5 (d) N_3' and N_5' (e) N_3'' and N_5''

(f) N_4 and N_6 (g) N_4' and N_6' (h) N_4'' and N_6''

Fig. 3.1 Shape functions and their derivatives.

Interpolations vectors **N** are defined, using the above defined shape functions, in eq.3.17:

$$\begin{aligned}
\mathbf{N}_u(x) &= \begin{Bmatrix} N_1(x) & 0 & 0 & 0 & 0 & N_2(x) & 0 & 0 & 0 & 0 \end{Bmatrix} \\
\mathbf{N}_v(x) &= \begin{Bmatrix} 0 & N_3(x) & 0 & 0 & N_4(x) & 0 & N_5(x) & 0 & 0 & N_6(x) \end{Bmatrix} \\
\mathbf{N}_w(x) &= \begin{Bmatrix} 0 & 0 & N_3(x) & -N_4(x) & 0 & 0 & 0 & N_5(x) & -N_6(x) & 0 \end{Bmatrix}
\end{aligned} \tag{3.17}$$

Mass and stiffness matrices of the non-linear beam element are defined considering that $\delta T^e = \int_0^l \delta \mathbf{u}^e \mathbf{M}^e \ddot{\mathbf{u}}^e dx$ and $\delta U^e = \int_0^l \delta \mathbf{u}^e \mathbf{K}^e \mathbf{u}^e dx$. Expression of mass (eq.3.18) and stiffness (eq.3.19) are hereafter reported.

$$\begin{aligned}
\mathbf{M}^e = \int_0^l & \begin{Bmatrix} \mathbf{N}_u^T & \mathbf{N}_v^T & \mathbf{N}_w^T & -(\mathbf{N}_w')^T & -(\mathbf{N}_v')^T \end{Bmatrix} \\
& \begin{Bmatrix} I_{00} & 0 & 0 & 0 & 0 \\ 0 & I_{00} & 0 & 0 & 0 \\ 0 & 0 & I_{00} & 0 & 0 \\ 0 & 0 & 0 & I_{02} & 0 \\ 0 & 0 & 0 & 0 & I_{20} \end{Bmatrix} \begin{Bmatrix} \mathbf{N}_u \\ \mathbf{N}_v \\ \mathbf{N}_w \\ -\mathbf{N}_w' \\ -\mathbf{N}_v' \end{Bmatrix} dx
\end{aligned} \tag{3.18}$$

$$\begin{aligned}
\mathbf{K}^e = \int_0^l & \begin{Bmatrix} \mathbf{N}_u' + \frac{1}{2}\mathbf{N}_v' \mathbf{u}^e \mathbf{N}_v' + \frac{1}{2}\mathbf{N}_w' \mathbf{u}^e \mathbf{N}_w' & -(\mathbf{N}_w'')^T & -(\mathbf{N}_v'')^T \end{Bmatrix} \\
& \begin{Bmatrix} A & 0 & 0 \\ 0 & D_z & 0 \\ 0 & 0 & D_y \end{Bmatrix} \begin{Bmatrix} \mathbf{N}_u' + \mathbf{N}_v' \mathbf{u}^e \mathbf{N}_v' + \mathbf{N}_w' \mathbf{u}^e \mathbf{N}_w' \\ -\mathbf{N}_w'' \\ -\mathbf{N}_v'' \end{Bmatrix} dx
\end{aligned} \tag{3.19}$$

The torsional behaviour is added to stiffness and mass matrices, considering the simple relations $k_\theta = \frac{G_b J_b}{l_b}$ and $m_\theta = \frac{1}{3}\rho_b I_{ob} l_b$, with J_b as the torsion constant and I_{ob} as the polar moment of inertia. No warping function is considered, contrary to [101].

It is necessary to note that in the expression of the stiffness matrix (eq.3.19) the displacement vector $\mathbf{u}^e$ is incorporated, making this matrix dependent on the displacements at the node of the beam, i.e. $\mathbf{K}^e = \mathbf{K}^e(\mathbf{u}^e)$, which will be translated, for the stiffness matrix of a generic structure, to $\mathbf{K} = \mathbf{K}(\mathbf{x})$, with $\mathbf{x}$ as the displacement vector. As a consequence, considering the static non-linear problem $\mathbf{K}(\mathbf{x})\mathbf{x} = \mathbf{F}$, the static displacement, $\mathbf{x}$ needs to be calculated by means of an iterative procedure.

The evaluation of the non-linear beam element characteristics is performed considering [101] as reference. Two benchmark examples have been considered:

- Beam A:
  - Aluminium: $E = 70 \times 10^9 \frac{\mathrm{N}}{\mathrm{m}^2}$, $\rho = 2778 \frac{\mathrm{kg}}{\mathrm{m}^3}$, $\nu = 0.34$
  - Clamped-clamped boundary conditions $\rightarrow x_A = 0 \quad x_B = 0$
  - $l = 0.580\mathrm{m}$, $b = 0.020\mathrm{m}$, $h = 0.002\mathrm{m}$
- Beam B:
  - Aluminium: $E = 70 \times 10^9 \frac{\mathrm{N}}{\mathrm{m}^2}$, $\rho = 2778 \frac{\mathrm{kg}}{\mathrm{m}^3}$, $\nu = 0.34$
  - Clamped-clamped boundary conditions $\rightarrow x_A = 0 \quad x_B = 0$
  - $l = 2.000\mathrm{m}$, $b = 0.020\mathrm{m}$, $h = 0.020\mathrm{m}$

3.1.1 Benchmark example - Beam A

A first comparison is provided by comparing numerical natural frequencies of the linear and non-linear (implemented here) Euler-Bernoulli beam model with the analytical ones, as proposed in Table3.1. Small amplitude of vibration are considered for these natural frequencies, which are therefore linear natural frequencies. The purpose of this step is to verify the consistency of the non-linear element in terms of its linear behaviour, while its non-linear performance is evaluated in Subsection 3.1.2.

Table 3.1 Beam A, natural frequencies comparison, with percentage error. Linear and non-linear Euler-Bernoulli beam models compared with analytical solution. Two (2-el) and four (4-el) elements.

	2-el (non-lin)	2-el (linear)	4-el (non-lin)	4-el (linear)	Analytical
ω_1	$195.7262\frac{\text{rad}}{\text{s}}$	$195.8751\frac{\text{rad}}{\text{s}}$	$192.8641\frac{\text{rad}}{\text{s}}$	$193.0066\frac{\text{rad}}{\text{s}}$	$192.7474\frac{\text{rad}}{\text{s}}$
ε_{ω_1}	1.54%	1.62%	0.06%	0.13%	-
ω_2	-	-	$533.2057\frac{\text{rad}}{\text{s}}$	$536.2395\frac{\text{rad}}{\text{s}}$	$531.3242\frac{\text{rad}}{\text{s}}$
ε_{ω_2}	-	-	0.35%	0.92%	-
ω_3	-	-	$1040.704\frac{\text{rad}}{\text{s}}$	$1063.855\frac{\text{rad}}{\text{s}}$	$1041.608\frac{\text{rad}}{\text{s}}$
ε_{ω_3}	-	-	0.09%	2.14%	-
ω_4	-	-	$1801.492\frac{\text{rad}}{\text{s}}$	$1930.066\frac{\text{rad}}{\text{s}}$	$1721.817\frac{\text{rad}}{\text{s}}$
ε_{ω_4}	-	-	4.63%	12.09%	-

The comparison shows good approximation of the first four natural frequencies, with percentage errors lowest in the non-linear case.

A static analysis is now proposed, comparing linear and non-linear models, and using different numbers of beam elements to model Beam A. Figure(3.2) shows the results obtained for a 8-element beam, with a force along the z axis applied in the centre of the beam, upward, with an intensity $F_z = 1 \times 10^{-3}$N. The number of elements used depends on the shape of the axial displacement, which requires at least 8 elements to be appreciated.

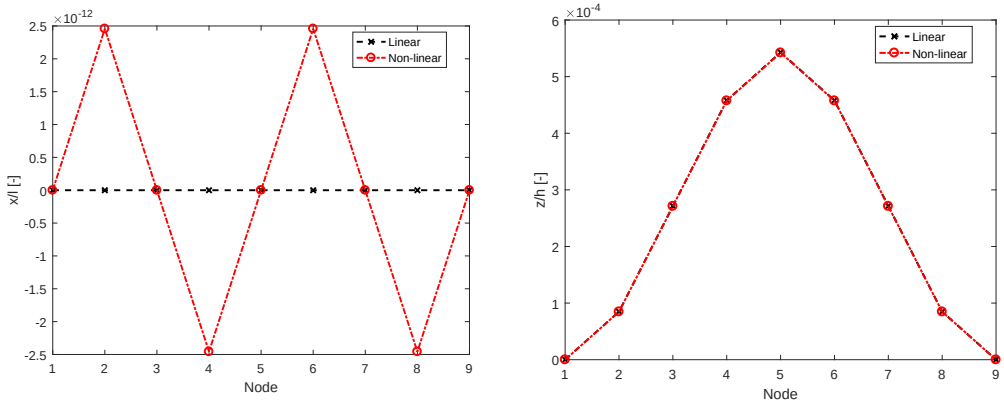

(a) Axial displacement (x).

(b) Bending displacement (z).

Fig. 3.2 Non-dimensional displacements along x and z, Beam A, 8-elements, $F_z = 1 \times 10^{-3}$N.

It can be noted that the expected axial-bending coupling of the non-linear model is not present in the linear one. Since the force applied is small, no significant differences are highlighted in the bending behaviour.

Increasing the number of nodes allows one to understand the number of elements necessary to describe Beam A with sufficient accuracy. Multiples of eight are considered, with the displacement field known. Figure(3.3) and Figure(3.4) show the same system, described with, 24 and 40 elements, respectively.

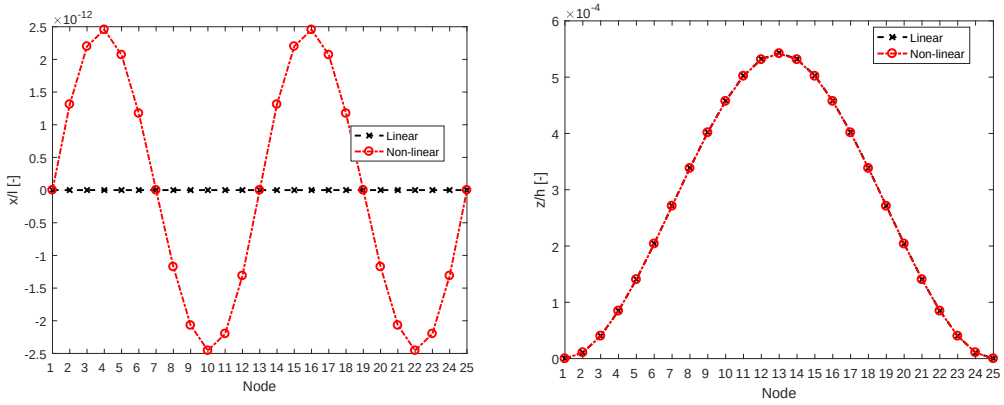

(a) Axial displacement (x). (b) Bending displacement (z).

Fig. 3.3 Non-dimensional displacements along x and z, Beam A, 24-elements, $F_z = 1 \times 10^{-3}$N.

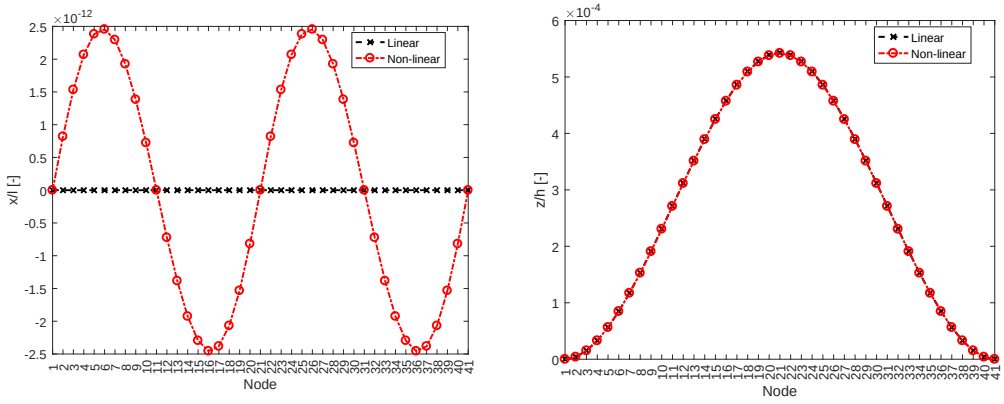

(a) Axial displacement (x). (b) Bending displacement (z).

Fig. 3.4 Non-dimensional displacements along x and z, Beam A, 40-elements, $F_z = 1 \times 10^{-3}$N.

The amplitude of the static force is increased to $F_z = 5$N; results are shown in Figure(3.5) to Figure(3.6).

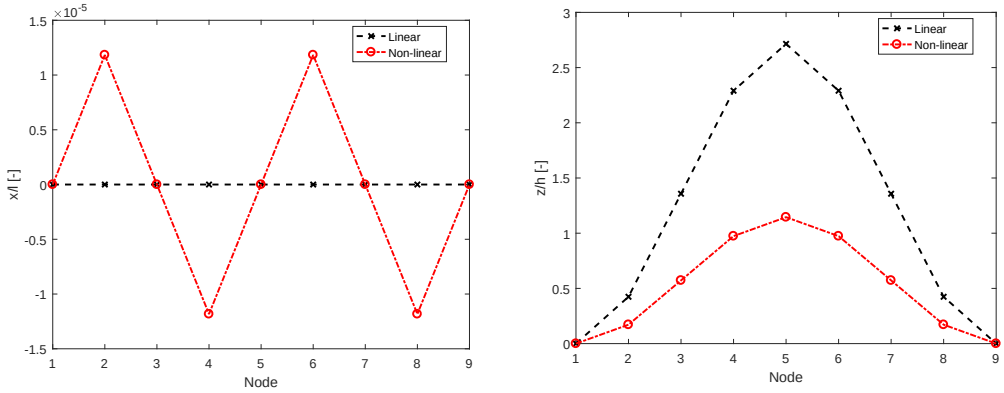

(a) Axial displacement (x). (b) Bending displacement (z).

Fig. 3.5 Non-dimensional displacements along x and z, Beam A, 8-elements, $F_z = 5$N.

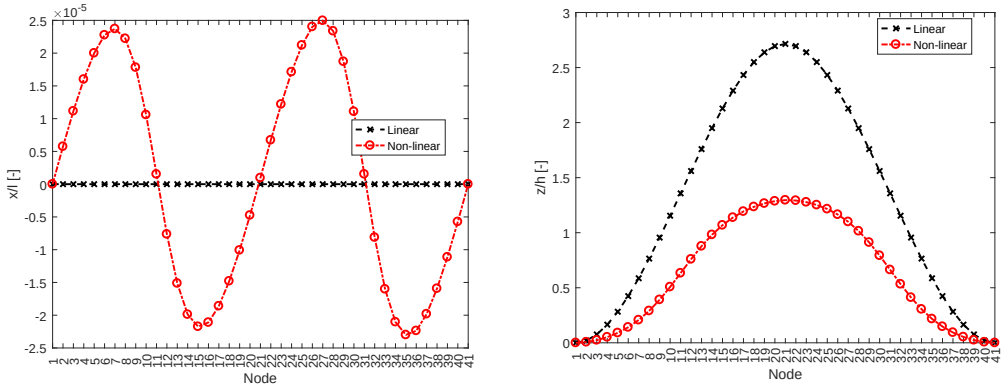

(a) Axial displacement (x). (b) Bending displacement (z).

Fig. 3.6 Non-dimensional displacements along x and z, Beam A, 40-elements, $F_z = 5$N.

Based on the results shown in the previous figure, it can be observed that:

- the non-linear element shows axial displacement as consequence of bending excitation, contrary to the linear element
- bending displacement of non-linear element differs from the one of the linear element
- the larger the excitation, the more elements are necessary to properly describe the displacement field (in particular the axial one)

In Figure(3.7) the axial and bending displacements, for the linear and the non-linear case, are compared.

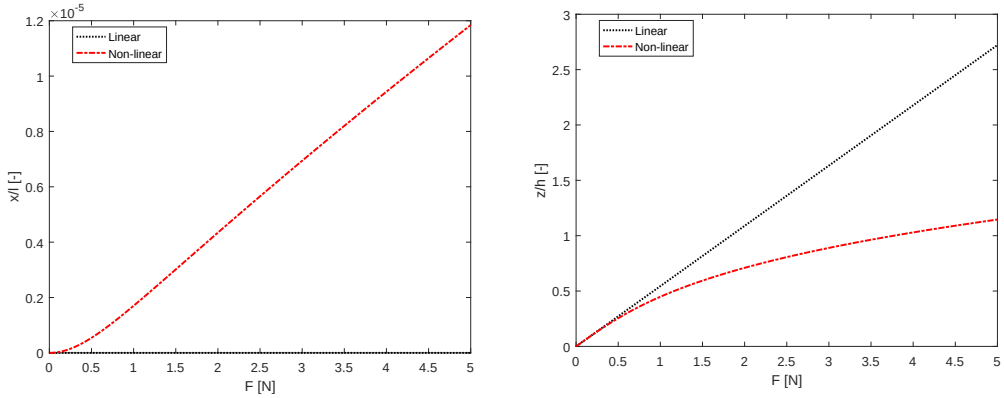

(a) Axial displacement (x). (b) Bending displacement (z).

Fig. 3.7 Comparison between linear (dotted black) and non-linear(dash-dot red) behaviour, Beam A, 8-elements.

It is evident that the non-linear element allows for coupling between bending and axial behaviour. Moreover, the non-linear element bending stiffness is dependent on the displacement, while it is constant in the linear beam element.

3.1.2 Benchmark example - Beam B

The second benchmark example considered, named Beam B, allows for a comparison with [101] of the static displacement of the beam centre point, considering a force applied at the centre of the beam, along the axis z and upwards. Table 3.2 reports static displacements and percentage error, with respect to the reference, of the centre of the beam, along z. Several force levels are considered.

Table 3.2 Static displacements and percentage error, beam centre, z direction, Beam B.

Force Amplitude	Linear	Non-linear	Reference
500N	2.232×10^{-2}m	1.543×10^{-2}m	1.560×10^{-2}m
	43.1%	1.09%	-
800N	3.571×10^{-2}m	2.037×10^{-2}m	2.053×10^{-2}m
	73.9%	0.78%	-
1000N	4.464×10^{-2}m	2.294×10^{-2}m	2.311×10^{-2}m
	93.2%	0.74%	-

Results reported in the table above show good agreement with the reference non-linear beam element.

3.2 Modal coefficients calculation

A generic multiple degrees-of-freedom (DoFs), viscously damped geometrically non-linear system can be described by means of eq.3.20,

$$\mathbf{M}\ddot{\mathbf{x}} + \mathbf{C}\dot{\mathbf{x}} + \mathbf{K}\mathbf{x} + \mathbf{\Gamma}(\mathbf{x}) = \mathbf{F} \tag{3.20}$$

where non-linear terms are expressed by the functional Γ as a function of the nodal displacements. It is then possible to use linear modeshapes to express the same equation of motion in terms of modal coordinates, as proposed in eq.3.21,

$$\tilde{\mathbf{M}}\ddot{\mathbf{q}} + \tilde{\mathbf{C}}\dot{\mathbf{q}} + \tilde{\mathbf{K}}\mathbf{q} + \boldsymbol{\gamma}(\mathbf{q}) = \tilde{\mathbf{F}} \tag{3.21}$$

where the matrices used are defined as per eq.3.22.

$$\begin{aligned}
\tilde{\mathbf{M}} &= \mathbf{\Phi}^T \mathbf{M} \mathbf{\Phi} = [1] \\
\tilde{\mathbf{C}} &= \mathbf{\Phi}^T \mathbf{C} \mathbf{\Phi} = [2\zeta_r \omega_r] \\
\tilde{\mathbf{K}} &= \mathbf{\Phi}^T \mathbf{K} \mathbf{\Phi} = \left[\omega_r^2\right] \\
\gamma &= \mathbf{\Phi}^T \mathbf{\Gamma} \\
\tilde{\mathbf{F}} &= \mathbf{\Phi}^T \mathbf{F}
\end{aligned} \tag{3.22}$$

The key point of the Modal Coefficient approach is then introduced by expressing the non-linear term as a polynomial function of modal coordinates, as per eq.3.23

$$\gamma_r(\mathbf{q}) = \sum_{i=1}^{L}\sum_{j=i}^{L} a_{ij}^r q_i q_j + \sum_{i=1}^{L}\sum_{j=i}^{L}\sum_{k=j}^{L} b_{ijk}^r q_i q_j q_k \tag{3.23}$$

The calculation of every modal coefficient is performed through 3 sequential steps:

1. Define coefficients with all equal indices: a_{ii} and b_{iii}
2. Define coefficients with two different indices: a_{ij}, b_{ijj} and b_{jji}
3. Define coefficients with three different indices: b_{ijk}

For each step, one or more *test displacement fields* are applied to the non-linear finite element model implemented in Section 3.1, to obtain the non-linear external force necessary to impose the prescribed displacement field. In this phase, only the non-linear part of the external force is considered, i.e. the part of the non-linear external force associated with the non-linear part of the stiffness, as defined in eq.3.24:

$$\mathbf{\Gamma}(\mathbf{x}) = \mathbf{K}_{nl}(\mathbf{x})\mathbf{x} \tag{3.24}$$

A detailed description of the procedure implemented for each step is provided in the following subsections. Generic indices i, j and k are used, to express the calculation of the generic modal coefficients vectors $\mathbf{a}_{ij}$ and $\mathbf{b}_{ijk}$. Such vectors are formed by the scalar values a_{ij}^r and b_{ijk}^r, for $r = 1 \dots L$. Given the polynomial form used for γ, this mean that each element γ_r of the vector γ, for $r = 1 \dots L$, is defined through the coefficients a_{ij}^r and b_{ijk}^r, with $i = 1 \dots L$, $j = i \dots L$ and $k = j \dots L$.

3.2.1 First Step

In the first step, two test displacement fields are used, obtaining the corresponding non-linear forces (as per eq.3.24), as reported in eq.3.25:

$$\begin{cases} \mathbf{X}_1 = +\mathbf{\Phi}_i q_i \Rightarrow \mathbf{\Gamma}_1 \\ \mathbf{X}_2 = -\mathbf{\Phi}_i q_i \Rightarrow \mathbf{\Gamma}_2 \end{cases} \tag{3.25}$$

The modal projection of the non-linear forces expressed in physical coordinates can be described by means of modal displacements as reported in eq.3.26:

$$\begin{cases} \mathbf{\Phi}^T \mathbf{\Gamma}_1 = \mathbf{a}_{ii} q_i q_i + \mathbf{b}_{iii} q_i q_i q_i \\ \mathbf{\Phi}^T \mathbf{\Gamma}_2 = \mathbf{a}_{ii} q_i q_i - \mathbf{b}_{iii} q_i q_i q_i \end{cases} \tag{3.26}$$

Finally, by using eq.3.27 it is possible to obtain the expression of the modal coefficients, by using sum and subtraction of the modal projections of the non-linear forces.

$$\begin{cases} \mathbf{a}_{ii} = \frac{\mathbf{\Phi}^T \mathbf{\Gamma}_1 + \mathbf{\Phi}^T \mathbf{\Gamma}_2}{2 q_i q_i} \\ \mathbf{b}_{iii} = \frac{\mathbf{\Phi}^T \mathbf{\Gamma}_1 - \mathbf{\Phi}^T \mathbf{\Gamma}_2}{2 q_i q_i q_i} \end{cases} \tag{3.27}$$

3.2.2 Second Step

In the second step, the modal coefficients vectors $\mathbf{a}_{ij}$, $\mathbf{b}_{iij}$ and $\mathbf{b}_{ijj}$ are obtained. It is assumed that all of the $\mathbf{a}_{ii}$ and $\mathbf{b}_{iii}$ modal coefficient vectors are already obtained in the previous step.

Three test displacement fields are used and expressed in eq.3.28, obtaining the corresponding non-linear forces in terms of modal coordinates:

$$\begin{cases} \mathbf{X}_3 = \mathbf{\Phi}_i q_i + \mathbf{\Phi}_j q_j \Rightarrow \mathbf{\Gamma}_3 \\ \mathbf{X}_4 = -\mathbf{\Phi}_i q_i - \mathbf{\Phi}_j q_j \Rightarrow \mathbf{\Gamma}_4 \\ \mathbf{X}_5 = \mathbf{\Phi}_i q_i - \mathbf{\Phi}_j q_j \Rightarrow \mathbf{\Gamma}_5 \end{cases} \tag{3.28}$$

Analogously to what was proposed in eq.3.26, the projections on the modal coordinates of the non-linear forces can be described by means of polynomials in terms of modal displacements, as per eq.3.29:

$$\begin{cases} \mathbf{\Phi}^T \mathbf{\Gamma}_3 = \mathbf{a}_{ii} q_i^2 + \mathbf{b}_{iii} q_i^3 + \mathbf{a}_{jj} q_j^2 + \mathbf{b}_{jjj} q_j^3 + \mathbf{a}_{ij} q_i q_j + \mathbf{b}_{iij} q_i^2 q_j + \mathbf{b}_{ijj} q_i q_j^2 \\ \mathbf{\Phi}^T \mathbf{\Gamma}_4 = \mathbf{a}_{ii} q_i^2 - \mathbf{b}_{iii} q_i^3 + \mathbf{a}_{jj} q_j^2 - \mathbf{b}_{jjj} q_j^3 + \mathbf{a}_{ij} q_i q_j - \mathbf{b}_{iij} q_i^2 q_j - \mathbf{b}_{ijj} q_i q_j^2 \\ \mathbf{\Phi}^T \mathbf{\Gamma}_5 = \mathbf{a}_{ii} q_i^2 + \mathbf{b}_{iii} q_i^3 + \mathbf{a}_{jj} q_j^2 - \mathbf{b}_{jjj} q_j^3 - \mathbf{a}_{ij} q_i q_j - \mathbf{b}_{iij} q_i^2 q_j + \mathbf{b}_{ijj} q_i q_j^2 \end{cases} \tag{3.29}$$

An explicit expression of the modal coefficient vectors sought is proposed in eq.3.30:

$$\begin{cases} \mathbf{a}_{ij} = \frac{\mathbf{\Phi}^T\mathbf{\Gamma}_3+\mathbf{\Phi}^T\mathbf{\Gamma}_4-2\mathbf{a}_{ii}q_i^2-2\mathbf{a}_{jj}q_j^2}{2q_iq_j} \\ \mathbf{b}_{iij} = \frac{2\mathbf{a}_{ii}q_i^2+2\mathbf{a}_{jj}q_j^2-2\mathbf{b}_{jjj}q_j^3-\mathbf{\Phi}^T\mathbf{\Gamma}_4-\mathbf{\Phi}^T\mathbf{\Gamma}_5}{2q_i^2q_j} \\ \mathbf{b}_{ijj} = \frac{\mathbf{\Phi}^T\mathbf{\Gamma}_5-\mathbf{a}_{ii}q_i^2-\mathbf{a}_{jj}q_j^2+\mathbf{a}_{ij}q_iq_j-\mathbf{b}_{iii}q_i^3+\mathbf{b}_{jjj}q_j^3+\mathbf{b}_{iij}q_i^2q_j}{2q_iq_j^2} \end{cases} \tag{3.30}$$

3.2.3 Third Step

The third and last step is necessary to determine the modal coefficient vector $\mathbf{b}_{ijk}$. A single test displacement field is used, reported in eq.3.31 with the corresponding non-linear force.

$$\mathbf{X}_6 = \mathbf{\Phi}_i q_i + \mathbf{\Phi}_j q_j + \mathbf{\Phi}_k q_k \Rightarrow \mathbf{\Gamma}_6 \tag{3.31}$$

The modal projection of the non-linear force obtained is reported in eq.3.32, while the explicit expression of the modal coefficient vector is proposed in eq.3.33.

$$\begin{aligned} \mathbf{\Phi}^T\mathbf{\Gamma}_6 = {} & \mathbf{a}_{ii}q_i^2+\mathbf{a}_{jj}q_j^2+\mathbf{a}_{kk}q_k^2+\mathbf{a}_{ij}q_iq_j+\mathbf{a}_{ik}q_iq_k+\mathbf{a}_{jk}q_jq_k+ \\ & +\mathbf{b}_{iii}q_i^3+\mathbf{b}_{jjj}q_j^3+\mathbf{b}_{kkk}q_k^3+\mathbf{b}_{iij}q_i^2q_j+\mathbf{b}_{iik}q_i^2q_k+\mathbf{b}_{ijj}q_iq_j^2+\mathbf{b}_{ikk}q_iq_k^2+ \\ & +\mathbf{b}_{jjk}q_j^2q_k+\mathbf{b}_{jkk}q_jq_kk^2+\mathbf{b}_{ijk}q_iq_jq_k \end{aligned} \tag{3.32}$$

$$\begin{aligned} \mathbf{b}_{ijk} = {} & \frac{\mathbf{\Phi}^T\mathbf{\Gamma}_6-\mathbf{a}_{ii}q_i^2-\mathbf{a}_{jj}q_j^2-\mathbf{a}_{kk}q_k^2-\mathbf{a}_{ij}q_iq_j-\mathbf{a}_{ik}q_iq_k-\mathbf{a}_{jk}q_jq_k}{q_iq_jq_k}+ \\ & -\frac{\mathbf{b}_{iii}q_i^3+\mathbf{b}_{jjj}q_j^3+\mathbf{b}_{kkk}q_k^3+\mathbf{b}_{iij}q_i^2q_j+\mathbf{b}_{iik}q_i^2q_k}{q_iq_jq_k}+ \\ & -\frac{\mathbf{b}_{ijj}q_iq_j^2+\mathbf{b}_{ikk}q_iq_k^2+\mathbf{b}_{jjk}q_j^2q_k+\mathbf{b}_{jkk}q_jq_k^2}{q_iq_jq_k} \end{aligned} \tag{3.33}$$

3.3 Applications

Once the non-linear modal coefficients are obtained, it is possible to formulate the non-linear static or dynamic problem in terms of modal coordinates, as per eq.3.21 (eventually considering only the static part). In order to effectively reduce the size of the problem, only a subset of the linear modes of the system should be considered,

so that $L << n$. Moreover, as it is highlighted in the following, the choice of the modes to be considered is a key point in the reduction procedure.

Two applications of this method are proposed: a static analysis, in Subsection 3.3.1, considering the same benchmarks used for the development of the non-linear beam element, and a dynamic comparison, in Subsection 3.3.2, with experimental data.

3.3.1 Static

The same two beams introduced as benchmarks in the developing of the non-linear beam element are used for the analysis of the performance of the Modal Coefficients method in its static application. Beam A is considered first, with two static forces of amplitude $F = 1$N, in Figure(3.8) and $F = 3$N, in Figure(3.9).

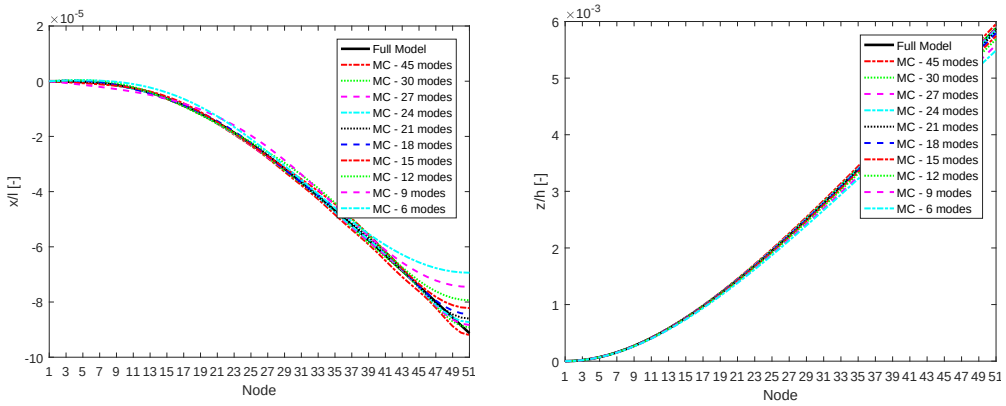

(a) Axial displacement (x). (b) Bending displacement (z).

Fig. 3.8 Comparison between full (solid black) and reduced models, Beam A, static displacement, $F_z = 1$N.

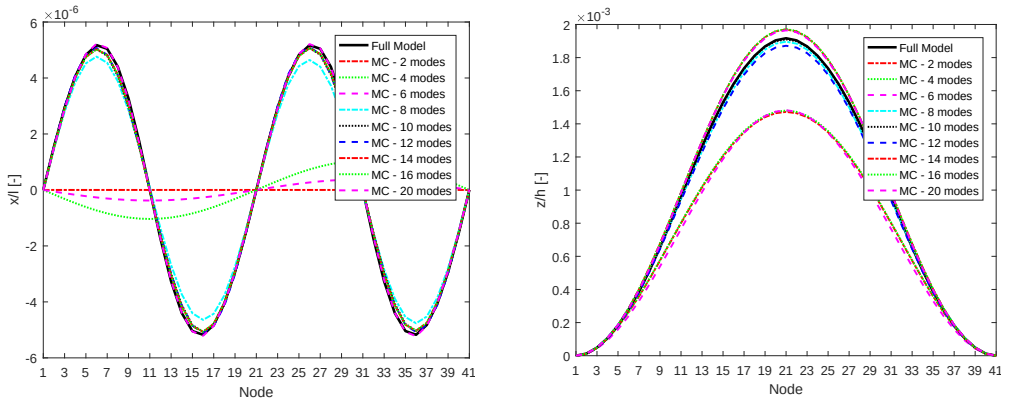

(a) Axial displacement (x). (b) Bending displacement (z).

Fig. 3.9 Comparison between full (solid black) and reduced models, Beam A, static displacement, $F_z = 3$N.

The number of modes used is not the only variable in the model reduction process. In fact, selecting the modes is of fundamental importance as this corresponds to an appropriate subset of the modeshapes. A simple modal truncation, considering therefore only the modes at lower frequency, would in fact significantly reduce the accuracy: axial modes are in fact fundamental in the description of the element deformation, but their frequency is significantly higher than bending modes (both along y and z). Figure(3.10) shows the comparison between two reduced model, both with 20 modes.

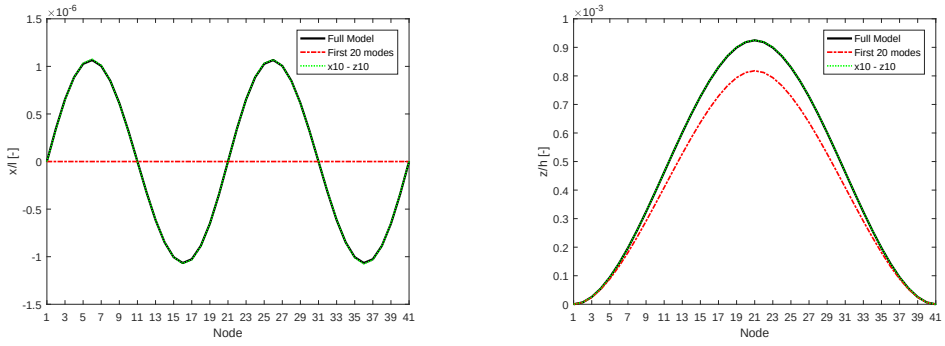

(a) Axial displacement (x). (b) Bending displacement (z).

Fig. 3.10 Comparison between full (solid black), reduced model with first 20 modes (dashed red) and reduced model with 10 bending and 10 axial modes (dot-dash green), Beam A, static displacement, $F_z = 3$N.

Using the first 20 modes (red line), according to the natural frequencies only, the non-linear axial behaviour of the beam is completely lost, while it is well approximated using 10 axial modes (green line). Moreover, also the bending behaviour is better approximated by using only 10 bending modes, combined with 10 axial modes.

Figure(3.11) shows the overall percentage error with respect to the full model, calculated according to eq.3.34, for two different levels of excitation ($F_z = 1$N in Figure(3.11a) and $F_z = 3$N in Figure(3.11b)).

$$\varepsilon = 100\frac{\sum_i |x_{red}(i) - x_{full}(i)|}{\sum_i |x_{full}(i)|} \tag{3.34}$$

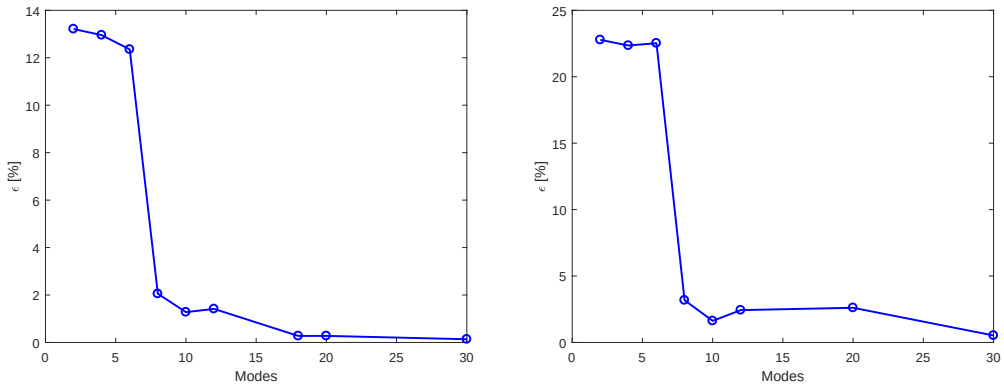

(a) $F_z = 1$N. (b) $F_z = 3$N.

Fig. 3.11 Percentage error with respect to full model, Beam A, static displacement.

One can note that, the larger the excitation the more non-linear the system is. Additionally, the percentage error increases with the external excitation, for a given number of modes used. It is also highlighted that the error is significantly reduced ($\varepsilon < 1.5\%$ for $F_z = 1$N) by using 10 modes or more (i.e. 5 bending and 5 axial modes).

3.3.2 Dynamic

The evaluation of the dynamic performance of the implemented method is evaluated through the comparison with the experimental data in [1]. A rod with annular cross section and the physical and geometrical characteristics reported in Table 3.3 is considered.

Table 3.3 Zirconium rod characteristics.

Name	Value
Length	$L = 0.900\text{m}$
Diameter (external)	$d_e = 9.49 \times 10^{-3}\text{m}$
Thickness	$t = 0.57 \times 10^{-3}\text{m}$
Density	$\rho = 6450 \frac{\text{kg}}{\text{m}^3}$
Young Modulus	$E = 95 \times 10^9\text{Pa}$
Poisson's Ratio	$\nu = 0.37$

The first four experimental natural frequencies of this configuration of the rod were measured in [1] and hereafter reported (Table 3.4).

Table 3.4 Zirconium rod experimental natural frequencies ([1]).

Mode	Frequency [Hz]
1	51.94
2	140.33
3	275.27
4	475.14

An optimization is performed to match the first four experimental natural frequencies with the numerical model of the rod, obtained with the formulation in Section 3.1. Results are reported in Table 3.5, obtained with $E = 92.1 \times 10^9\text{Pa}$ and $\rho = 6843 \frac{\text{kg}}{\text{m}^3}$.

Table 3.5 Zirconium rod experimental natural frequencies ([1]).

Mode	Frequency (Exp) [Hz]	Frequency (Num) [Hz]
1	51.94	50.94
2	140.33	140.41
3	275.27	275.27
4	475.14	455.03

In order to suppress the companion mode, shifting it outside the frequency of interest, in [1] a lumped mass glued at the centre of the rod is used, reporting a new first natural frequency $f_1 = 33.815$Hz. A lumped mass is considered in the numerical model as well, tuning its value in order to match the new first natural frequency. The mass value identified is $m = 51.61 \times 10^{-3} kg$.

Experimental conditions are reproduced, introducing a harmonic forcing function located at $f = 50 \times 10^{-3}$m and the displacement along the same direction at the centre ($x = 0.450$m) is measured. The frequency response function (FRF) was experimentally obtained through a stepped-sine technique, reproduced here numerically. The MATLAB routine *ode45*, which implements an explicit Runge-Kutta (4,5) scheme, is used. The same force amplitude levels used in [1] are considered here, while a simpler viscous proportional damping is used, with respect to the non-linear one proposed in [1]. An additional simplification is used, assuming $\boldsymbol{C} = \beta \boldsymbol{K}$, with a damping proportional to the stiffness matrix only and assuming an initial value for β based on the linear part of the damping identified in [1] and reported in Table 3.6.

Table 3.6 Zirconium rod identified linear damping ([1]).

Force Amplitude [N]	Damping ratio ζ_{exp} [-]
0.05	4.3709×10^{-4}
0.10	4.4151×10^{-4}
0.15	5.7694×10^{-4}
0.20	6.0298×10^{-4}
0.25	6.6411×10^{-4}
0.30	7.1960×10^{-4}
0.35	8.0128×10^{-4}

The value of $\beta = \frac{2\zeta_{exp}}{\omega_{exp,1}}$ is in the numerical simulations here proposed adjusted to match the peak amplitude of the experimental FRFs in [1].

Firstly, a 1-DoF linear reduced model (no non-linear cubic force is considered) is used to tune the damping and match the peak amplitude. Despite the use of the data in Table 3.6, it is necessary an additional correction. Figure 3.12 shows the results obtained, comparing experimental (cross marks) with numerical (circles).

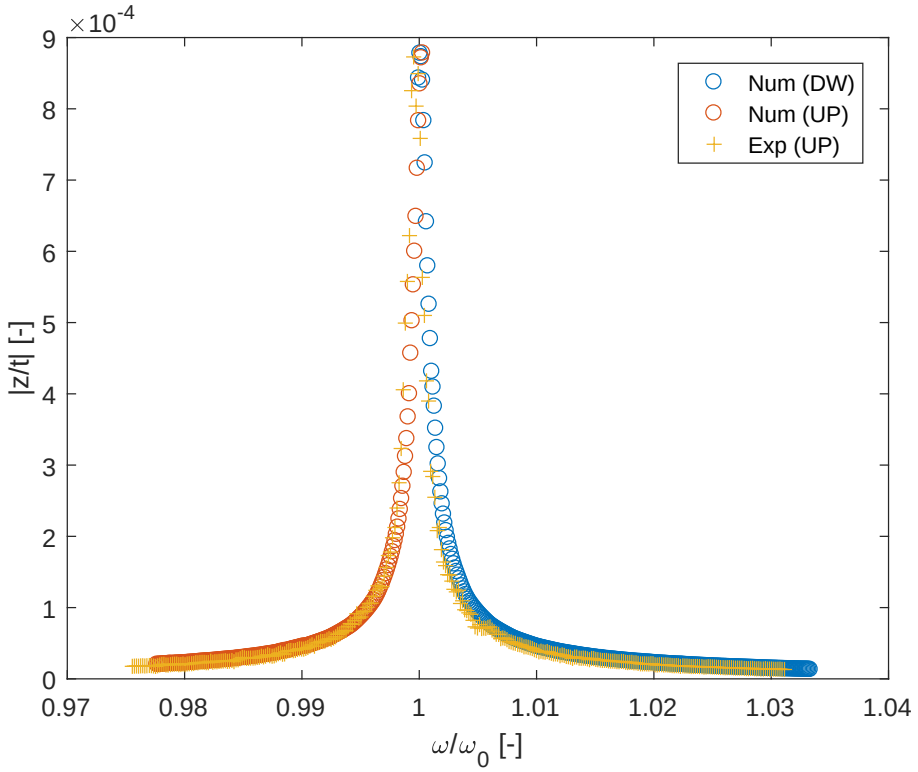

Fig. 3.12 Experimental (cross marks) and numerical (circles) comparison, linear case $F = 0.05$N, ζ_{opt}.

Such a simple model (1-DoF, linear) accurately reproduces the experimental linear response, with damping ratios as per Table 3.7.

Table 3.7 Zirconium rod numerical/optimized linear damping.

Force Amplitude [N]	Damping ratio ζ_{exp} [-]
0.05	4.9309×10^4
0.10	4.6967×10^4
0.15	6.2138×10^4
0.20	6.6011×10^4
0.25	7.3822×10^4
0.30	8.0578×10^4
0.35	9.0117×10^4

Now introducing the non-linear terms, but retaining the 1-DoF reduced model, Figure 3.13 shows the results for the same force amplitude ($F = 0.05$N, i.e. the linear experimental case). This simplest non-linear model is presented in the following and is named "$x0$ $z1$". It includes only one bending mode (z axis) and no axial ones (x axis). A similar notation is used for all other numerical models.

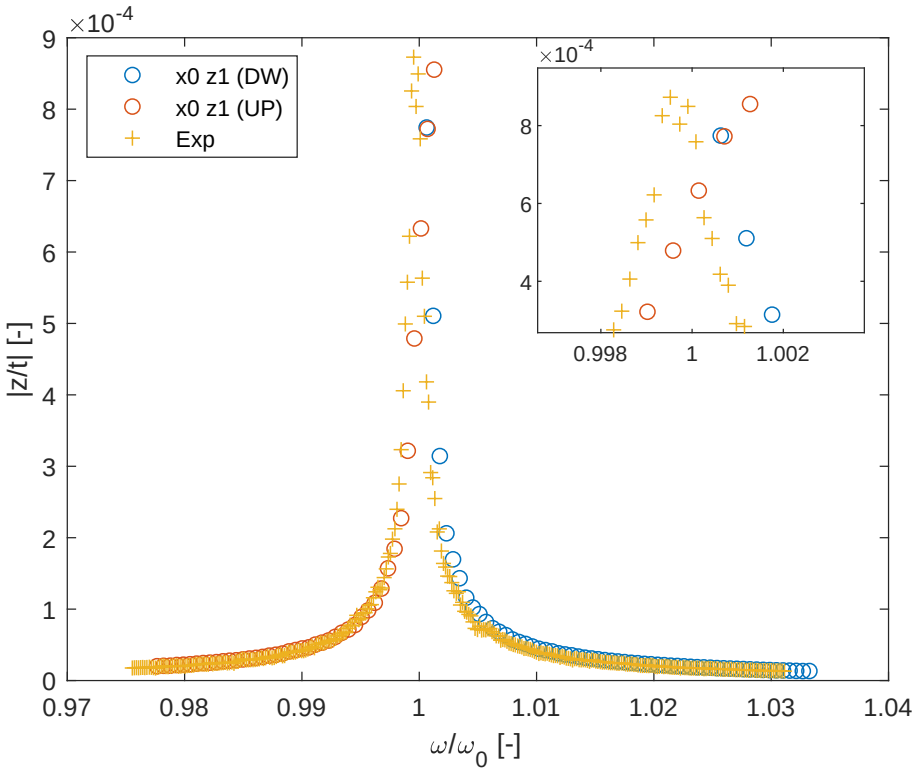

Fig. 3.13 Experimental (cross marks) and $x0$ $z1$ model (circles) comparison $F = 0.05$N, ζ_{opt}.

The non-linear terms introduce stronger non-linearity as compared to the experimental one, for the smallest force amplitude experimentally tested. Figure 3.14 confirms this trend for an increased amplitude ($F = 0.10$N), showing that it is necessary to add more modes to more precisely match the experimental data.

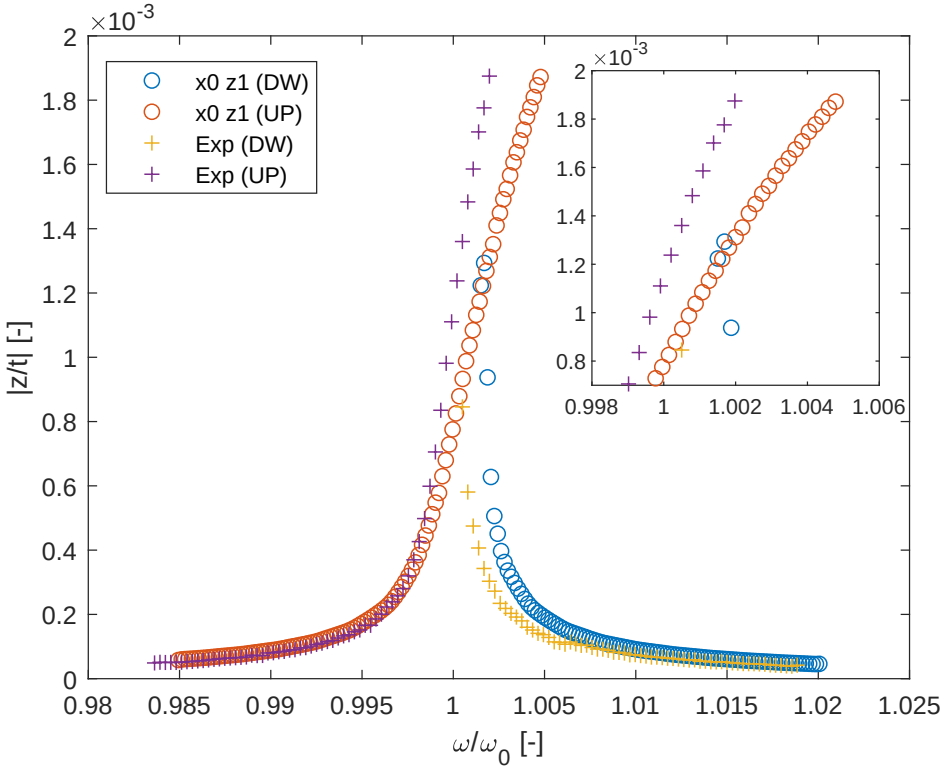

Fig. 3.14 Experimental (cross marks) and $x0\ z1$ model (circles) comparison $F = 0.10$N, ζ_{opt}.

In order to improve the accuracy of the reduced model, axial modes can be added. The 4^{th} axial mode, showed in Figure 3.15, was found to be the most effective in reducing the non-linearity of the numerical model and better fitting the experimental data.

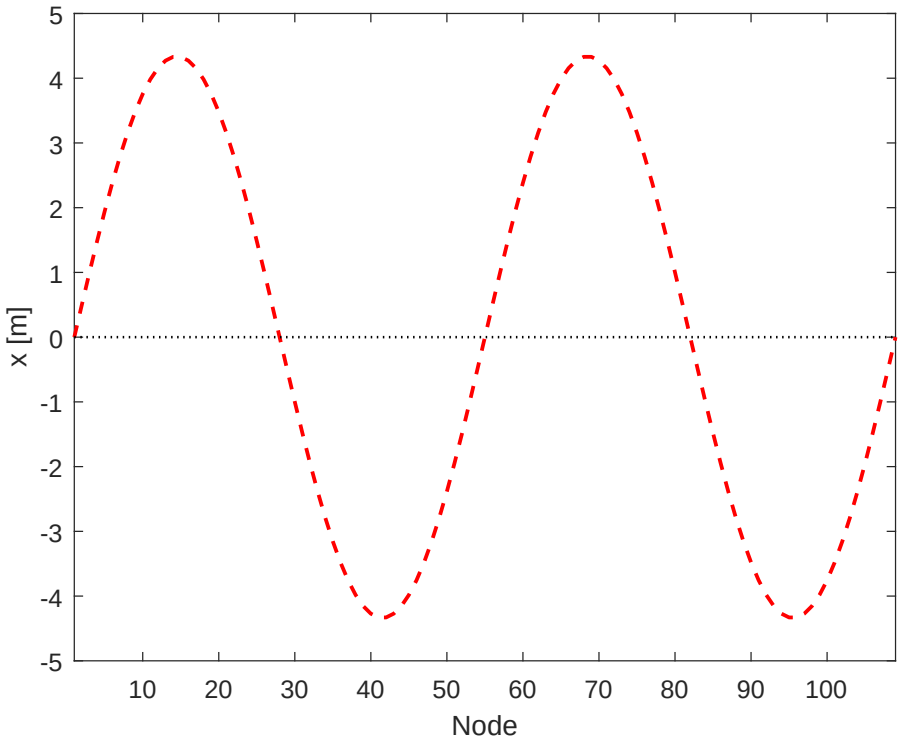

Fig. 3.15 Axial displacements, 4^{th} axial modeshape.

Figure 3.16 shows a comparison between the experimental data and the two reduced models introduced above. The last one, with the 4^{th} axial mode introduced, is named $x1(4)\ z1$, to highlight the number of axial modes used (1) and to specify which one(s) (4). A force amplitude $F = 0.10$N is used in this example.

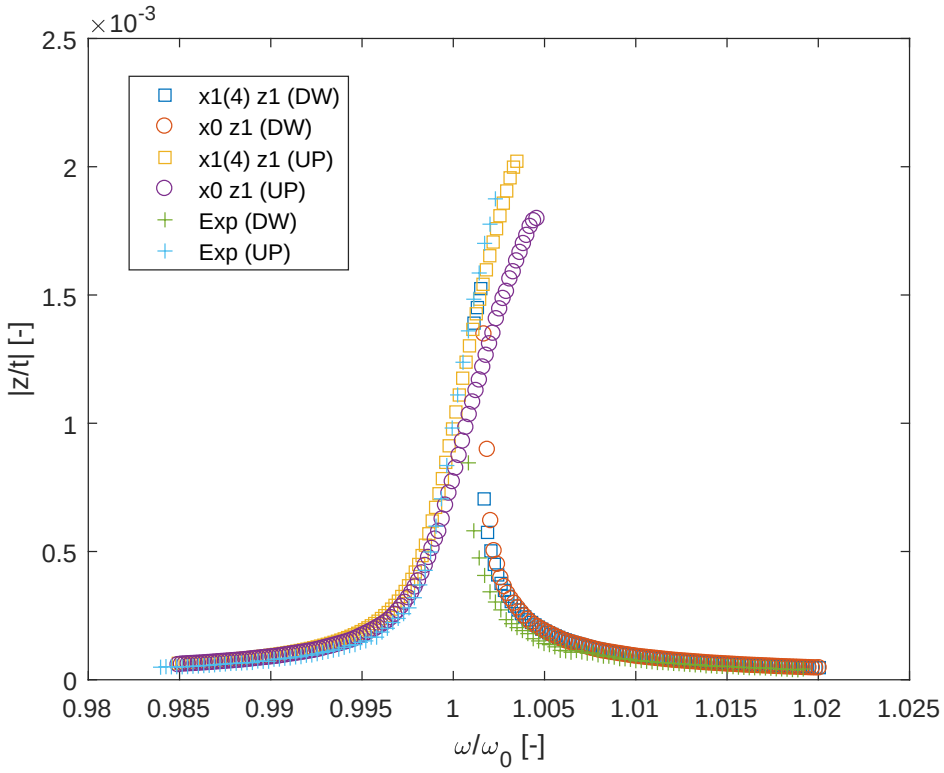

Fig. 3.16 Experimental (cross marks), $x0\ z1$ (circles) and $x1(4)\ z1$ (squares) comparison, $F = 0.10$N, ζ_{opt}.

A substantial improvement in replicating the experimental response is obtained with the addition of this second mode. By increasing the force amplitude, Figure 3.17 and Figure 3.18 summarize the results obtained.

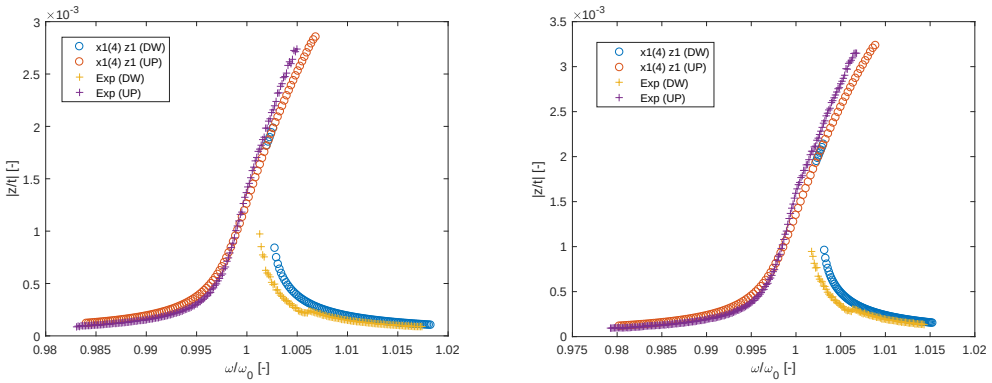

(a) $F = 0.20$N (b) $F = 0.25$N

Fig. 3.17 Experimental (cross marks) and $x1(4)\ z1$ model (circles) comparison.

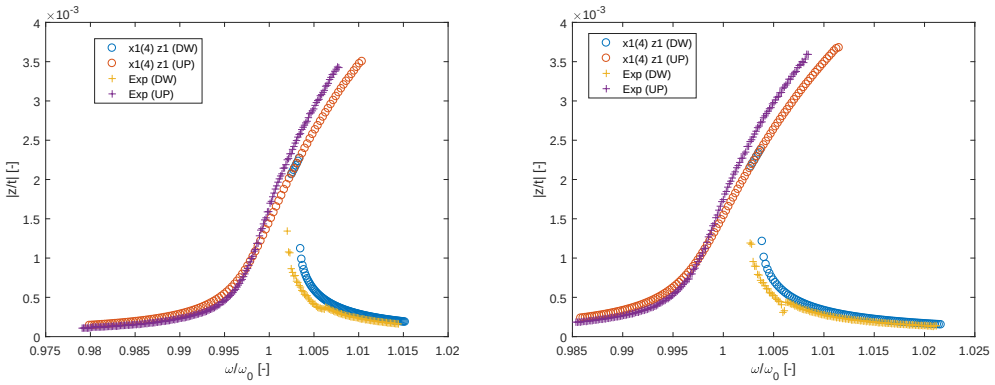

(a) $F = 0.30$N (b) $F = 0.35$N

Fig. 3.18 Experimental (cross marks) and $x1(4)$ $z1$ model (circles) comparison.

It can be observed that the reduced model still overestimates the non-linearity. It is then considered the addiction of other axial modes. A new reduced model, containing all the first 8 axial modes was introduced and named $x8$ $z1$; results of this last model, compared with experimental data and the $x1(4)$ $z1$ model, are showed in Figure 3.19.

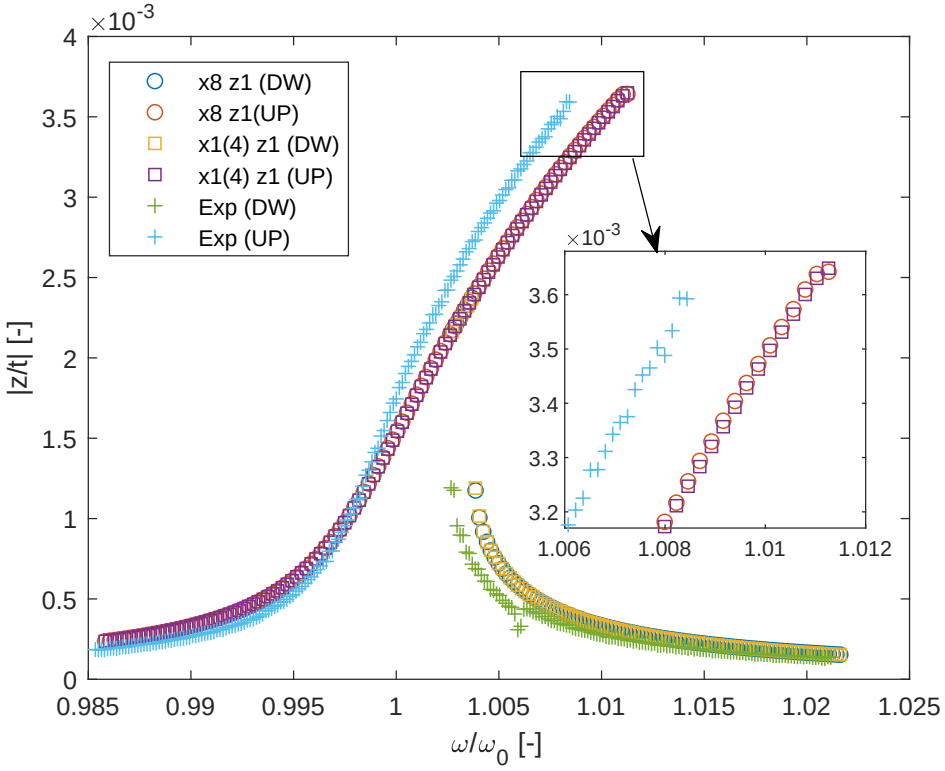

Fig. 3.19 Experimental (cross marks), $x8$ $z1$ (circles) and $x1(4)$ $z1$ (squares) comparison, $F = 0.35$N.

No significant improvements are observed including the first 8 axial modes. The addition of other bending modes (up the the 3^{rd}) and of other axial modes (up to the 20^{th}) shows similar results. It is then concluded that the full non-linear model, obtained through the beam element introduced in Section 3.1, overestimates the system's non-linearity. Explanations of this behaviour can be found in geometrical imperfections, residual axial forces or imperfect boundary conditions, present in the experiment but not modelled numerically. Both conditions are known for inducing a softening behaviour, which would partially compensate the hardening non-linearity, leading to a less non-linear system.

Considering a geometry defect, with the beam curved according to the first mode, with a maximum displacement of $x_{def} = 1.8 \times 10^{-3}$m, the results in Figure 3.20 show an almost perfect agreement with experimental data.

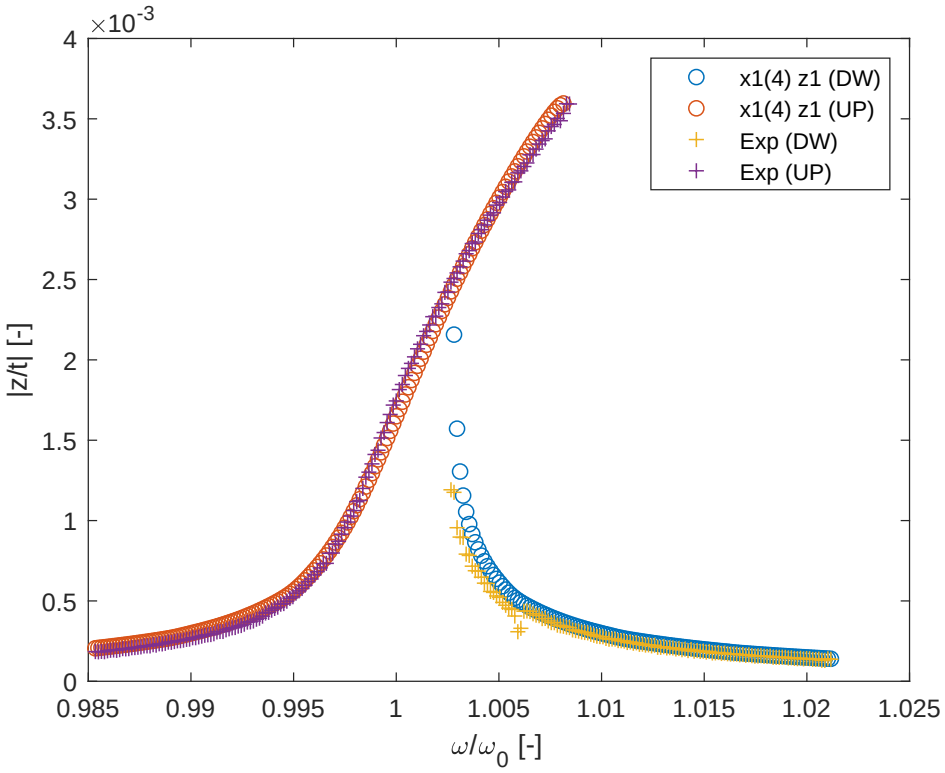

Fig. 3.20 Experimental (cross marks), $x1(4)$ $z1$ (circles) comparison, $F = 0.35$N and $x_{def} = 1.8 \times 10^{-3}$m.

Chapter 4

Multi Level Modal Analysis

Linear modal analysis is a consolidated tool, used in several engineering fields and as reported in Section 2, it can be effectively used for model order reduction purposes. It serves in fact as an excellent base for linear systems and it can be used, with approximation, in non-linear applications. The method proposed here is called Multi-Phi and is for dynamical non-linear systems in which the non-linearity considered can be modelled as a piecewise non-linearity, function of the configuration space. Beside this main characteristic, the Multi-Phi method targets non-linear systems with the following additional characteristics:

- interest of the analysis behind the steady state response, but focused on the transient
- damping of the system approximated with proportional damping
- linear modeshapes obtainable at a low computational cost

In this Chapter 4 the representation of a generic non-linear dynamical system by means of a set of linear systems (here and in the following called subsystems), projected into the modal coordinate space is considered. Here all available modes of each subsystem are used. Also, details about non-null boundary conditions, time integration and the switch between subsystems is described and discussed.
In Chapter 5, the procedure of reducing the model order by selecting only a subset of the available modes, for each subsystem is discussed.
Finally, in Chapter 6 the method is applied to several numerical examples.

4.1 Multi-Phi method idea

The idea of representing or approximating non-linearities as piecewise is not a novelty and many references have been discussed in Chapter 2. In particular, the TPWL method ([28, 91–99]) considers the non-linear equations of motion as per eq.2.31. An adaptation to mechanical systems can be obtained starting from the generic non-linear system expressed in eq.4.1:

$$\mathbf{M}(\mathbf{x},\dot{\mathbf{x}})\,\ddot{\mathbf{x}} + \mathbf{C}(\mathbf{x},\dot{\mathbf{x}})\,\dot{\mathbf{x}} + \mathbf{K}(\mathbf{x},\dot{\mathbf{x}})\,\mathbf{x} = \mathbf{f} \tag{4.1}$$

A generic non-linear system is described here by state-dependent matrices, which can be linearised at specific points in the space-state. By using lv linearisation points, eq.4.1 can be approximated by eq.4.2,

$$\sum_{l=1}^{lv} w_l(\mathbf{x},\dot{\mathbf{x}})\,(\mathbf{M}_l\ddot{\mathbf{x}} + \mathbf{C}_l\dot{\mathbf{x}} + \mathbf{K}_l\mathbf{x}) = \mathbf{f} \tag{4.2}$$

with w_l as weights described as functionals depending on the state-space and dictating the participation of each linear subsystem in the equation of motion. The weights are defined based on the distance of each linearisation point with respect to the current state of the system $(\boldsymbol{x},\ddot{\boldsymbol{x}})$. In eq.4.2 l describes the generic linear subsystem and lv is the number of linearisation points.

A straightforward application of the TPWL approximation method would imply the use of a single projection matrix for all the linear subsystems, as proposed in eq.2.25. The choice is, in the Multi-Phi method, to use a specific projection matrix, i.e. the modal matrix, for each subsystem. This guarantees the diagonalization of all the matrices involved (assuming proportional damping), as proposed in eq.4.3,

$$\sum_{l=1}^{lv} w_l(\boldsymbol{x},\dot{\boldsymbol{x}})\left(\tilde{\boldsymbol{M}}_l\ddot{\boldsymbol{\eta}}_l + \tilde{\boldsymbol{C}}_l\dot{\boldsymbol{\eta}}_l + \tilde{\boldsymbol{K}}_l\boldsymbol{\eta}_l\right) = \sum_{l=1}^{lv} w_l(\boldsymbol{x},\dot{\boldsymbol{x}})\,\boldsymbol{\Phi}_l^T\boldsymbol{f} \tag{4.3}$$

in which:

- $\boldsymbol{\eta}_l = \boldsymbol{\Phi}_l^{-1}\boldsymbol{x}$
- $\tilde{\boldsymbol{M}}_l = \boldsymbol{\Phi}_l^T\boldsymbol{M}\boldsymbol{\Phi}_l = \boldsymbol{I}$
- $\tilde{\boldsymbol{C}}_l = \boldsymbol{\Phi}_l^T\boldsymbol{C}\boldsymbol{\Phi}_l = diag(2\zeta_l\omega_l)$

- $\tilde{\boldsymbol{K}}_l = \boldsymbol{\Phi}_l^T \boldsymbol{K} \boldsymbol{\Phi}_l = diag\left(\omega_l^2\right)$

At this point an additional restriction is used, assuming that the weighting functionals are dependent on the configuration space only, so that $w_l = w_l(\boldsymbol{x})$. Even though it is possible to relax this assumption, having weighting functionals dependent on the configuration space only allows for extreme simplification of the formulation of the reduced model. In fact, keeping the weight as a functional of both displacements and velocities would require a modelling procedure similar to the one used by TPWL approximation method.

One should note that a major difference between the proposed Multi-Phi method and the TPWL approximation method can be highlighted. Referring to eq.4.3: in the Multi-Phi method the reduction matrix $\boldsymbol{\Phi}_l$ is specific for each linearisation point, whereas in the TPWL approximation method it was unique for the whole non-linear system. While it is possible to define a common reduction base, only the use of a specific base for each linear subsystem allows full decoupling of the equations of motion. The main point of Multi-Phi is in fact to deal with linear equations of motion of linear subsystems, using the weighting functionals w_l to reproduce the non-linear behaviour.

Based on the above introduced additional assumption, eq.4.3 can be simplified, leading to eq.4.4:

$$\sum_{l=1}^{lv} w_l(\boldsymbol{x}) \left(\tilde{\boldsymbol{M}}_l \ddot{\boldsymbol{\eta}}_l + \tilde{\boldsymbol{C}}_l \dot{\boldsymbol{\eta}}_l + \tilde{\boldsymbol{K}}_l \boldsymbol{\eta}_l\right) = \sum_{l=1}^{lv} w_l(\boldsymbol{x}) \boldsymbol{\Phi}_l^T \boldsymbol{f} \tag{4.4}$$

A straightforward application of eq.4.4 leads to a reduced model composed of a number of linear subsystems equal to the number of linearisation points, all to be solved contemporaneously. This approach would require a reduced number of linearisation point or extremely reduced linear subsystems, to be fully effective, in spite of the fact that the decoupling of the equations of motion and the use of linear equations would be in any case beneficial.

In order to improve the effectiveness of this method, it can be assumed that only a limited number of configurations (and therefore of linear subsystems) contributes to the system's dynamics. This means that only a few weighting functionals w_l are non-null, so that it is not necessary to simulate all of the lv subsystems. In the following, it is therefore assumed that all the weighting functionals w_l depend on a

small set of parameters, in the following named α_i, with $i = 1, \ldots, p$, with $p << lv$. The number of linear subsystems to be simultaneously simulated is in this way reduced to 2^p.

In the simplest example of $p = 1$, this assumption leads to eq.4.5, in which only two subsystems, named a and b are considered for a single parameter α.

$$w_a(\alpha)\left(\tilde{\boldsymbol{M}}_a\ddot{\boldsymbol{\eta}}_a + \tilde{\boldsymbol{C}}_a\dot{\boldsymbol{\eta}}_a + \tilde{\boldsymbol{K}}_a\boldsymbol{\eta}_a - \boldsymbol{\Phi}_a^T\boldsymbol{f}\right) + w_b(\alpha)\left(\tilde{\boldsymbol{M}}_b\ddot{\boldsymbol{\eta}}_b + \tilde{\boldsymbol{C}}_b\dot{\boldsymbol{\eta}}_b + \tilde{\boldsymbol{K}}_b\boldsymbol{\eta}_b - \boldsymbol{\Phi}_b^T\boldsymbol{f}\right) = 0 \quad (4.5)$$

It should be noted that $w_a + w_b = 1$.

4.2 Asymptotic configuration

In the proposed method all of the linear modeshapes of the subsystems analysed are calculated by imposing homogeneous Dirichlet boundary conditions at all of the boundary conditions nodes. This is analogous to the Craig-Bampton reduction scheme ([61]), so that interface modes need to be introduced. In the proposed method this concept is implemented in a way that allows for the calculation of a single displacement vector, called the *asymptotic configuration*. This vector represents the superposition of all interface modes for a specific set of boundary conditions and is therefore a specific configuration, which can be defined as the steady state response of the system, considering only imposed displacements (non-homogeneous Dirichlet boundary conditions) and neglecting all external forces. The steady state response of the system due to external force is in fact described by means of the subsystems modeshapes. Any other deviation from the undeformed configuration needs to be described differently, however.

Considering only the generic l linear subsystem, its configuration is described by eq.4.6

$$\mathbf{x} = \boldsymbol{\Phi}_l\eta_l + \mathbf{x}_{\infty,l} \quad (4.6)$$

in which the term $\mathbf{x}_{\infty,l}$ represents the *asymptotic configuration* of the subsystem l.

It is possible that $\mathbf{x}_{\infty,l}$ is undetermined during the definition of the reduced model, but only during the simulation itself. An example of this problem is represented when a node is locked once it reaches zero velocity: the position of the node cannot be determined before the simulation itself, so that an on-line evaluation of the asymptotic configuration is necessary.

To determine $\mathbf{x}_{\infty,l}$, the Guyan reduction ([59]) is applied. Firstly, all of the DoFs are split into known ($\mathbf{x}_k$) and unknown ($\mathbf{x}_u$), the first being the non-homogeneous Dirichlet boundary conditions and the latter being the remaining DoFs. Then a reordering matrix $\mathbf{T}_R$ is defined, such that eq.4.7 is satisfied.

$$\boldsymbol{x} = \boldsymbol{T}_R \begin{Bmatrix} \boldsymbol{x}_k \\ \boldsymbol{x}_u \end{Bmatrix} \tag{4.7}$$

The asymptotic configuration $\mathbf{x}_{\infty,l}$ is then defined by means of eq.4.8:

$$\mathbf{x}_{\infty,l} = \boldsymbol{T}_R^{-1} \begin{bmatrix} -(\boldsymbol{K}_{uu,l})^{-1}\boldsymbol{K}_{uk,l} \\ \boldsymbol{I} \end{bmatrix} \mathbf{x}_k \tag{4.8}$$

4.3 Time integration

The main goal of this thesis is to develop a reduction procedure for non-linear dynamic mechanical systems, having as final purpose their use in numerical time integration schemes. This last phase plays a major role in the use of model order reduction techniques, so that significant importance is given to the formulation of reduced models having interesting characteristics from a time integration point of view. The time integration scheme implemented is not, however, the main focus on this thesis, so that a standard `ode23tb` in a MATLAB environment is used. This solution has several advantages, providing a common tool for the evaluation of the reduction scheme performances and allowing the use of a piecewise integration, using the built-in `ODE event location`. It also permits one to identify and to address the development of specific time integration tools. Drawbacks of this choice are the relatively limited size of the models reasonably handled, in particular in providing a direct integration reference, and the impossibility of providing a comparison with other commercial non-linear solvers.

The `ode23tb` solver is an implementation of an implicit Runge-Kutta formula with a trapezoidal rule step as its first stage and a backward differentiation formula of order two as its second stage. This algorithm is also known as `TR-BDF2` and it was developed by [102, 103]. This algorithm was chosen for its stability and versatility.

Some assumptions are made, based on the kind of time integration considered. In particular, the class of problem targeted is the one in which:

1. the external actions are potentially non-periodic;
2. the interest lies in the transient solution as well as in the steady state.

The implementation of eq.4.5 suggests an event-driven time integration problem, with (for the generic case) two linear subsystems for each parameter α_i considered. This choice, in fact, greatly reduces the number of subsystems to be integrated contemporaneously but it requires the switching of subsystems (as described in Subsection 4.3.3) every time that α_i falls outside the validity range of the subsystems a_i and b_i. Each subsystem is in fact characterized by a reference value α_i^a or α_i^b, so that $\alpha_i^a \leq \alpha_i \leq \alpha_i^b$. It is assumed that a_i refers to the lower bound and b_i represents the upper bound, for the parameter i.

4.3.1 Continuous or Discrete Level

A specific subset of non-linear systems can be accurately modelled by means of linear piecewise models without losing accuracy. An example of this category is represented by contact problems, which can be modelled by means of two linear models: one with no contact and one with contact, considered as additional boundary condition. In this thesis this class of systems and this modelling approach are also considered, since it is possible to simplify the formulation of the non-linear model reported in eq.4.5. As reported by eq.4.9, in fact, only one linear subsystem at the time can be used:

$$\tilde{\boldsymbol{M}}_l \ddot{\boldsymbol{\eta}}_l + \tilde{\boldsymbol{C}}_l \dot{\boldsymbol{\eta}}_l + \tilde{\boldsymbol{K}}_l \boldsymbol{\eta}_l = \boldsymbol{\Phi}_l^T \boldsymbol{f} \tag{4.9}$$

In the following, this class of models will be referred at as *Discrete Levels* or *DL*, while the class of models governed by eq.4.5 will be called *Continuous Levels* or *CL*. The time integration scheme used for the simulation of Discrete Levels models is

simplified since it is not necessary to obtain the simulation results through a weighted mix of several models, as it is necessary for Continuous Levels models.

For CL models, at each time step all the linear subsystems involved need to be mixed, in order to obtain the instantaneous configuration of the non-linear model. This is obtained by defining the weighting functionals w_i, which are themselves functions of the instantaneous configuration, requiring an iterative procedure to be performed. Details regarding the algorithm implemented are reported in Subsection 4.3.2.

Even though every non-linear system can be defined via a DL or a CL approach, it is useless to use a Continuous Level approach for contact-like systems. Using a Discrete Level approach for a system characterized by a non-linear spring would lead to significant approximation errors.

An explanatory single-parameter non-linear system ($p = 1$) is now considered, with a non-linear characteristic showed in Figure 4.1.

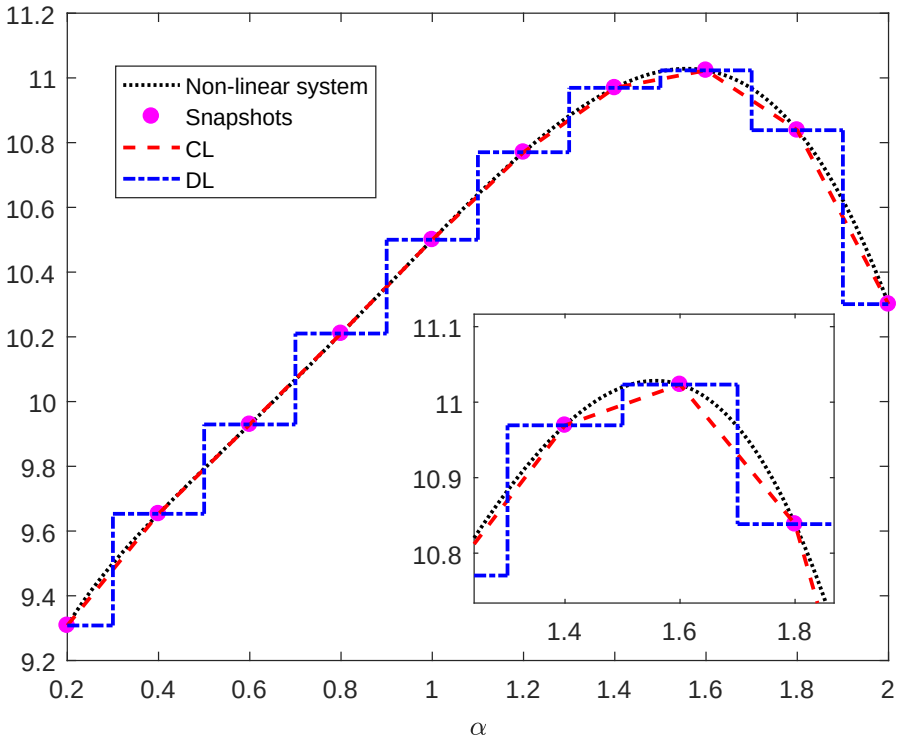

Fig. 4.1 Non-linear characteristic (dotted black), snapshots (magenta dots), CL approximation (dashed red) and DL approximation (dash-dot blue).

The original non-linear characteristic (dotted black) is approximated by using a limited number of linearisation points, named snapshots (magenta dots), which define the linear subsystems. Depending on the modelling strategy used, the system's characteristics reproduced for all the continuous values of α can be extremely close to the original one (by using CL, dashed red line) or significantly different (considering DL, dash-dot blue).

Despite the significant advantage in terms of approximation error, a major drawback of the CL approach is that the number of linear subsystems contemporary simulated, considering p governing parameters, is equal to 2^p. Taking into account r modes for all the linear subsystems and using a first order integrator as `ode23tb`, the size of the reduced problem is $2r2^p$. It has to be remember that in order to effectively reduce the original model it is necessary that $n >> 2r2^p$.

The use of the DL approach allows a significant reduction in the number of linear systems to be used. In Figure 4.2 an explanatory non-linear characteristic is shown, considering a 2-parameters system ($p = 2$). This kind of characteristic can be representative of a non-linear system with two contact points.

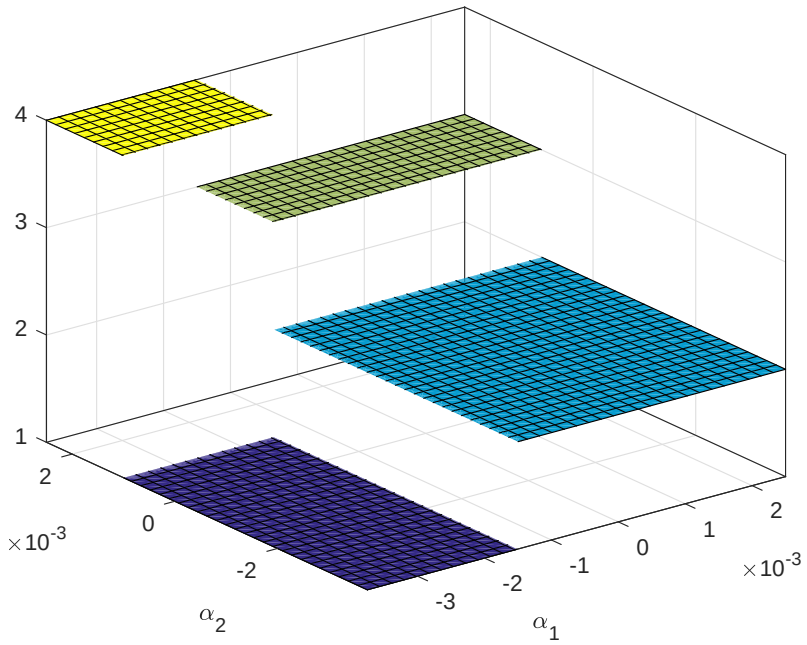

Fig. 4.2 Non-linear characteristic, piecewise explanatory non-linear system.

One can appreciate that once the whole parameter space is mapped, a single reduced system can be used for each couple of parameters $\boldsymbol{\alpha} = [\alpha_1 \alpha_2]$. The size of the reduced problem is therefore equal to $2r$, considering r modes and a first order differential equations solver.

In conclusion, the choice between CL and DL approach depends on the characteristics of the non-linear system, on the number of parameters used and on the amount of the reduction, which can be defined as $\frac{r}{n}$ and it is further discussed in Section 5.

4.3.2 Weighting functionals calculation

Considering a Continuous Levels modelling approach, it is necessary to calculate the weighting functionals at each time step. A generic iterative scheme is hereafter reported, with the purpose of illustrating how the assumption made to obtain eq.4.5 limits the iterative process in obtaining the values of the parameters α_i.

```
err = 2*tol;
while err > tol
     % Initialization displacements and velocities
     x = zeros(n,1);
     xd = zeros(n,1);
     % For each linear subsystem
     for l = 1 :  2^p
          % Displacements and velocities of the current system
          x = x + wOld(l)*Phi{i}*eta(l,:);
          xd = xd + wOld(l)*Phi{i}*etad(l,:);
     end
     % For each parameter
     for i = 1 :  p
          % Define the real system parameter i
          alpha(i) = alphaFun{i}(x,xd);
     end
     % For each linear subsystem
     for l = 1 :  2^p
          % Define the current weight
          w(l) = wFun{l}(alpha);
     end
```

```
    % Determine the error wrt the previous iteration
    err = sum(abs(w-wOld));
    % Update the weights
    wOld = w;
end
```

In the algorithm depicted above two functions need to be defined:

1. `alphaFun` extracts the parameters from the system's state
2. `wFun` calculates the weighting functional of each linear subsystem

The first is defined as part of the model and allows one to extract the p parameters from the n DoFs, while the second has a more generic formulation and it is described in the following.

Is important to note that the only purpose of the algorithm reported above is to illustrate the iterative procedure to determine the weighting functionals. The implementation through a MATLAB code of this procedure takes into account that it is not necessary to calculate the whole state space of the system, but it is possible to obtain an estimate of each parameter α_i from every l linear subsystem. All of the 2^p estimates can be *mixed*, through the weighting functionals, to provide a single estimate for each parameter then used in the iterative process.

The definition of the weighting functionals is based on the p parameters of the model and it follows two main concepts:

1. Higher weights to more representative linear subsystems
2. Unitary overall weight

The first point implements the idea that the closer the *real* state space point is to a linearised subsystem, the more representative the linear subsystem. At each time step the set of parameters identified with $\boldsymbol{\alpha}$ represents what is here called a *real non-linear system*, while each linearised subsystem l has a reference and fixed set of parameters, identified by $\boldsymbol{\alpha}_l$. The second constraint is necessary to retain the physical meaning of the non-linear system represented.

Two assumptions are made in order to introduce the weighting calculation procedure:

- Parameters α_i in the configuration space only
- $p = 3$, so that $2^p = 8$ linear subsystems are used

The calculation of the weighting functionals is based on the first stage of the *Multi-linear interpolation* procedure, which consists of defining 8 (for $p = 2$) volumes, as shown in Figure 4.3, representing the distance from the real non-linear system from the linear subsystems.

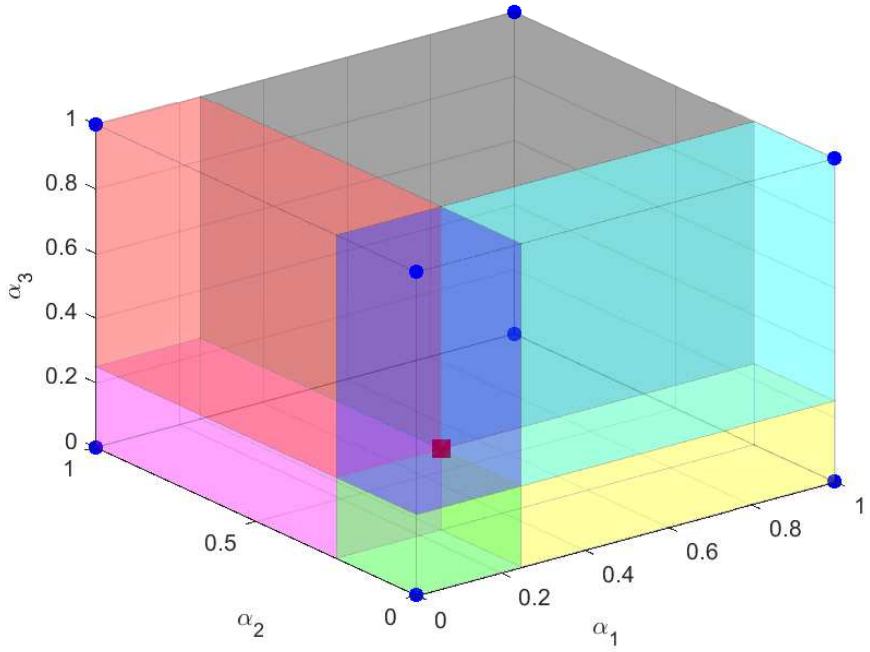

Fig. 4.3 Unitary cube in configuration space. Linear subsystems (blue circles) and real non-linear system (red square).

The weighting functionals for each linear subsystem are inversely proportional to the overall volume. From an implementation point of view, it is useful to define a *distance* (here named $\boldsymbol{w}_d$) as per eq.4.10

$$\boldsymbol{w}_d(l) = \frac{V(l)}{V_{all}} \tag{4.10}$$

where $V(l)$ represent the volume between the real non-linear system and the l linear subsystem and V_{all} the volume defined by the 8 linear subsystems. From a

mathematical point of view, $V(l)$ is defined through eq.4.11:

$$V(l) = |(\boldsymbol{\alpha}_l(1) - \boldsymbol{\alpha}(1))(\boldsymbol{\alpha}_l(2) - \boldsymbol{\alpha}(2))(\boldsymbol{\alpha}_l(3) - \boldsymbol{\alpha}(3))| \tag{4.11}$$

An interesting property of $\boldsymbol{w}_d$ is that the sum of all its component is equal to 1 if the real non-linear system is in the volume defined by the linear subsystems and greater than 1 otherwise. This helps in understanding when it is necessary to update the linear subsystems used.

The weighting functionals w_l can then be defined by ordering the elements of $\boldsymbol{w}_d$ and reversely assigning them to the linear subsystems, as illustrated hereafter through a portion of MATLAB code:

```
wd = V/Vall;
[~,idx] = sort(wd,'descend');
idxFlip = fliplr(idx);
for ii = 1 :  numel(idx)
    w(idxFlip(ii)) = wd(idx(ii));
end
```

Relaxing the restriction of $p = 2$ it is possible to define any number of parameters and to calculate the weighting functionals through hyper-volumes, defined by eq.4.12:

$$V(l) = |(\boldsymbol{\alpha}_l(1) - \boldsymbol{\alpha}(1))(\boldsymbol{\alpha}_l(2) - \boldsymbol{\alpha}(2)) \ldots (\boldsymbol{\alpha}_l(p) - \boldsymbol{\alpha}(p))| \tag{4.12}$$

It is necessary to note that what is reported and illustrated in this section is implemented in the `wFun` introduced in Subsection 4.3.1.

4.3.3 Level switch

A key point of the proposed method is the switch between the linear subsystem, which is event driven and it is the mechanism that allows one to reproduce the non-linear behaviour of the system. The reduced model produced by Multi-Phi is composed of lv linear subsystems, of which only 2^p at the time are effectively used in the time-domain simulation. In the following it is referred to these subsystems as

active subsystems, while the remaining $lv - 2^p$ are defined as *inactive*. Whenever the parameters of the real system fall outside the range of reference parameters of the active subsystems, it is necessary to interrupt the simulation and change the subsystems used, in a process here described as *Level switch*. In this phase it is fundamental to reduce the inevitable approximation errors introduced by the linearisation procedure and the event-driven simulation.

The definition of the exact instant of the level switch is pivotal in this process and represents the first kind of approximation, i.e. the *timing approximation*. In the current work it is handled by the `event` functionality of MATLAB `ode`, plus additional corrections necessary to ensure a successful switch, due to machine epsilon errors. Thresholds and tolerances can be used in the definition of the switching procedure, in order to avoid repeated level switch due solely to numerical approximations. On the other hand, the pursue of the best possible accuracy suggests maximum reduction of such tolerances, to be as precise as possible.

A second approximation is introduced by describing the same physical configuration of the full non-linear system with two different sets of linear subsystems and it is named *discretization approximation*. This kind of error increases with the level of reduction used (a procedure more detailing described in Section 5) and it also depends on how close to one of the 2^p linear subsystems is the full non-linear system. Considering in fact $p = 1$ and a CL modelling strategy, the level switch occurs when the full non-linear system coincides with one of the linear ones, reducing the level switch approximation to the timing one only. Aside for this specific (yet significant) zero-error case, the discretization approximation depends on how close it is to the closest linear subsystem, which is directly related to the number of linearisation points lv. In each level switch several parameters may change, but from a practical point of view it can be assumed that only one parameter at the time is exceeding the range defined by the 2^p linear subsystems, so that 2^{p-1} linear subsystems remain the same. The worst case scenario is therefore represented by the real non-linear system equally distant from all the 2^{p-1} linear subsystems.

The level switch procedure is hereafter described and consists of calculating the initial modal displacements and velocities of the new linear subsystems for the new timespan. Additionally, the initial weighting functionals need to be defined, based on the new linear subsystems involved and the configuration (or state) of the real non-linear system at the level switch instant.

A Discrete Levels (DL) model strategy is now considered, which involves the use of only one linear subsystem at the time. The time instant t_e of the level switch is taken into account and it is assumed to update of the previous linear subsystem to the new one. The new modal initial conditions can be determined by considering the last modal configuration of the old level and by expressing it with the new modal base, as reported by eq.4.13.

$$\begin{cases} \eta_{new} = \mathbf{\Phi}_{new}^{+}(\mathbf{\Phi}_{old}\eta_{old} + \mathbf{x}_{\infty,old} - \mathbf{x}_{\infty,new}) \\ \dot{\eta}_{new} = \mathbf{\Phi}_{new}^{+}\mathbf{\Phi}_{old}\dot{\eta}_{old} \end{cases} \tag{4.13}$$

where $\mathbf{\Phi}^{+}$ is the Moore-Penrose pseudoinverse for a generic non-square subset of eigenvectors matrix. It results in $\mathbf{\Phi}^{+} = \mathbf{\Phi}^{-1}$ if the complete set of eigenvectors is adopted in eq.4.13.

In recent years a method named *Static Modes Switching* (SMS) was introduced and developed (see [19, 17, 18]), consisting of dynamically selecting the static modes effectively contributing to the solution at each time step. This method is applied in multi-body dynamics and it is particularly beneficial in gear contact simulations. The level switch method proposed here presents several similarities with the SMS method, but the selection of the modes performed here is only a response of specific events and not completed at each time step. Additionally, the whole set of modes used is updated.

Chapter 5

Model Reduction

5.1 General

In Chapter 4 the focus is on the description of a full non-linear system by means of linear subsystems in modal coordinates. In this chapter the focus is on the selection of the modes to be included, realising the effective *reduction* of the system. It should be noted that even if the reduction phase is mainly responsible for the reduction of the computational time, the description of a physical non-linear systems by means of a set of linear subsystems has some benefits. The first-order differential equation of motion (in physical coordinates) reported in eq.5.1 is now taken into account.

$$\begin{Bmatrix} \dot{\boldsymbol{x}} \\ \ddot{\boldsymbol{x}} \end{Bmatrix} = \begin{Bmatrix} \boldsymbol{0} \\ \boldsymbol{M}^{-1}\boldsymbol{f} \end{Bmatrix} + \begin{bmatrix} \boldsymbol{0} & \boldsymbol{I} \\ -\boldsymbol{M}^{-1}\boldsymbol{K} & -\boldsymbol{M}^{-1}\boldsymbol{C} \end{bmatrix} \begin{Bmatrix} \boldsymbol{x} \\ \dot{\boldsymbol{x}} \end{Bmatrix} \tag{5.1}$$

Considering n DoFs, the size of the problem expressed by eq.5.1 is now $2n$. The use of `ode23tb` in MATLAB suggests the definition of the Jacobian's pattern (as it is for any other implicit integration scheme), allowing the reduction of the number of effectively calculated terms. Without this information, in fact, the number of terms is $4n^2$, while in the worst case, for a completely full system, it is $2n^2+n$. The effective number of terms depends on the specific system and on how coupled are the degrees of freedom, but even if it is unusual to have completely full matrices it is impossible to have completely diagonal ones. This last and ideal case (fully

uncoupled equations) is a prerogative of modal coordinates of linear system, as expressed in eq.5.2.

$$\begin{Bmatrix} \dot{\boldsymbol{\eta}} \\ \ddot{\boldsymbol{\eta}} \end{Bmatrix} = \begin{Bmatrix} \mathbf{0} \\ \boldsymbol{\Phi}^T \boldsymbol{f} \end{Bmatrix} + \begin{bmatrix} \mathbf{0} & \boldsymbol{I} \\ -\boldsymbol{\omega}^2 & -2\boldsymbol{\zeta}\boldsymbol{\omega} \end{bmatrix} \begin{Bmatrix} \boldsymbol{\eta} \\ \dot{\boldsymbol{\eta}} \end{Bmatrix} \tag{5.2}$$

All matrices in eq.5.2 are diagonal, so that the number of terms to be calculated is $3n$ and only when all n modes are considered.

Despite this initial advantage in the use of modal coordinates, the main point of the proposed method is to use a subset of the modes available. Several approaches can be used to determine the modeshapes to be retained and the ones to be discarded. The common starting point of all of them is to consider a number of coordinates $r_l < v_l \leq n$ for the generic linear system l. In the following the hereafter listed notation is used, where the subscript l refers to the generic l linear subsystem:

- n is the number overall DoFs
- $v_l \leq n$ is the number of unknowns, due to boundary conditions, which is considered to be equal to the number of modes available
- $r_l \leq v_l$ modal coordinates to be used

It is important to note that, by considering a reduction of the modal base of each linear system, an approximation of the already linearised (and therefore approximated) system is introduced. The consequent error is called the *modal approximation error*. Such approximation is introduced and accepted based on the key point that in mechanical systems few modes are usually representative of the system's behaviour.

The value of r_l can be defined as a constant value for every linear system or it can be dynamically chosen and varies for every time span, depending on the approach used. In the next subsections the following approaches are introduced and described:

1. Modal Truncation(MT)
2. Automatic Mode Selection (AMS)
3. Automatic Dynamic Mode Selection (ADMS)
4. variable Automatic Dynamic Mode Selection (vADMS)

These approaches differ in the way in which the reduced set of modes is determined, when this operation is performed and if the number of modes is constant or variable. For each method, the aim is to obtain the reduced modal matrix $\mathbf{\Phi}_{l,red}$. As starting point, it is assumed that the complete $(n\ x\ v_l)$ modal matrix and of the initial conditions in terms of modal coordinates $(\eta_0,\ \dot{\eta}_0)$ are known. The result of the model reduction and selection process is represented by the following matrices and vectors, listed here with their dimensions:

- $\boldsymbol{x}\ (n\ x\ 1)$
- $\mathbf{\Phi}_{l,red}\ (n\ x\ r_l)$
- $\boldsymbol{\eta}_l\ (r_l\ x\ 1)$

All of the proposed methods are based on the energy of the system; from an energetic point of view, total (L), kinetic (T) and potential elastic (U) energy are expressed at each time instant by means of eq.5.3:

$$\begin{cases} T = \frac{1}{2}\dot{\mathbf{x}}(t)^T\mathbf{M}(t)\dot{\mathbf{x}}(t) \\ U = \frac{1}{2}\mathbf{x}(t)^T\mathbf{K}(t)\mathbf{x}(t) \end{cases} \quad L(t) = T + U \tag{5.3}$$

It must be noted that mass and stiffness matrices are not assumed to be constant but variable in time to describe a non-linear system. For the mass matrix such time-dependent nature does not mean that the overall mass of the system is lost, but that it may be redistributed or that the boundary conditions (BCs) of the system may vary. Finally, the overall energy in the system (L) is expected to be constant or decreasing in time due to dissipations.

5.2 Modal Truncation

The first approach proposed is based on the idea that in mechanical systems the modeshapes associated with lower natural frequencies usually have more influence on system behaviour than the modeshapes associated with higher natural frequencies. The truthfulness of this assumption depends largely on the external forces applied, but mechanical excitations tend to be characterized by low frequencies, if compared with the natural frequencies of the system.

Since in the modal matrix the modeshapes are ordered based on increasing natural frequency, modes for the generic linear subsystem l are selected as per eq.5.4:

$$\mathbf{\Phi}_{l,red} = \begin{bmatrix} \Phi_l(1,1) & \Phi_l(2,1) & \dots & \Phi_l(r,1) \\ \Phi_l(1,2) & \Phi_l(2,2) & \dots & \Phi_l(r,2) \\ \vdots & \vdots & \ddots & \vdots \\ \Phi_l(1,n) & \Phi_l(2,n) & \dots & \Phi_l(r,n) \end{bmatrix} \tag{5.4}$$

In this approach a truncation threshold is defined for each linear subsystem, fixing therefore r_l and using the reduced modal matrices $\mathbf{\Phi}_{l,red}$ during the entire time integration process. An additional advantage of this procedure is the reduction of the matrices memorized, since truncated modes can be simply eliminated.

5.3 Automatic Mode Selection

The second approach proposed is based on the idea that the most significant modeshapes are the ones most excited by the external actions and by the initial conditions. The concept of *significance* is expressed by means of the energy content of each modeshape, so that the modes containing more energy are assumed to be the most significant in defining the system's behaviour.

In the following, the generic m modeshape of the generic l linear system is considered, with the purpose of illustrating the procedure followed. Firstly, the modal coordinate amplitude is calculated according to eq.5.5,

$$\begin{gathered} \dot{\eta} = \dot{\eta}_0 \\ \omega^2 \eta = f_\eta \Rightarrow \eta = \eta_0 + \frac{f_\eta}{\omega^2} \end{gathered} \tag{5.5}$$

in which the projection of the external force on the considered mode is named f_η. A static approach is used in eq.5.5, to evaluate the external force effect on the system. This passage has the purpose of giving the same importance to the free response of the system due to initial conditions (represented by $\boldsymbol{\eta}_0$) and to the forced response.

In a second step the energy contained in the generic mode l is calculated as per eq.5.6,

$$\begin{cases} T = \frac{1}{2}\dot{\eta}_0^2 \\ U = \frac{1}{2}\omega^2\eta_0^2 + \frac{1}{2}\frac{f_\eta^2}{\omega^2} \end{cases} \qquad L = T + U \tag{5.6}$$

where T is a scalar value indicating the kinetic energy of the considered mode, while U indicates its potential elastic energy. Lastly, L represents the overall energy. All of the v modes are then sorted according to L: the modal matrix of the linear subsystem Φ_l is rearranged as Φ_l^L, which indicates that the sorting is obtained according to the overall energy. The first r modes are then considered as per eq.5.7.

$$\boldsymbol{\Phi}_{l,red} = \begin{bmatrix} \Phi_l^L(1,1) & \Phi_l^L(2,1) & \dots & \Phi_l^L(r,1) \\ \Phi_l^L(1,2) & \Phi_l^L(2,2) & \dots & \Phi_l^L(r,2) \\ \vdots & \vdots & \ddots & \vdots \\ \Phi_l^L(1,n) & \Phi_l^L(2,n) & \dots & \Phi_l^L(r,n) \end{bmatrix} \tag{5.7}$$

The procedure described above is performed before the time integration and the modes unselected are discarded, as done in MT. The advantages are therefore the same of the previous method, but low frequency modes that are not excited by initial conditions or external forces are not retained, further reducing the DoFs of the reduced system.

A drawback of this approach is described hereafter. In the following the term *intermediate initial conditions* is used to describe the modal initial displacements calculated at a level switch, as per eq.4.13. This term is used to distinguish the initial conditions at $t = 0$, known and defined before the time integration simulation, from the unknown (a priori) intermediate conditions at $t > 0$.

During the switch between linear modal bases the energy is redistributed according to the similarity between the modes of the two bases (in the simplest case of DL or CL with $p = 1$). The projection of the external forces into the modal base of each subsystem is already taken into account, but it is possible that the configuration of the full non-linear system described by the old base is not fully represented by means of the intermediate initial conditions of the new subsystem. This may happen in the reduction procedure (performed before the time integration) as each subsystem is considered separately, so that if the intermediate initial conditions differ from the

initial conditions at $t = 0$, modes useful in describing the intermediate configuration may be deleted. This may result in a loss of overall energy at the level switch.

It should be noted that this approach serves as starting point for the following ones, described in Section 5.4 and Section 5.5. Its use however presents several limitations. It is difficult to forecast before the simulation which modes will be more representative of the system for the whole simulation. Contrary to the idea of MT, in which it is correctly assumed that the higher frequency modes have a limited influence on the overall behaviour of the system, with the AMS approach there is the risk of neglecting low frequency modes that will be excited at the switch event. This approach is therefore not used in the examples of Section 6, containing the examples proposed in this thesis.

5.4 Automatic Dynamic Mode Selection

The AMS procedure is used as a starting point for the ADMS strategy, trying to correct the drawbacks highlighted in the previous Section 5.3. The same energy-based criterion is used to obtain the reordered modal matrix $\mathbf{\Phi}_l^L$. In this third approach, however, the calculation is performed for each level change, using the initial conditions (in terms of modal coordinates) of the new linear system. Considering a generic level change from the old to the new subsystem, eq.5.8 expresses how the full set of r modal coordinate amplitudes are determined:

$$\begin{aligned} \eta_{new} &= (\mathbf{\Phi}_{new})^{+}\mathbf{\Phi}_{old,red}\eta_{old} + (\omega_{new}^2)^{-1}\mathbf{f}_{\eta,new} \\ \dot{\eta}_{new} &= (\mathbf{\Phi}_{new})^{+}\mathbf{\Phi}_{old,red}\dot{\eta}_{old} \end{aligned} \tag{5.8}$$

where the vector $\mathbf{f}_{\eta,new} = \mathbf{\Phi}_{new}^T\mathbf{f}$ is the modal force vector, obtained projecting the external forces on the considered modal base. In eq.5.8 all of the available modal coordinates are used. The previous level is considered to be already reduced. To obtain $\mathbf{\Phi}_{new}^L$, eq.5.6 is used, for each modal coordinate; then, by applying eq.5.7, the reduced modal matrix $\mathbf{\Phi}_{l,red}$ is obtained, considering l as the new level. It should be noted that this procedure is used to obtain the reduced modal matrix only and not to define the actual initial conditions of the new level.

For the first step of the simulation, the same procedure of the AMS approach is used. The number of modes to be considered is fixed and equal to r.

This approach can be considered computationally effort-driven, since the size of the problem is defined beforehand and it is maintained constant.

5.5 Variable Automatic Dynamic Mode Selection

The last approach proposed is identical, in terms of equations, to ADMS, except for the value of r_l, which is different in each level switch. At the beginning of the simulation, the matrix $\boldsymbol{\Phi}_{l_0,red}$ is obtained by using the first $r_l = r_{l_0}$ modes in terms of energy content. Eq.5.9 is used to define the energy content of all the modes:

$$\boldsymbol{L}_l = \frac{1}{2}(\dot{\boldsymbol{\eta}}_{0,l} + diag(\boldsymbol{\omega}_l^2))\boldsymbol{\eta}_{0,l} + diag(\boldsymbol{\omega}_l^2)^{-1}\boldsymbol{f}_{\eta,l}) \tag{5.9}$$

Once the energy contribution of each mode is defined, $\boldsymbol{L}_l$ is sorted in decreasing order of energy content, obtaining $\boldsymbol{L}_{sort}$ (l is drop in the notation for clarity). After this, a cumulative energy vector is defined, with the generic k element defined as per eq.5.10:

$$\boldsymbol{L}_{cum}(k) = \frac{\boldsymbol{L}_{cum}(k-1)+\boldsymbol{L}_{sort}(k)}{\sum_{m=1}^{v} \boldsymbol{L}_{sort}(m)} \tag{5.10}$$

where $\boldsymbol{L}_{sort}(j)$ is the j^{th} element of $\boldsymbol{L}_{sort}$ and $\boldsymbol{L}_{cum}(k)$ is the k^{th} element of $\boldsymbol{L}_{cum}$. This vector represents the normalized cumulative energy, so that $\boldsymbol{L}_{cum}(v) = 1$.

A fixed value of energy threshold (L_{th}) is calculated at the beginning of the simulation, as $L_{th} = \boldsymbol{L}_{cum}(r_{l0}) < 1$, with r_{l0} as the size of the first reduced linear subsystem. In a generic level change to level l, $\boldsymbol{L}$, $\boldsymbol{L}_{sort}$ and $\boldsymbol{L}_{cum}$ are calculated, and r_l is determined so that $L_{th} = \boldsymbol{L}_{cum}(r_l)$. This approach can be considered as error-driven, since it is based on the definition of the portion of energy to be neglected, with the number of DoFs to be used (computational cost) as consequence.

5.6 Error correction through x_∞

The switch between linear subsystem without the complete set of eigenvectors implies approximation errors, which may cause the imperfect correspondence between the final physical configuration of the previous time span and the initial physical configuration of the following one. In order to avoid small approximation errors

causing unexpected level switches, it is possible to compensate the approximation errors by using $\boldsymbol{x}_\infty$.

By using eq.5.11, it is possible to obtain a *corrected* version of $\boldsymbol{x}_\infty$, named $\boldsymbol{x}'_\infty$.

$$\boldsymbol{x}'_{\infty,new} = \boldsymbol{x}_{\infty,new} + (\boldsymbol{x}_{old} - \boldsymbol{x}'_{\infty,old}) - \boldsymbol{\Phi}_{new}\boldsymbol{\eta}_{new} \tag{5.11}$$

The use of this vector as an asymptotic configuration ensures no discrepancies in the physical configurations across the level switch event. It does however alter the asymptotic configuration, so that it should be used carefully.

5.7 Performance estimation

The performance of the reduced model needs to be evaluated on two criteria:

- Accuracy
- Computational time

The accuracy of the model is determined through a comparison between the full non-linear model and the results obtained with the numerical simulation of the reduced one. It must be noted that the use of MATLAB for the time-domain simulations implies limitation in the size of the models which can be handled through the *ode* function, in particular for what concern non-linear differential equation. Even though it is always technically possible to obtain the response of the full non-linear model, the computational time associated with the results is not indicative when compared with those of the reduced models. This is due, as discussed in Section 4.3, to the different nature of the differential equations: full non-linear model should be simulated with physical coordinates and non-diagonal matrices, while the reduced models should always use diagonal matrices.

Since the correspondence between the 0 reduction model, handled through the MT approach, and the full non-linear model was proved to be acceptable (see Subsection 6.1.1), all the comparisons, in terms of both accuracy and computational time, are performed according to this solution, defined in the following as *Reference* (shortened ar *ref* in formulas).

The computational cost is evaluated through the *computational time (CT)*, defined as per eq.5.12:

$$CT_s = 100\frac{t_{comp,s}}{t_{comp,ref}} \tag{5.12}$$

For the accuracy, a more complex indicator needs to be defined. The *global mean square error* (gMSE), based on the *normalised mean square error* (MSE) [104, 105], is obtained as described in eq.5.12, eq.5.13, eq.5.14:

$$MSE_s(j) = \frac{100}{M\sigma^2_{ref,j}}\sum_{r=1}^{M}(x_j(r\Delta t) - x_{j,ref}(r\Delta t))^2 \tag{5.13}$$

$$gMSE_s = \frac{1}{N}\sum_{j=1}^{N} MSE_s(j) \tag{5.14}$$

The subscript s indicates the evaluated simulation, with a specific level of reduction, expressed as a percentage through the variable *model reduction* (MR).

For each simulation, M time instants are considered, so that $t_{end} = M\Delta t$. Each DoF, identified by the subscript j is been taken into account separately. Eq5.13 defines, for each simulation, a vector composed by the *MSE* of each DoF. In order to provide a global value, not affected by the number of nodes, eq5.14 is used to give a mean value of the percentage error. Eq5.15 is then used to add a weight to each percentage error, defining a *global weighted mean square error* (gwMSE).

$$gwMSE_s = \frac{1}{N}\sum_{j=1}^{N} w(j)MSE_s(j) \qquad with \quad w(j) = \frac{\sigma^2_{ref,j}}{\bar{\sigma}^2_{ref}} \tag{5.15}$$

Chapter 6

Applications

In this chapter several applications of the proposed Multi Phi method are presented. The purpose is firstly to demonstrate and to verify its effectiveness in reproducing the non-linear behaviour of the original system. Then, the performance in terms of accuracy and computational time saved are analysed.

The complexity of the examples proposed is progressively increased, starting from a simple lumped parameter system (Section 6.1), with no reduction used.
A second class of examples is proposed in Section 6.2, characterised by continuous systems with non-linearities due to contact, modelled as *hard contacts*. In this section, the proposed reduction strategies are evaluated on increasingly complex examples.
A third class of examples is proposed in Section 6.3, in which continuous systems characterised by non-linearities due to non-linear stiffness components are analysed. Analogously to Section 6.2, reduction strategies are compared and performance of the reduction method proposed are analysed.

6.1 Lumped masses

In the first example the system shown in Figure 6.1 is considered, and first, an academic example is considered to evaluate the effectiveness of a time-domain simulation performed in the modal coordinate domain. Additionally, the algorithm used for switching between the linear subsystems used is assessed. Because of the simplicity of the system, no reduction is used.

The system considered is a lumped system with 8 masses, 7 springs and 7 dampers; the first and the last masses are fixed and a rigid wall is placed at $c = 0.2$mm with respect to the equilibrium position of the 5^{th} mass (positive direction: left to right). This rigid wall is modelled as an additional boundary constraint on the 5^{th} mass, defining therefore a hard contact. All of the masses are considered to be free to move along the x coordinate only. The physical coordinates used are expressed as x_i and they represent the deviation from the undeformed configuration and they can therefore be described as *local coordinates*.

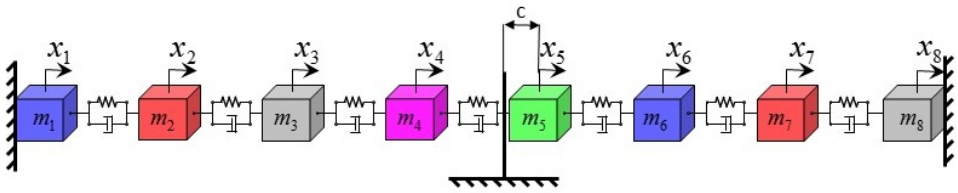

Fig. 6.1 8-DOFs lumped system, with asymmetrical contact on the 5^{th} mass.

The values of masses and springs stiffnesses are summarized in Tab.6.1.

Table 6.1 Masses and stiffness values.

Mass	**Value** [kg]	**Spring**	**Value** $\left[\frac{\text{N}}{\text{m}}\right]$
m_1	0	k_{12}	1
m_2	1	k_{23}	2
m_3	2	k_{34}	3
m_4	3	k_{45}	4
m_5	4	k_{56}	5
m_6	5	k_{67}	6
m_7	6	k_{78}	7
m_8	0		

The full non-linear system can be easily discretized through 2 linear subsystems, based on the position of the 5^{th} mass. It has to be noted that the reaction force applied by the constraint representing the rigid wall must to be considered for the transition between the linear subsystems.

1. No contact between mass and rigid wall: if $x_5 > 0.2$mm. $R_5 = 0$N

2. Contact between mass and rigid wall: if $x_5 = 0.2$mm then $R_5 > 0$ N

Depending on the linear subsystem considered, the modal properties vary: natural frequencies for each level are reported in Tab.6.2.

Table 6.2 Modal Properties.

	Frequency [Hz]	
Mode	*Subsystem*1	*Subsystem*2
1	2.29	4.23
2	4.71	5.25
3	6.87	8.14
4	8.64	9.11
5	9.93	10.69
6	10.86	-

Differences can be observed also in terms of modeshapes, depending on the linear subsystem analysed, as shown in Figure 6.2.

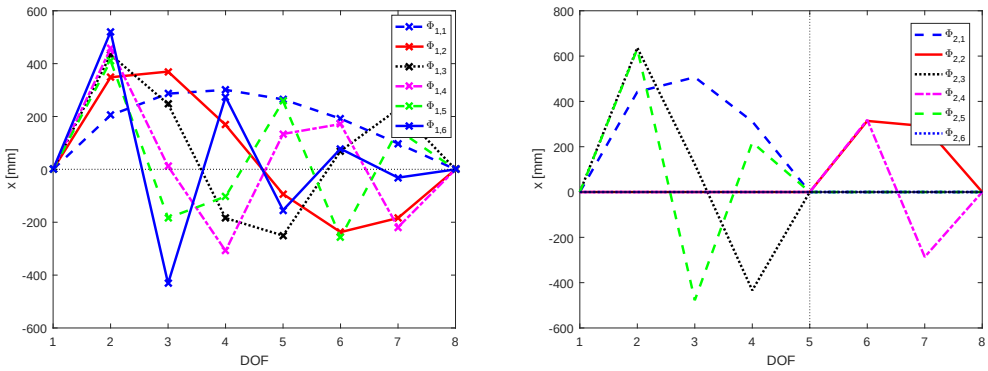

(a) (b)

Fig. 6.2 Modeshapes of linear subsystem without contact (a) and with contact (b).

The difference in terms of boundary conditions implies a clear difference in terms of modeshapes: considering the 5^{th} mass fixed, the first 3 modes pertain to the first 3 masses, while the last 2 modes pertain to the last 2 masses. The linear subsystem considered is in fact composed by two uncoupled systems, as highlighted by the vertical line in Figure 6.2.

A proportional damping is considered, as $\boldsymbol{C} = \alpha\boldsymbol{M} + \beta\boldsymbol{K}$, with $\alpha = 1\frac{1}{\text{s}}$ and $\beta = 1 \times 10^{-2}$s. Initial conditions are defined so that the first and the last masses have zero relative displacement, while the relative displacements of the others increase linearly, between $x_2 = 0$mm and $x_7 = 8$mm. This configuration leads the 5^{th} mass to have a relative displacement of $x_5 = 6.4$mm, resulting this mass relocating to the right of the rigid wall. It is as a consequence expected that in the final configuration the 5^{th} mass remains in contact with the wall.

Figure 6.3 shows simulation results for all DoFs, highlighting the position of the wall. The absolute reference system is used to better identify masses displacements.

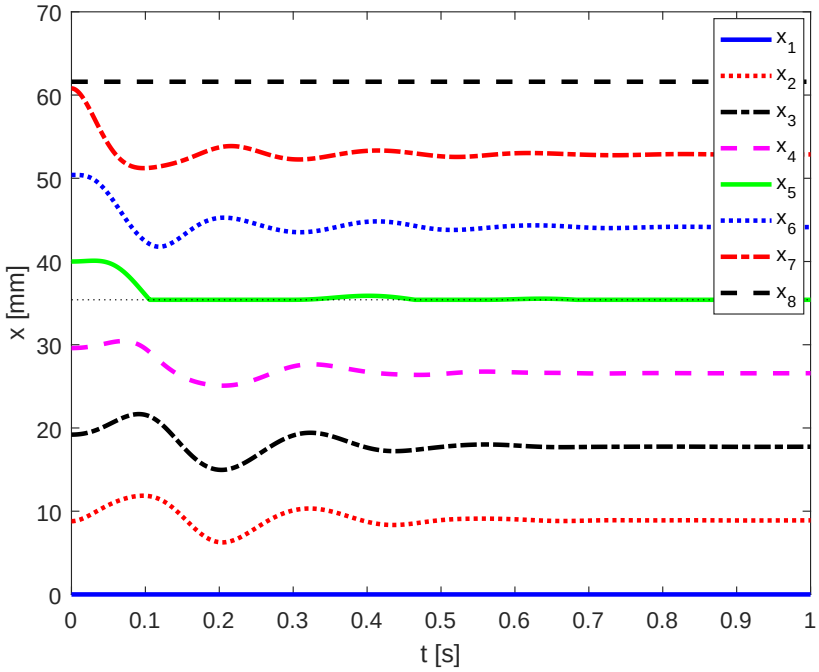

Fig. 6.3 Absolute displacements for all DoFs.

Focusing on the 5^{th} mass, Figure 6.4 shows both its relative displacement and the associated reaction force.

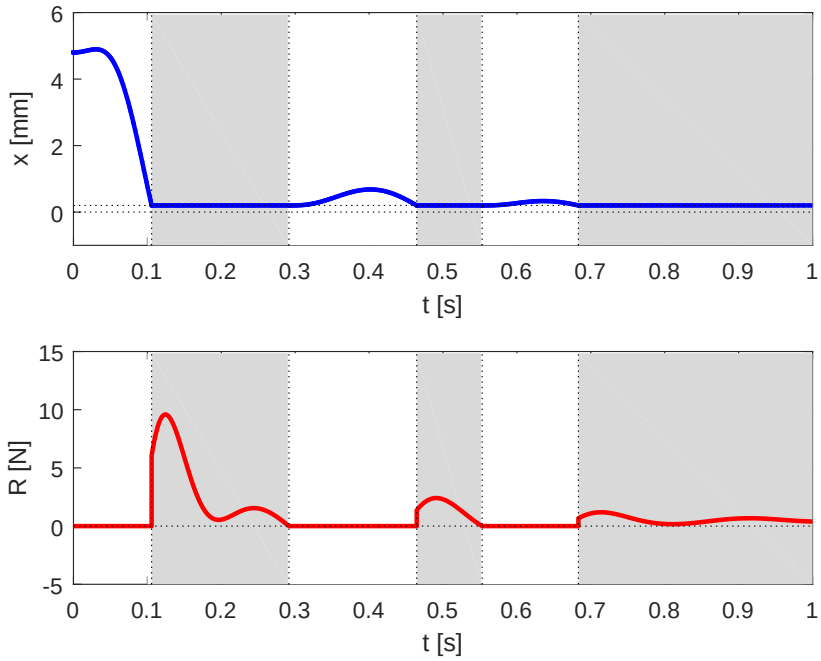

Fig. 6.4 Relative displacement and reaction force of the 5^{th} mass.

Two different background colours, in Figure 6.4, identify the subsystem used: the white colour identifies the no contact subsystem while the grey colour identifies the one with contact. As expected, for the first linear subsystem the reaction force is zero and no contact is detected. The result is different from zero when the second linear subsystem is used.

Figure 6.5 shows the time history of modal coordinates, highlighting discontinuities at each subsystem switch.

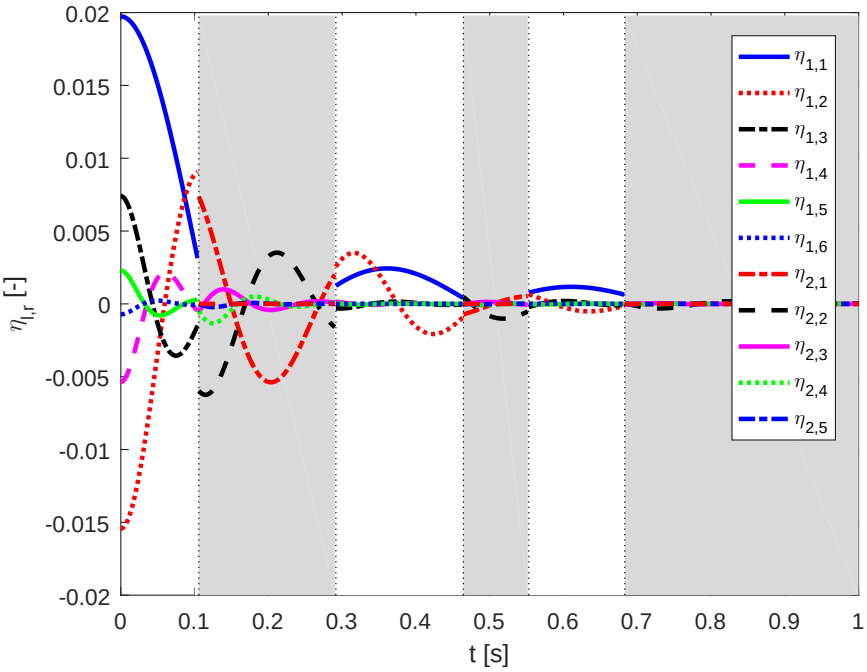

Fig. 6.5 Modal coordinates displacements.

The switch between linear subsystems, as discussed in Subsection 4.3.3, implies a change in the modal coordinates, as if a new simulation starts from the switching instant, so that new initial conditions are used. In Figure 6.5 it is possible to appreciate the lack of continuity in terms of modal coordinates, these being representative of modes which vary across the switching event. Despite the lack of continuity of the modal coordinates, at the switching instant the same physical configuration is represented with two different bases. The two representations are perfectly coincident only if all the modes of the system are used and if the switching event is perfectly captured. The first assumption is dropped when a model reduction is performed, while the precision in capturing the switch instant depends on the algorithm used. In this thesis the `ODE Event Location` function of MATLAB is used, with additional measures necessary to perform the switching as correctly as possible.

This last point was one of the most challenging aspects of the MATLAB implementation of the method proposed in this thesis.

In Figure 6.5, as highlighted in the legend, 11 modal coordinates are used: 6 for the first subsystem and 5 for the second. At each transition from subsystem 1 (no contact) to subsystem 2 (contact), all of the energy associated with the modal

coordinates of the system with no contact is transferred to the modal coordinates associated with the contact subsystem, except for the kinetic energy of the 5^{th} mass, which is therefore dissipated. This is better highlighted in Figure 6.6, which shows the loss of kinetic energy at every impact, while the elastic energy is continuous.

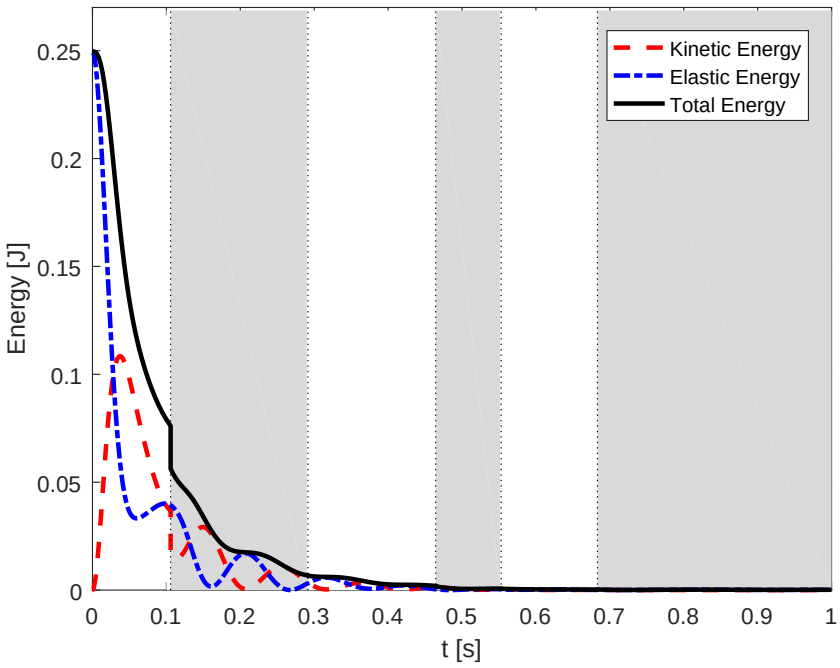

Fig. 6.6 Kinetic, elastic and total energy.

Summarizing, the consequences of the use of multiple modal coordinates transformation are:

- the physical coordinates are continuous at each instant;
- the modal coordinates are continuous at each instant except for the switching ones.

6.1.1 Direct integration comparison

In order to validate the the effectiveness of the time integration by means of a piecewise linear subsystems described through modal coordinates, the same system has been simulated by means of the physical coordinates only. Figure 6.7 shows a

comparison between the direct integration (DI) and the proposed approach (MPhi) about the contact point and the reaction force.

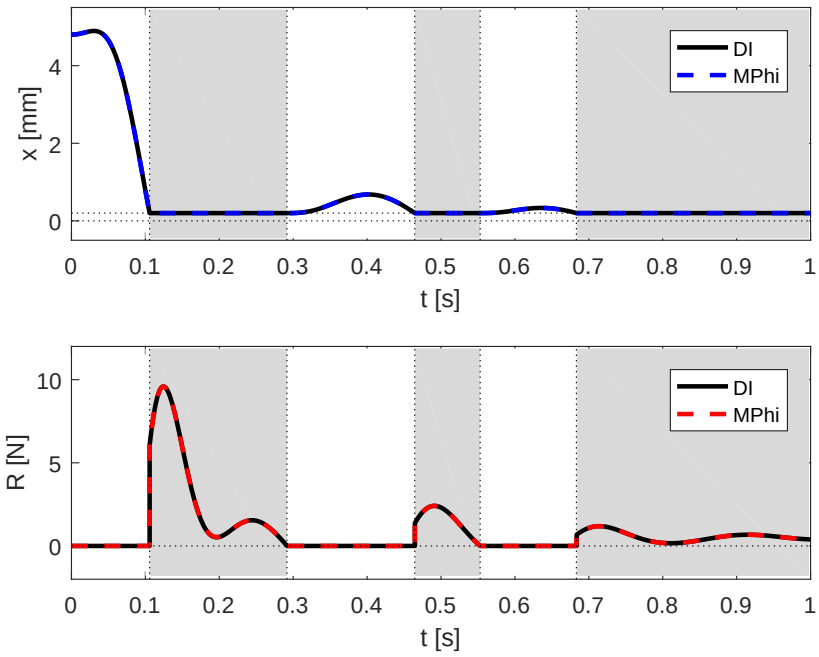

Fig. 6.7 Relative displacement (x) and reaction force (R) of the 5^{th} mass, with Direct Integration (DI) and Multi-Phi (MPhi) approaches.

No meaningful differences are observable between the two methods and the change of coordinates, from physical to modal coordinates, does not introduce any significant error. It must be noted that this is obtained by using all of the modes of the system and therefore performing no model reduction.

6.2 Discrete Levels

In this section, several applications of the Multi-Phi method are proposed, with the common characteristic of containing a non-linearity due to one or more contacts. The approach used in this section is the Discrete Levels one, since it is possible to clearly identify a limited number of linear subsystems able to represent with good approximation the non-linear system. This class of non-linear systems is often referred to as *piecewise linear* systems. For what concern the approaches introduced

in Chapter 5, only MT, ADMS and vADMS will be used in this Section, and not AMS. The reason is the nature of the system examined here: contacts introduce what can be described as an *internal excitation*, in the sense that the frequency content and the physical distribution of the response can vary and differ significantly from the ones excited by the external force. The AMS approach evaluates the effect of the external force and initial conditions beforehand, defining modes to retain and to delete for the whole duration of the simulation. Deleted modes are no longer considered and they cannot be excited by the contact, making a significant loss of accuracy likely; in this phase AMS is sought as a means for obtaining ADMS and vADMS, but it is not used in any of the examples of this section.

The same base system, i.e. a beam with the characteristics reported in Table 6.3, is used for all the examples in this section. 51 nodes are used to provide a sufficiently precise physical description and the location of contacts, localized non-linearities and external force application points.

Table 6.3 Beam characteristics.

Name	Value
Length	$L = 1\text{m}$
Width	$w = 0.05\text{m}$
Height	$h = 0.006\text{m}$
Density	$\rho = 2700\frac{\text{kg}}{\text{m}^3}$
Young Modulus	$E = 69 \times 10^9\text{Pa}$
Poisson's Ratio	$\nu = 0.30$

Based on this common linear system, several non-linear ones are obtained by means of contact points, varying their number, location and clearance. The following non-linear systems are considered:

- *Falling Beam*, in Subsection 6.2.1. Hinged left end, free right end, with a support. Initial displacement as per the first mode (rigid body motion) and no external forces, except for the gravity effect;
- *Contact Beam*, in Subsection 6.2.2. Clamped-free beam, with a support. Null initial displacements and velocities and harmonic external force;

- *Multiple Contacts Beam*, in Subsection 6.2.3. Clamped-free beam, with two supports in different position. Null initial displacements and velocities and harmonic external force.

Each non-linear system is integrated in time by using the proposed approach, analysing the system's response and evaluating accuracy and performance of the reduction scheme.

6.2.1 Falling Beam

In this subsection a beam named *Falling Beam* is considered, with the characteristics reported in Table 6.4 added to the generic beam model introduced in Section 6.2:

Table 6.4 Falling Beam characteristics.

Name	Value	
Constraint Position (x)	$e = 0.7\text{m}$	
Tip Initial Displacement (z)	$z_0 = 0.025\text{m}$	
Constraint Height (z)	$c = 0.001\text{m}$	
Damping	$\alpha = 0.0025\frac{\text{rad}}{\text{s}}$	$\beta = 5 \times 10^{-5}\frac{\text{s}}{\text{rad}}$

As reported in Section 6.2, the boundary conditions for this example consist of a hinge at the left end ($x = 0\text{m}$), while the right end ($x = l$) remains free. Moreover, the x-z plane only is considered. Figure 6.8 shows a scheme of the system.

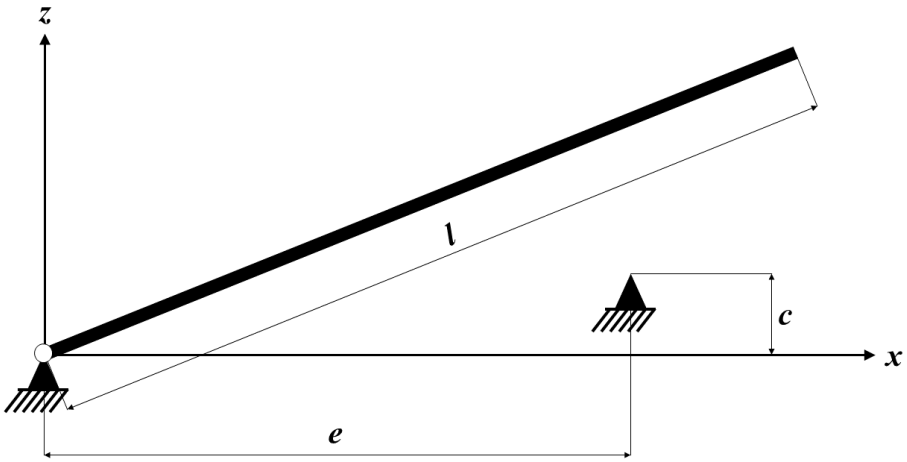

Fig. 6.8 Falling Beam.

Figure 6.9 shows the simulation of the system with no reduction, highlighting the contact point (Figure 6.9a) and the free end (Figure 6.9b) of the beam.

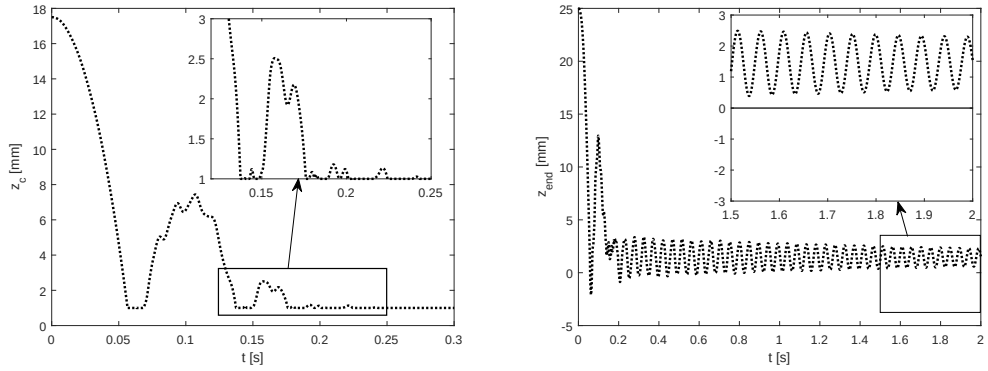

(a) Contact point displacement (b) Free end displacement

Fig. 6.9 Falling Beam, displacements, full model.

Figure 6.9a shows that the beam bounces on the support multiple times, dissipating at each contact part of its kinetic energy. After $t \approx 0.3$s the beams remains in contact with the support, but the free end continues to vibrate, as shown in Figure 6.9b. Damped oscillations not centred around the x axis can be observed, as expected since $c \neq 0$m. These oscillations confirm that the impact with the support activate higher frequency modes, with the initial displacement involving the first modeshape only.

Figure 6.10 shows a comparison between the full model and the two reduced ones, obtained by means of Modal Truncation (MT) and Automatic Dynamic Modal Selection (ADMS). In both cases, only half of the modes are used, defining a reduction of 50%. The beam here is modelled with 110 beam elements, resulting in 220 overall modes, after all boundary conditions are applied; as a consequence, the reduction used in Figure 6.10 uses 110 modes, for both MT and ADMS.

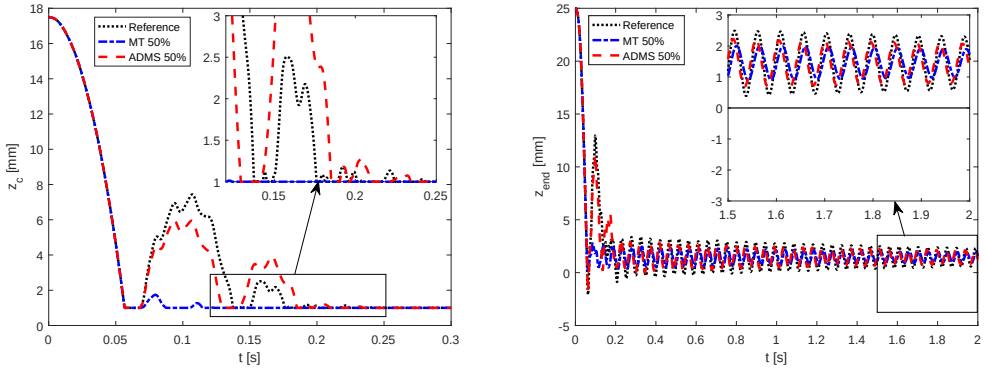

(a) Contact point displacement (b) Free end displacement

Fig. 6.10 Falling Beam, displacements, comparison between MT and ADMS, 50% reduction.

Despite having similar computational costs, the results obtained through the ADMS approach show a significantly improved accuracy when compared with the MT approach, especially concerning the contact point.

The use of the vADMS approach, introduced in Section 5.5, is difficult to compare with MT or ADMS, because of the way in which the reduction threshold is defined. As reported in 5.5, the reduction threshold is defined by specifying the number of modes used for the first time span, based on which an *energy threshold* is calculated. Such threshold is then used in all of the subsequent level switches, so that depending on the initial conditions the mean number of modes used during the simulation varies. In this example, in the first time span the full system is well represented by the first few modes, which contain most of the energy of the system, while during and after the first contact other modes get involved and the energy of the system results more widespread. Figure 6.11 shows the energy contribution of each mode normalized to 1 (blue dashed line) of the initial conditions. The black dotted line represents the *floating-point relative accuracy*, so that the contribution of each mode below the black line cannot be appreciated from a numerical point of view.

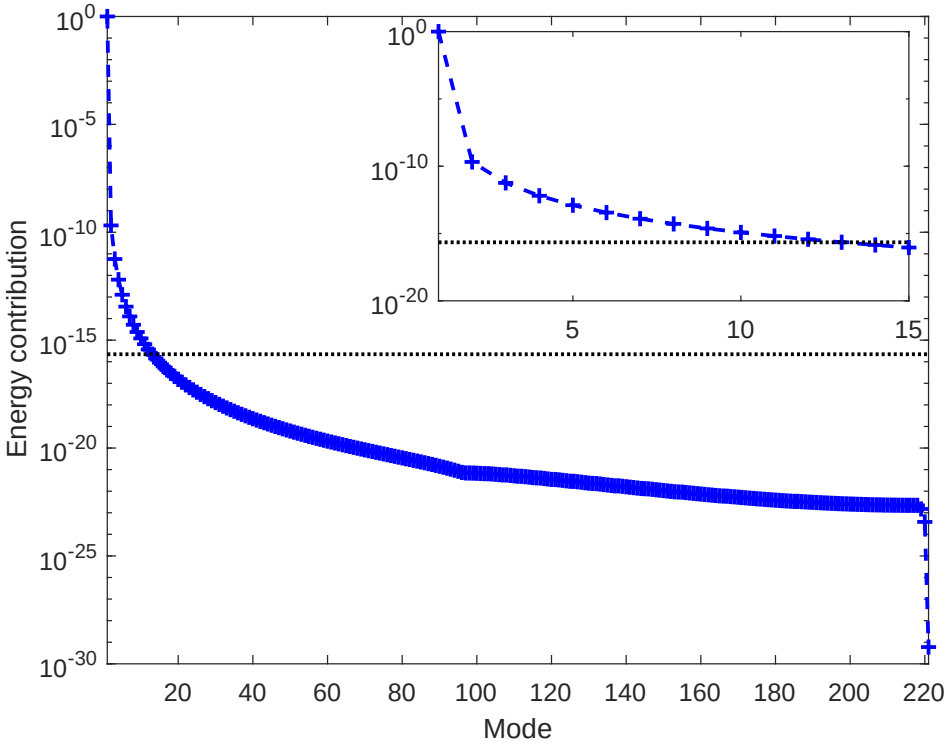

Fig. 6.11 Falling Beam, energy contribution of each mode.

The first 14 modes contain all of the energy of the system, so that the first time span is simulated by using only this subset. Figure 6.12 shows the number of modes used during the simulation, the dash-dotted blue line for the *no contact* linear system (on the left) and in dashed red line for the *contact* one (on the right).

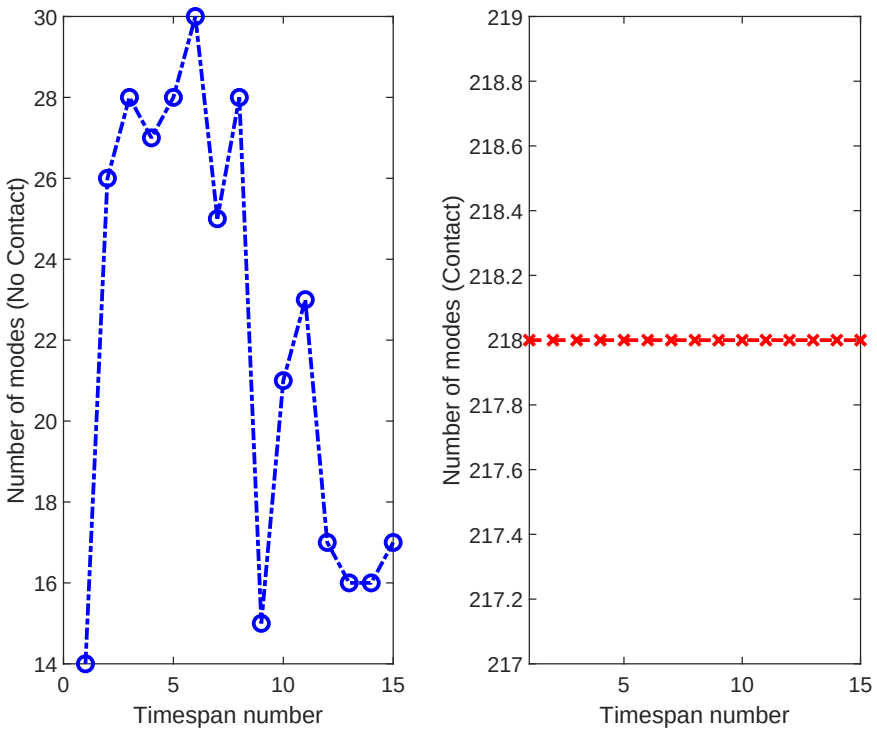

Fig. 6.12 Falling Beam with no reduction, number of modes considered, no-contact subsystem in dash-dotted blue (left) and contact subsystem in dashed red (right).

It can be observed that the number of modes used to describe the beam having no contact with the support varies, since for some cases a different number of modes produces results below the floating point accuracy. Contrarily, the same number of modes, coincident with the maximum number of modes available, is used for the simulation of the beam that is in contact with the support.

Figure 6.13 provides an explanation of the observed behaviour, highlighting how the energy distribution is radically different between the no-contact (blue) and the contact (red) subsystem.

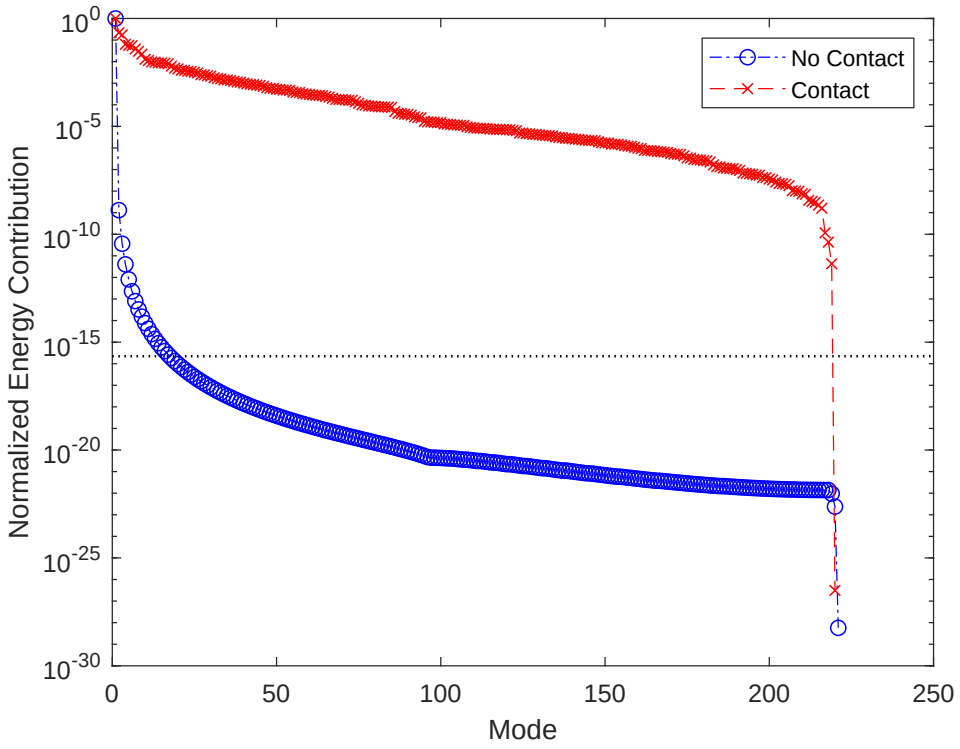

Fig. 6.13 Falling Beam, energy contribution of each mode, for the no-contact subsystem (blue) and for the contact subsystem (red).

Energy distributions refer to different time instant but, being normalized to 1, give an explanation of the different number of modes used for the two subsystems.

Figure 6.14 and Figure 6.15 show data analogous to those reported in Figure 6.12 and Figure 6.13, but refer to a case with more severe model reduction.

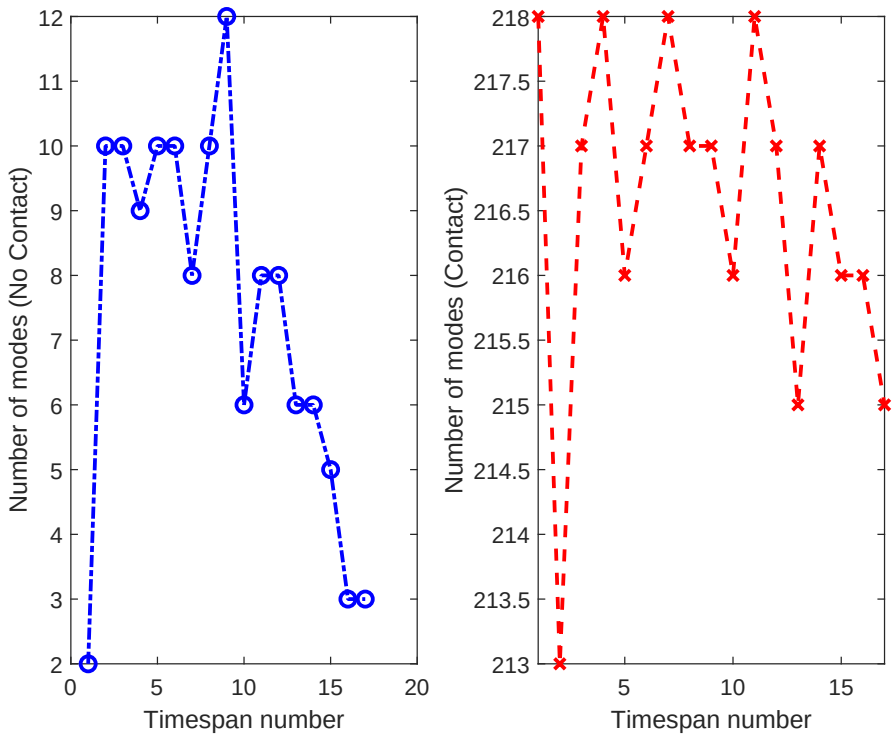

Fig. 6.14 Falling Beam, number of modes considered for 98.80% reduction, no-contact subsystem in dash-dotted blue(left) and contact subsystem in dashed red (right).

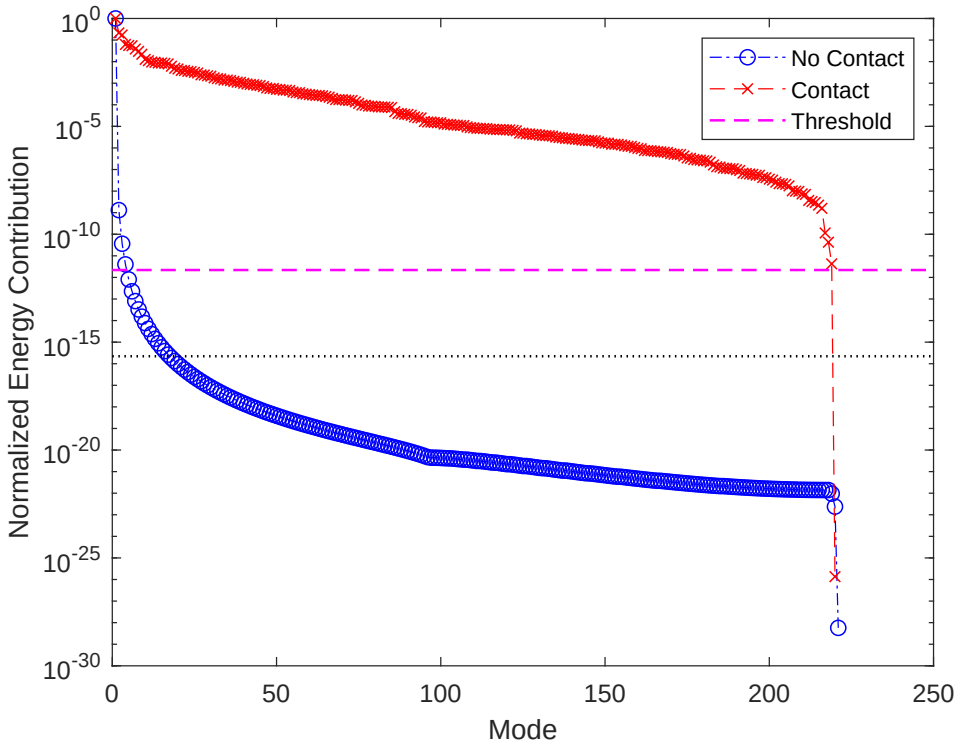

Fig. 6.15 Falling Beam, energy contribution of each mode, with98.80% reduction. No-contact subsystem (blue), contact subsystem (red) and energy threshold (magenta).

In this second case, the number of modes varies for both the contact and the contact-free linear subsystem, even though the number of modes considered in the contact conditions (red line) remains high.

The horizontal magenta line in Figure 6.15 represents the energy threshold used to reduce the model. The approach used in vADMS is different from MT, AMS and ADMS, which use a vertical threshold. It should be remembered that vADMS is an *error-driven* approach, so that a certain level of accuracy is prescribed while the number of modes (and therefore the computational cost) results as a consequence.

Figure 6.16 shows a comparison between the full model and the model simulated through the vADMS approach, with no reduction (blue) and a 50% reduction (red). Small differences can be observed between the non-reduced version of vADMS, which is practically identical to the full model, and the 50% reduced one.

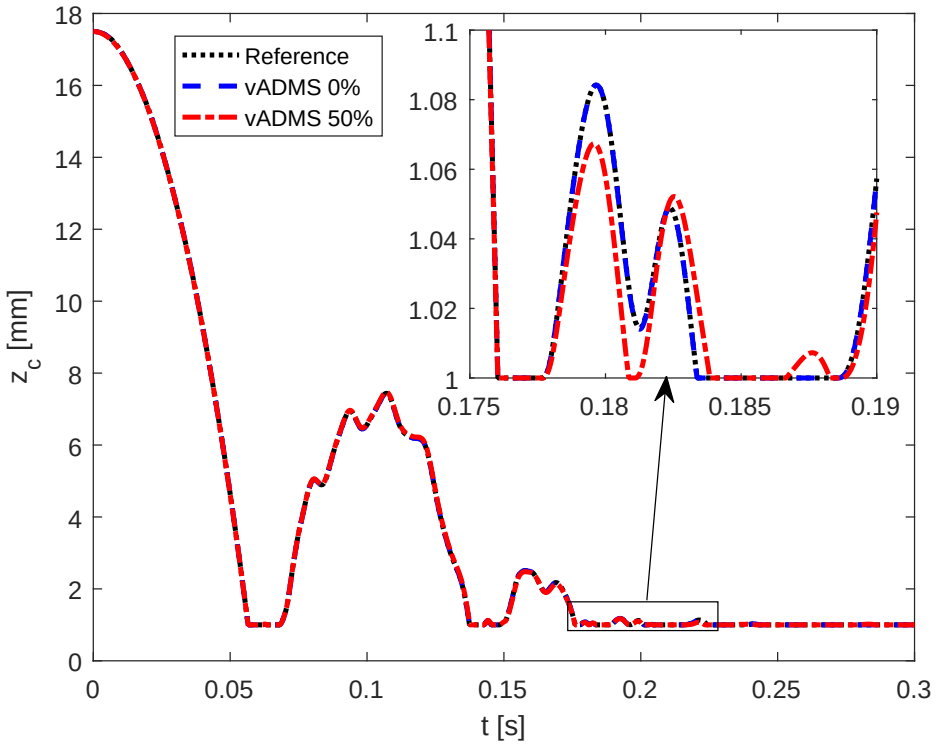

Fig. 6.16 Falling Beam, displacements, comparison between MT and vADMS, 0% (dashed blue line) and 50% reduction (dash-dot red line).

It is necessary to note that the percentage reduction, for the vADMS reduced model, is calculated after the simulation by using the mean number of modes retained, defining an *effective* reduction percentage. In Figure 6.16 the *effective* 50% reduction is obtained by setting an initial reduction of 98.80%.

In Figure 6.17 a comparison is proposed, between full model (dotted black) and a 50% reduction, according to MT (dash-dotted blue), ADMS (dashed red) and vADMS (dash-dotted magenta).

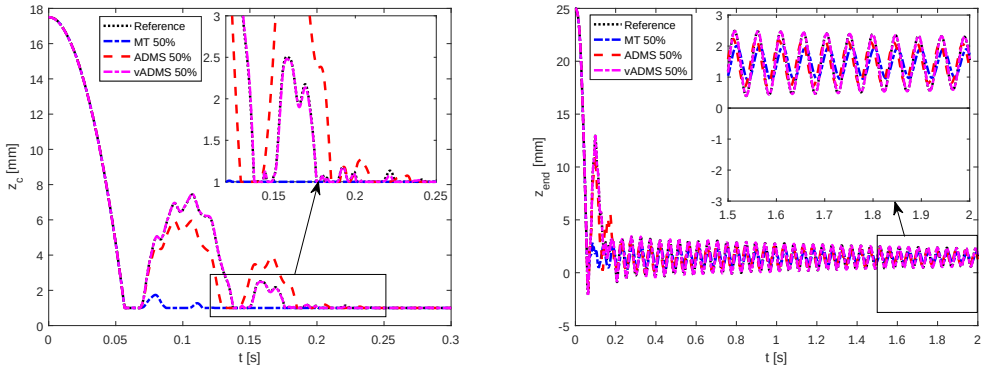

(a) Contact point displacement (b) Free end displacement

Fig. 6.17 Falling Beam, displacements, comparison between MT, ADMS and vADMS, 50% reduction.

The performance of the reduced model is analysed according to Section 5.7, i.e. through the indicators CT and gwMSE. Figure 6.18 shows percentage error (red) and percentage computational time (blue), with respect to the reference. Different model reduction strategies are identified by means of different line and marker styles.

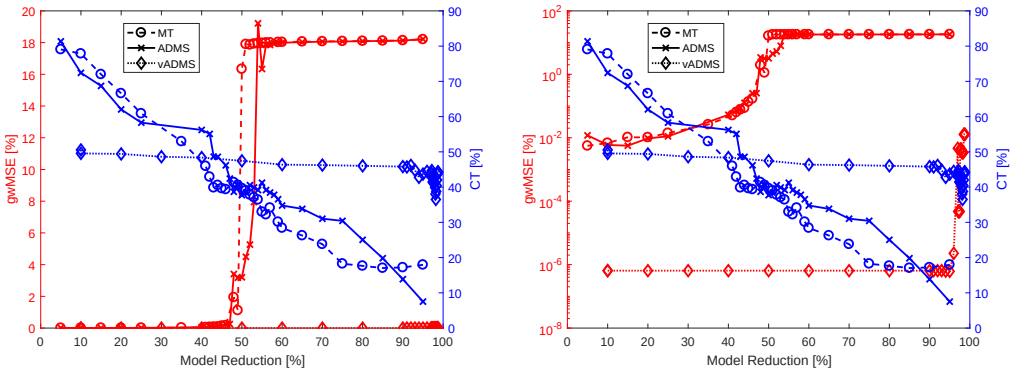

(a) Linear scale (b) Logarithmic scale

Fig. 6.18 Falling Beam, performance evaluation, percentage error (gwMSE, red) and computational time (CT, blue) as a function of the model reduction percentage.

For what concern MT and ADMS, it is possible to observe a continuously decreasing computational time (CT, in blue), in accordance with the reduced computational burden. The error (gwMSE, in red) remains low up to a percentage reduction of about 50%, after which it increases significantly, remaining then constant at $gwMSE \approx 18\%$. Referring to Figure 6.18a, this is the percentage error associated

with a beam falling on the support without bouncing back. It is possible to reduce the system slightly more by using the ADMS approach, due to the more sophisticated selection of the modes. Such procedure implies however higher computational time as compared to those obtained with the MT approach.

For what concern vADMS, the model reduction percentages reported in Figure 6.18 are the *prescribed* ones, as discussed above. This approach guarantees the lowest percent errors for a wide prescribed model reduction, but it does not allow for the computational cost reduction in an intuitive and straightforward way.

6.2.2 Contact Beam

The second example proposed in this subsection assumes different boundary conditions, replacing the hinge used in Subsection 6.2.1 with a clamped end, while the other end remains free, obtaining a cantilever beam. A scheme of the non-linear system considered in this example is showed in Figure 6.19.

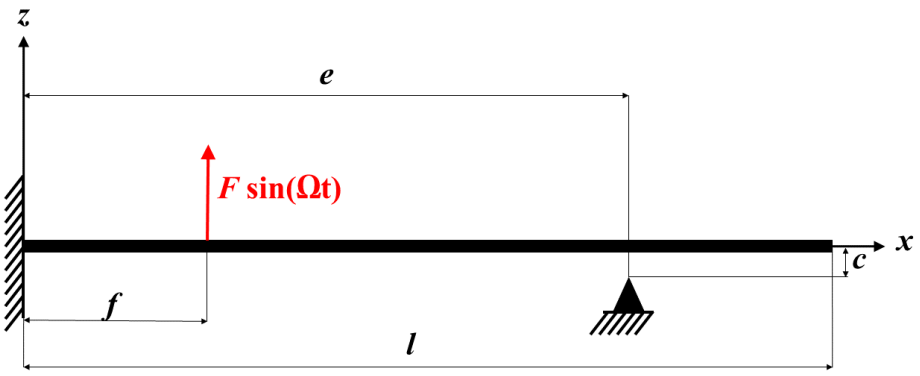

Fig. 6.19 Contact Beam.

A harmonic external force is introduced, located at f from the fixed end of the beam, while a support with clearance c is placed at e. Characteristics additional to those in Table 6.3 are reported in Table 6.5

Table 6.5 Contact Beam characteristics.

Name	Value
Constraint Position (x)	$e = 0.78\text{m}$
Constraint Clearance (z)	$c = 0.25 \times 10^{-3}\text{m}$
Force Position (x)	$f = 0.50\text{m}$
Force Amplitude	$F = 10\text{N}$
Force Pulsation	$\Omega = 192.90\frac{\text{rad}}{\text{s}}$ $(\approx 30.70\text{Hz})$
Damping	$\alpha = 0.0025\frac{\text{rad}}{\text{s}}$ | $\beta = 5 \times 10^{-5}\frac{\text{s}}{\text{rad}}$

Analogous to the example in Subsection 6.2.1, the non-linear system is modelled through two linear subsystems, the first one as a simple cantilever beam and the second one with an additional boundary condition to represent the contact with the support. The first 4 modeshapes of the two linear subsystems are shown in Figure 6.20.

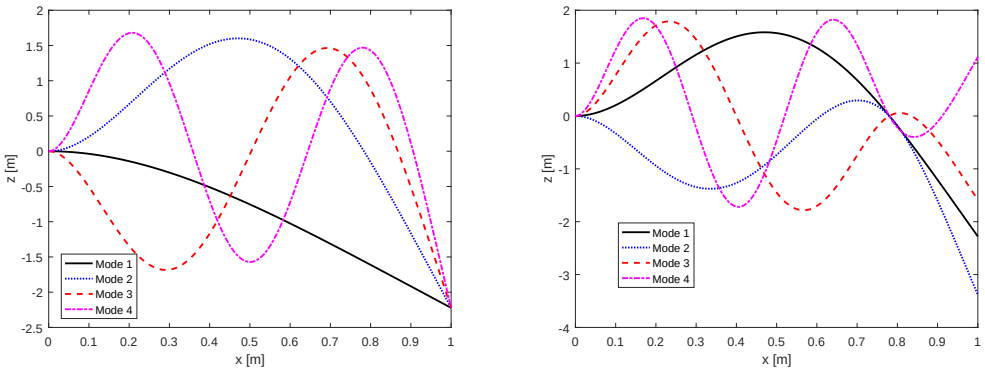

(a) Subsystem 1 (no contact). (b) Subsystem 2 (contact).

Fig. 6.20 Contact Beam, mass-normalized modeshapes.

Figure 6.20b highlights the contact point, considered as an additional boundary condition. In this formulation, the node corresponding to the contact point is set as fixed, with null displacement. Since the contact point is not on the beam axis, as reported in Table 6.5, the asymptotic configuration x_∞ introduced in Section 4.2 is non-null. Figure 6.21 shows the pre-determined configuration.

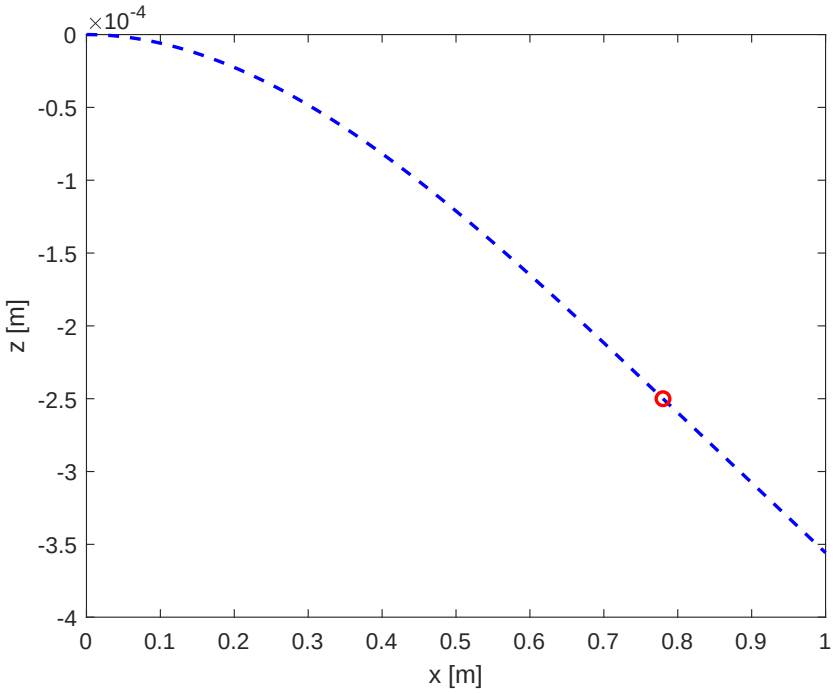

Fig. 6.21 Contact Beam, asymptotic configuration (contact subsystem).

Finally, the first natural frequencies of the two subsystems are reported in Table 6.6.

Table 6.6 Contact Beam natural frequencies.

	Frequency [Hz]	
Mode	No contact	Contact
1	4.90	30.69
2	30.70	67.74
3	85.95	134.37
4	168.37	256.24

Figure 6.22 shows the whole simulation, considering the contact point (Figure 6.22a) and the free end of the beam (Figure 6.22b). The reference (dotted black line) is compared with a 50% reduction, with the MT (dash-dotted blue), ADMS (dashed red) and vADMS (dash-dotted magenta) approaches.

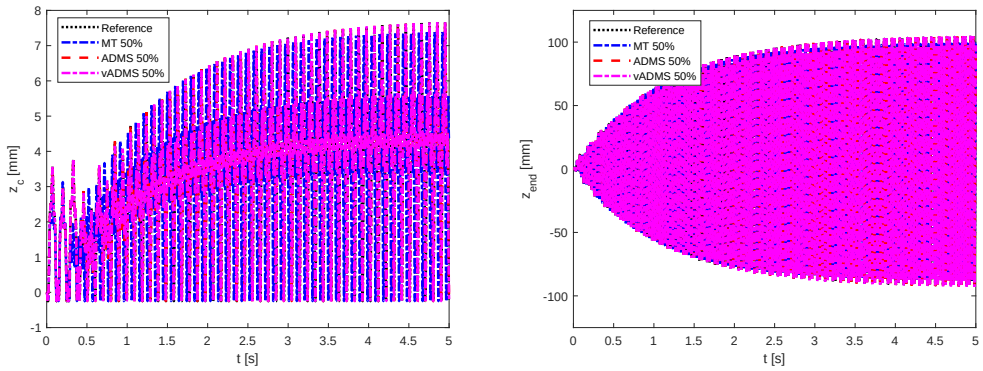

(a) Contact point displacement (b) Free end displacement

Fig. 6.22 Contact Beam displacements, comparison between Reference (dotted black) and MT (dash-dotted blue), ADMS (dashed red) and vADMS (dash-dotted magenta) at the contact point, with 50% reduction.

The simulation is performed until the steady state is reached, but the focus is also on the transient part. Figure 6.23 shows the comparison between the reference and a 50% reduction, considering the first 0.5s of the response.

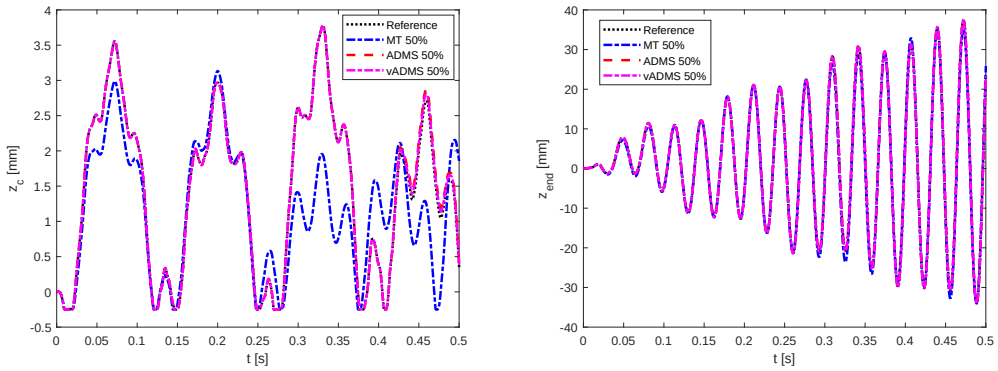

(a) Contact point displacement (b) Free end displacement

Fig. 6.23 Contact Beam, transient response, comparison between MT, ADMS and vADMS, 50% reduction.

Figure 6.23a shows the contact point, highlighting the importance of the mode selection. The ADMS and vADMS approaches show an almost perfect comparison with respect to the reference whereas the MT approach shows a significantly worse approximation. Despite the lack of accuracy in describing the contact point, the overall response result is consistent, as shown by Figure 6.23b, referring to the free

end of the beam. The behaviour in this case is well approximated by all of the considered approaches.

Figure 6.24 shows the same DoFs in the steady state regime, confirming the trend observed in Figure 6.23.

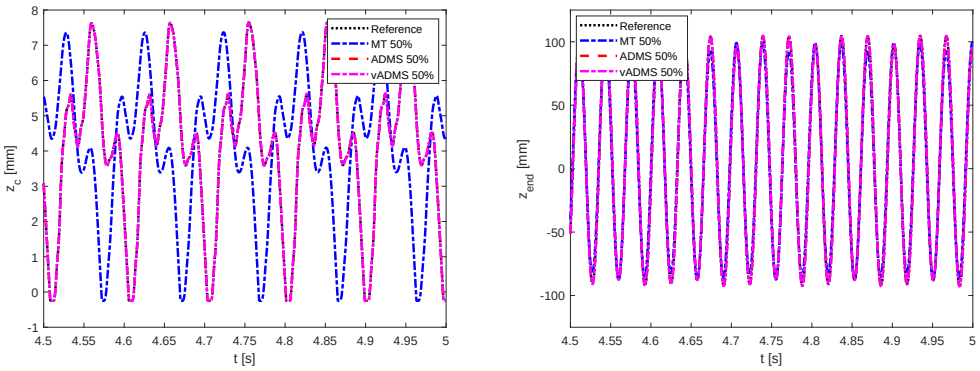

(a) Contact point displacement (b) Free end displacement

Fig. 6.24 Contact Beam, steady state response, comparison between MT, ADMS and vADMS, 50% reduction.

Figure 6.25 shows a more severe reduction, with 80% of the modes neglected, for both transient (Figure 6.25a) and steady state (Figure 6.25b) responses.

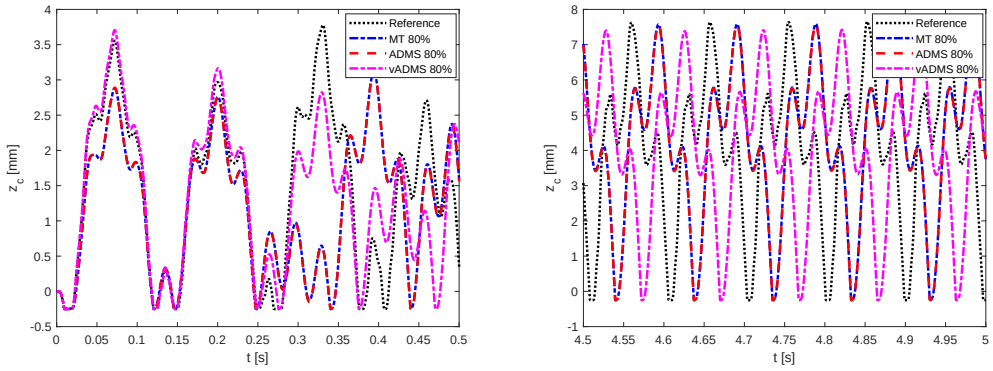

(a) Contact point, transient (b) Contact point, steady state

Fig. 6.25 Contact Beam displacements, comparison between MT, ADMS and vADMS at contact point, 80% reduction.

The error in both transient and steady state behaviours increases for all considered approaches. In this example, the differences between ADMS and vADMS approach

are highlighted, whereas for the 50% reduction example the two approaches show very similar results.

Figure 6.26 shows an evaluation of the reduction approach performances. The idea of the proposed method is to retain the overall behaviour of the original non-linear system, with no particular focus on a specific DoF: all DoFs are in fact taken into account for the calculation of the gwMSE, shown in both a linear (Figure 6.26a) and logarithmic (Figure 6.26b) scale.

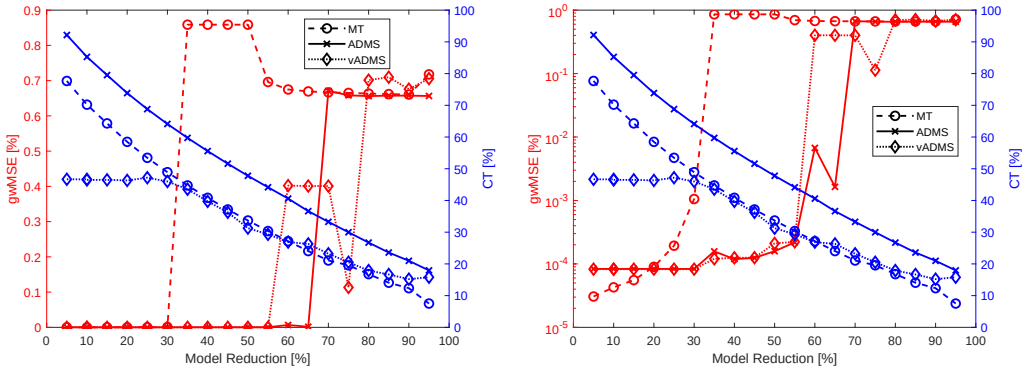

(a) Linear scale (b) Logarithmic scale

Fig. 6.26 Contact Beam, performance evaluation, percentage error (gwMSE, red) and computational time (CT, blue) as a function of the model reduction percentage.

In Figure 6.26, results clearly show the increased computational cost of the ADMS approach, due to the evaluation and mode selection procedure performed at each time span. Such fixed cost is somehow compensated, in the vADMS approach, by the number of modes used, which varies in each portion of the simulation. It also highlights the *minimum reduction* used by vADMS for any non-null prescribed reduction threshold, as discussed in Subsection 6.2.1.

6.2.3 Multiple Contacts Beam

The example proposed here considers two contact points, with a system described in Figure 6.27. The same base beam introduced in Section 6.2 (Table 6.3) is used, with additional parameters as reported in Table 6.7.

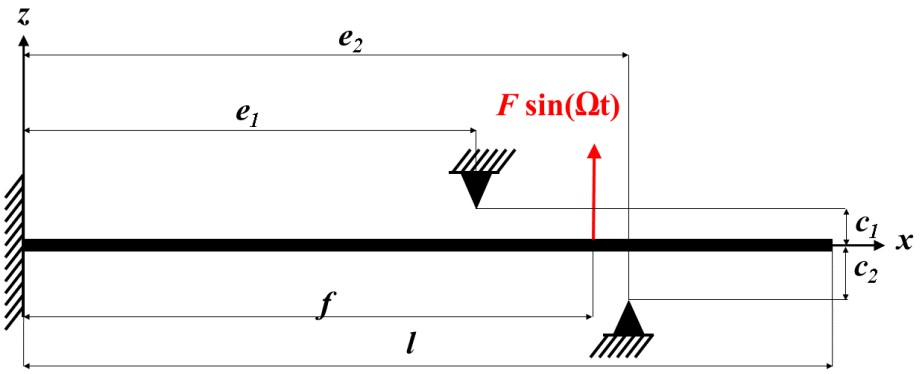

Fig. 6.27 Multiple Contacts Beam.

Table 6.7 Multiple Contacts Beam characteristics.

Name	Value
Contact 1 position (x)	$e_1 = 0.45\text{m}$
Contact 1 clearance (z)	$c_1 = 1 \times 10^{-3}\text{m}$
Contact 2 position (x)	$e_2 = 0.85\text{m}$
Contact 1 clearance (z)	$c_1 = 1.5 \times 10^{-3}\text{m}$
Force Position (x)	$f = 0.70\text{m}$
Force Amplitude	$F = 5\text{N}$
Force Pulsation	$\Omega = 31\frac{\text{rad}}{\text{s}}$ $(\approx 4.93\text{Hz})$

Four linear subsystems are used to model the non-linear system analysed:

1. Contact on e_2 only
2. No contact
3. Contact on e_1 only
4. Contact on both e_1 and e_2

Modeshapes and natural frequencies vary significantly, as shown in Figure 6.28(first two modeshapes) and reported in Table 6.8 (natural frequencies).

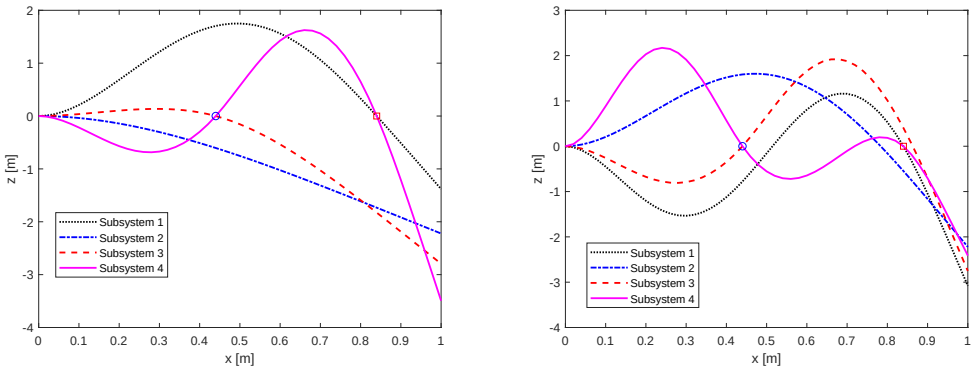

(a) 1^{st} modeshape (b) 2^{nd} modeshape

Fig. 6.28 Multiple Contacts Beam, mass-normalized modeshapes.

Table 6.8 Multiple Contacts Beam natural frequencies.

	Frequency [Hz]			
Mode	Subsys. 1	Subsys. 2	Subsys. 3	Subsys. 4
1	29.27	4.90	11.64	75.88
2	83.51	30.70	78.00	129.46
3	138.13	85.95	138.42	182.62
4	232.31	168.37	247.55	372.94

As shown in Figure 6.28, modeshapes are obtained by simply applying a Dirichlet boundary condition at the specific node, with a value equal to 0. Non-zero clearance is obtained through the asymptotic configuration x_∞, as shown in Figure 6.29. This means that a change of clearance in the system can be implemented modifying x_∞ only.

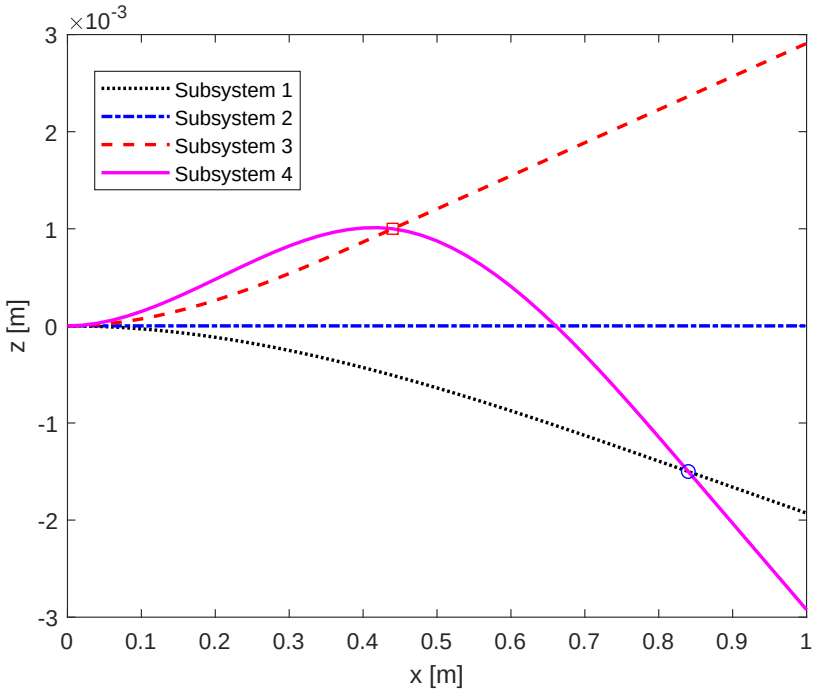

Fig. 6.29 Multiple Contacts Beam, asymptotic configurations (x_∞).

Figure 6.30 shows a comparison between the reference (dotted black) and two reduced model simulations with a reduction of 90%, with MT (dash dotted blue) and vADMS (dashed magenta) approaches.

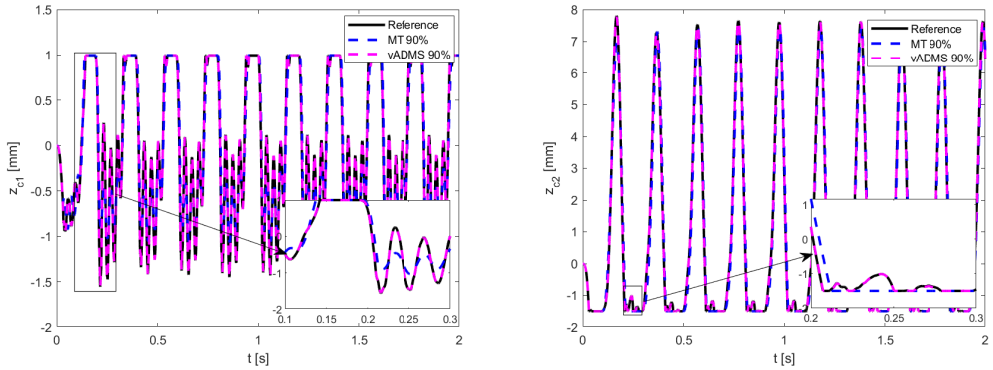

(a) Contact point 1 (b) Contact point 2

Fig. 6.30 Multiple Contacts Beam, contact displacements, comparison between MT and vADMS at contact points, 90% reduction.

A good approximation is obtained with both approaches, with the vADMS showing an almost perfect approximation ($gwMSE = 0.88\%$ in the example). Some error in correctly representing the full dynamic of the non-linear system can be observed in the MT approach ($gwMSE = 36.18\%$), highlighting the importance of the mode selection procedure. Similar results can be observed by considering the free end of the beam, as shown in Figure 6.31.

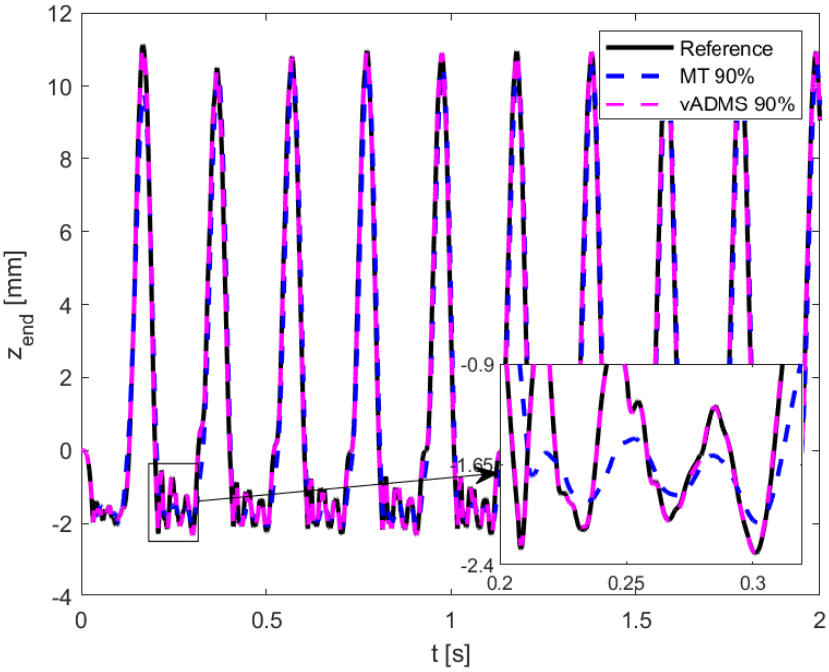

Fig. 6.31 Multiple Contacts Beam, free end displacement, comparison between MT and vADMS at contact points, 90% reduction.

Figure 6.32, finally, shows the performance of the reduction method proposed, considering MT and vADMS approaches. The expected reduction of the computational time with the increasingly reduced model is observed, as well as an increase in the percentage error.

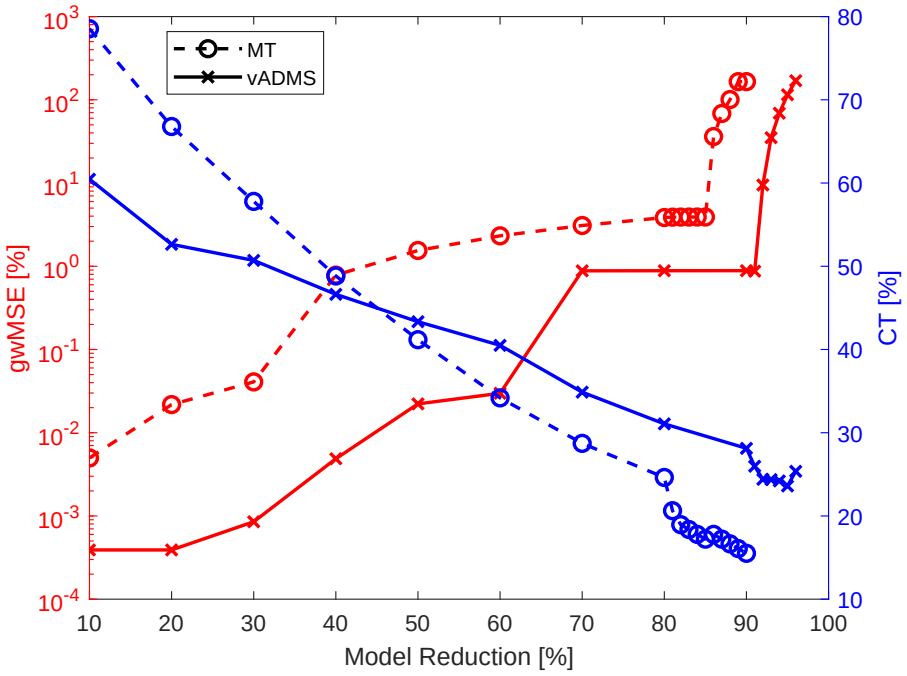

Fig. 6.32 Multiple Contacts Beam, performance evaluation, percentage error (gwMSE, red) and computational time (CT, blue) as a function of the model reduction percentage.

For a given prescribed reduction, the vADMS approach always shows a lower percentage error with respect to the MT approach. The computational time results are similar, with differences based on the different modes used and the variations in the implemented algorithms.

6.3 Continuous Levels

In this section the proposed Multi-Phi method is applied on several Continuous Level systems (CL), as defined in Subsection 4.3.1.

One of the main challenges of this kind of system is the interaction between two or more linear subsystems considered at the same time during the time integration. This involves the calculation of one or more weighting functionals, as discussed in Subsection 4.3.2. Such procedure needs to be performed at each time step, in order to describe intermediate configurations, not exactly corresponding to any linearisation

point; moreover, it is necessary to correctly evaluate the parameter(s) indicating the linear subsystem to be selected.

Contrary to the examples in Section 6.2, a linearisation error is introduced, with the non-linear characteristic which is approximated, as shown in Figure 4.1. It is possible to reduce such error by increasing the number of linearisation points. In the following examples it is investigated the convergence, obtained with higher number of linearisation points: it has to be noted that the stronger the non-linearity, the higher the number of points necessary to achieve a good approximation.

Increasing the number of linearisation points increases the cost of defining the reduced model in a straightforward manner, while the effect on the computational time in the simulation is more complexly affected. More linearisation points leads to more switch events, but the size of the problem does not change, as the number of DoFs simulated in each time span is dependent on the entity of the reduction only.

6.3.1 Cubic Stiffness Beam

Starting from the beam described in Section 6.2, with the characteristics reported in Table 6.3, a non-linear system is obtained by means of a cubic spring, with the additional characteristics listed in Table 6.9. A schematic of the system is shown in Figure 6.33, while the non-linear spring characteristic is shown in Figure 6.34.

Table 6.9 Cubic Stiffness Beam characteristics.

Name	Value
Non-linear spring Position (x)	$e = 0.65\text{m}$
Force Position (x)	$f = 0.50\text{m}$
Force Amplitude	$F = 10\text{N}$
Force Pulsation	$\Omega = 40\frac{\text{rad}}{\text{s}}$ $(\approx 6.37\text{Hz})$
Stiffness Coefficients	$k_1 = 750\frac{\text{N}}{\text{m}}$ $k_{3,UP} = 3 \times 10^7 \frac{\text{N}}{\text{m}^3}$ | $k_{3,DW} = 7.5 \times 10^7 \frac{\text{N}}{\text{m}^3}$

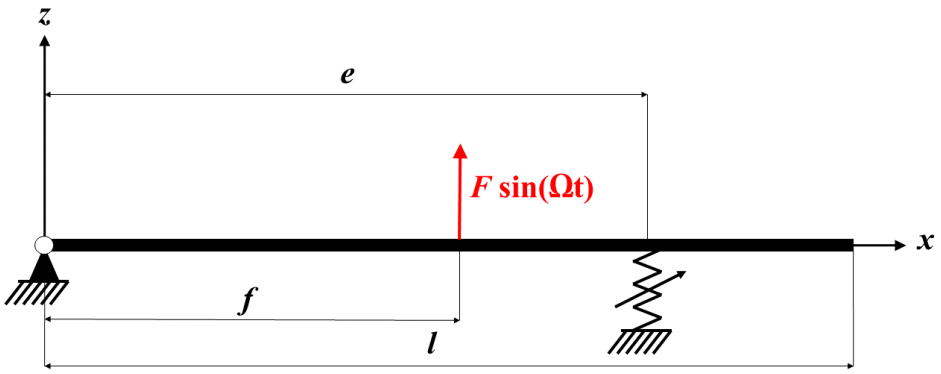

Fig. 6.33 Cubic Stiffness Beam, non-linear cubic spring beam.

As shown in Figure 6.34, a non-symmetric non-linear spring is considered, with a stiffness described by Figure 6.34a, which gives a non-linear characteristic as shown in Figure 6.34b

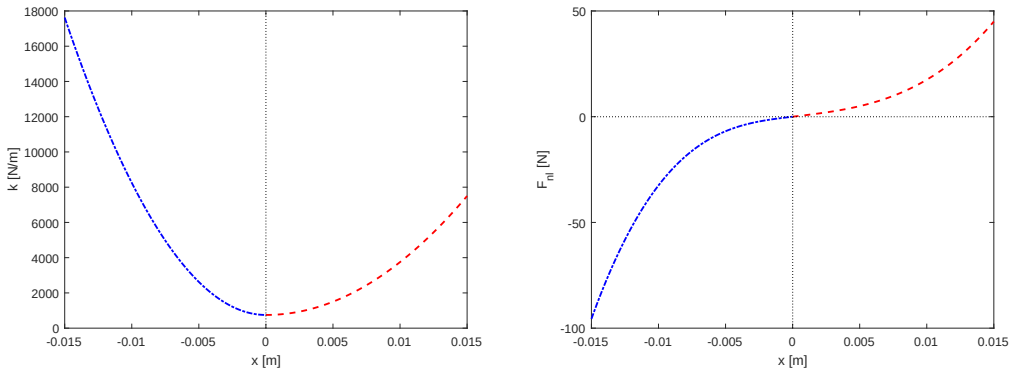

(a) Non-linear stiffness (b) Non-linear force

Fig. 6.34 Cubic Stiffness Beam, non-linear stiffness characteristic.

Modal properties of the system vary depending on the spring elongation Δx; Table 6.10 reports the first 2 natural frequencies of the linear system ($\Delta x = 0$) and of the linearised one, corresponding to minimum ($\Delta x = min$) and maximum ($\Delta x = max$) elongation.

Table 6.10 Cubic Stiffness Beam natural frequencies.

	Frequency [Hz]		
Mode	$\Delta x = 0$	$\Delta x = min$	$\Delta x = max$
1	5.48	14.36	10.56
2	21.62	23.17	22.11

The corresponding modeshapes are also a function of the spring elongation and are shown in Figure 6.35, highlighting how the modal matrix is different for each linearised subsystem. The position of the attachment point of the non-linear spring is highlighted with a vertical dotted black line.

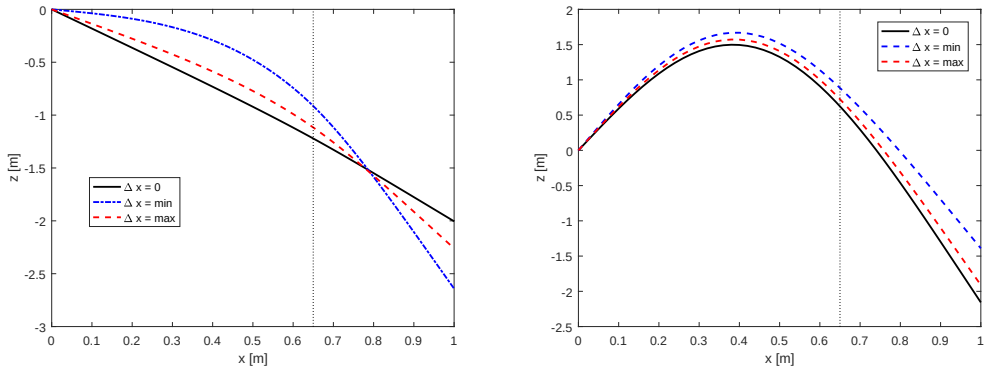

(a) 1^{st} modeshape (b) 2^{nd} modeshape

Fig. 6.35 Cubic Stiffness Beam, linearised modeshapes, for $\Delta x = 0$ (solid black line) $\Delta x = min$ (dash dotted blue line) $\Delta x = max$ (dashed red line).

A non-reduced model is considered to estimate the linearisation error, which is then used to evaluate the model reduction performance. Figure 6.36 shows the results in terms of displacement of the free end (z_{end}), obtained with several numbers of linearisation points.

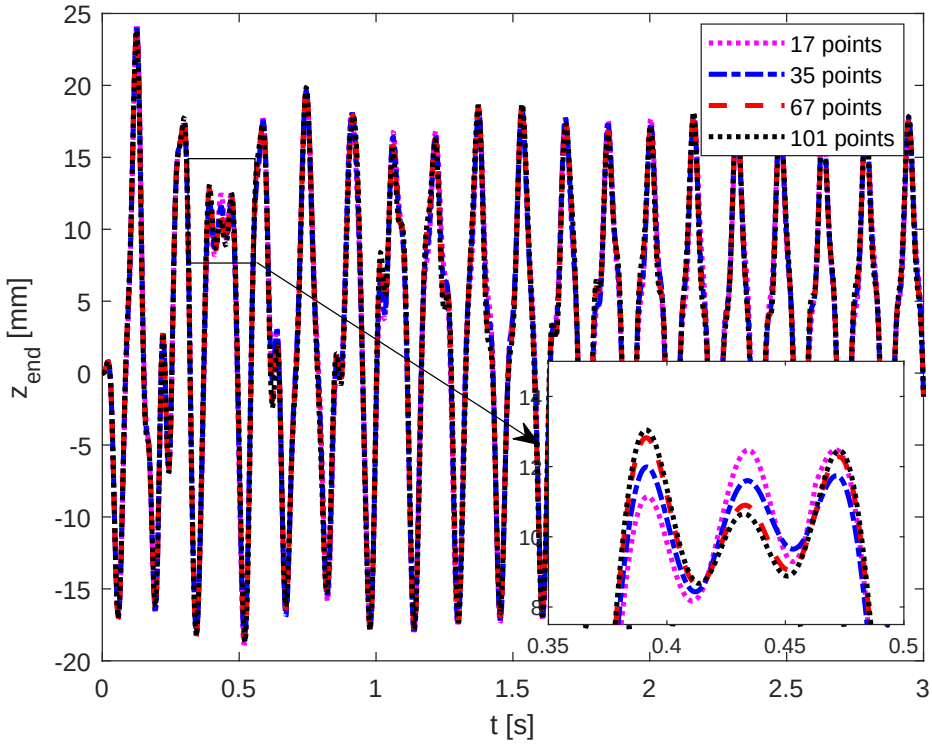

Fig. 6.36 Cubic Stiffness Beam, free end displacements for several non-reduced models.

The results suggest that a reasonable convergence can be reached. The linearisation point non-reduced model with 101 points is in the following used as reference. Figure 6.37 shows the performance of the proposed reduction algorithm (using the MT approach) for a low reduction level (10%) and several numbers of linearisation points.

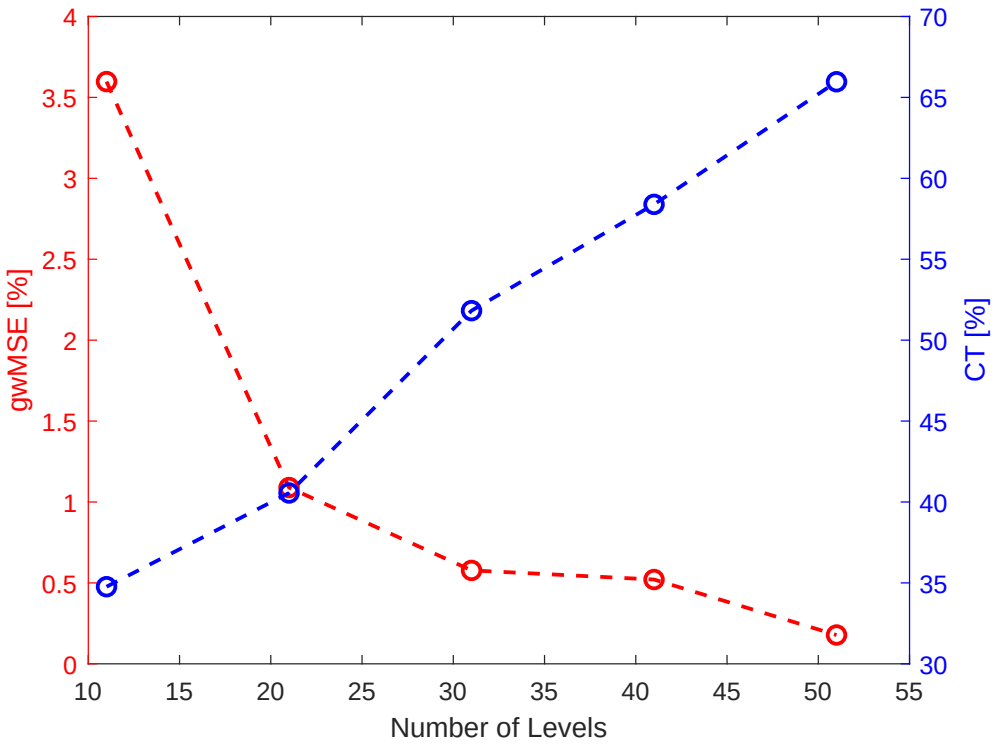

Fig. 6.37 Cubic Stiffness Beam, performance evaluation with 10% reduction (MT).

Figure 6.38 shows a longer simulation (10 seconds) obtained with the reference non-reduced model, showing the transient portion (Figure 6.38a) and the steady state one (Figure 6.38b), indicating a non-linear behaviour.

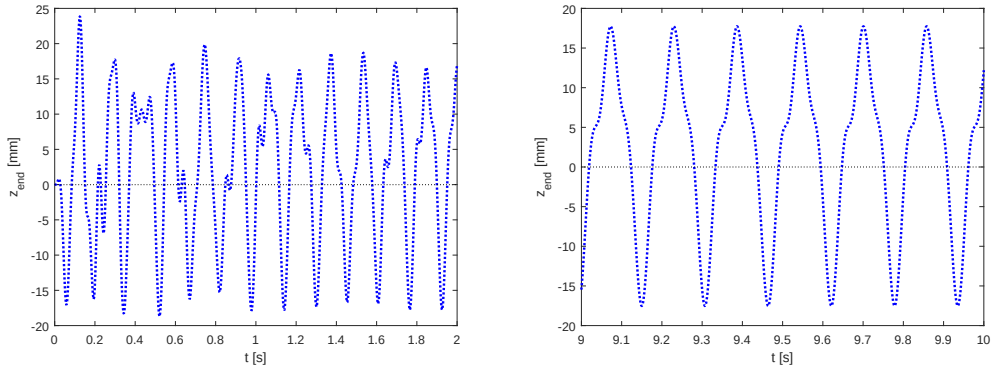

(a) Transient (b) Steady state

Fig. 6.38 Cubic Stiffness Beam, comparison between reference (dashed red), a 51 linearisation points non-reduced model (dotted black) and MT, with 90% reduction and 51 linearisation points.

In order to further highlight the non-linearity of the system, Figure 6.39 shows the frequency contents of the steady state response, which exhibits multiple frequencies, in addition to the external force one.

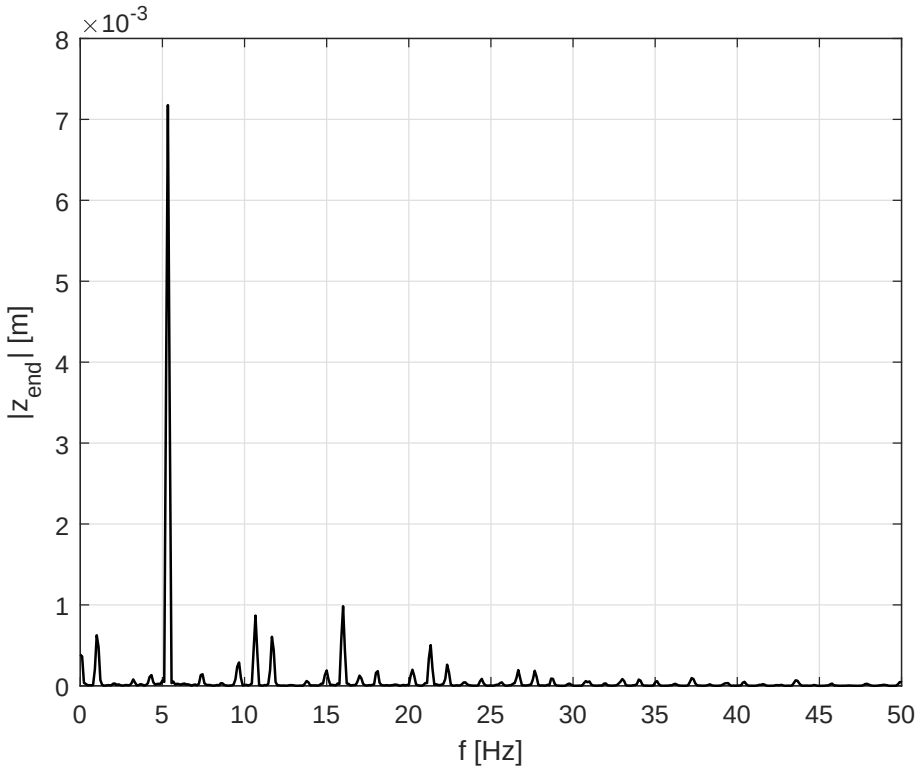

Fig. 6.39 Cubic Stiffness Beam, frequency contents analysis.

Figure 6.40 shows a comparison of the free end displacement between the reference, as defined above, and a 90% reduction case. A 51 linearisation point non-reduced case is added to the comparison, highlighting that the error is mainly due to the linearisation procedure, rather than to the reduction one.

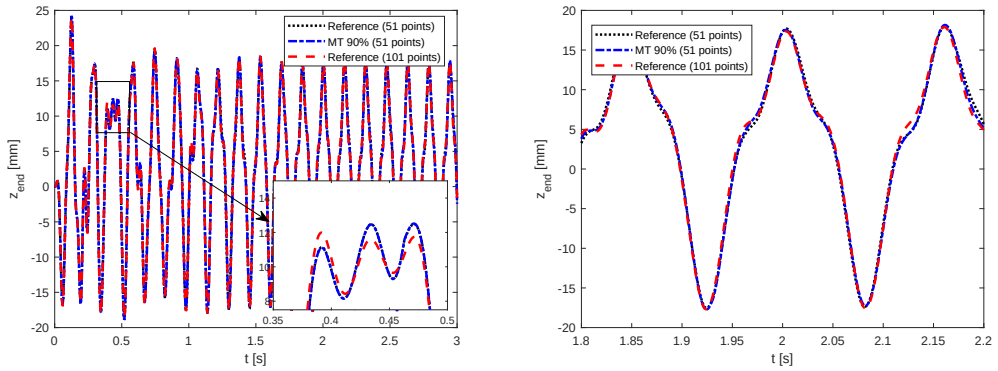

(a) Free end displacement

(b) Free end displacement, steady state

Fig. 6.40 Cubic Stiffness Beam, comparison between reference (dashed red), a 51 linearisation points non-reduced model (dotted black) and MT, with 90% reduction and 51 linearisation points.

An analysis of the model reduction method performance is proposed in Figure 6.41, in which the MT and the ADMS approaches are applied with several reduction levels. The same 51 linearisation point model is used.

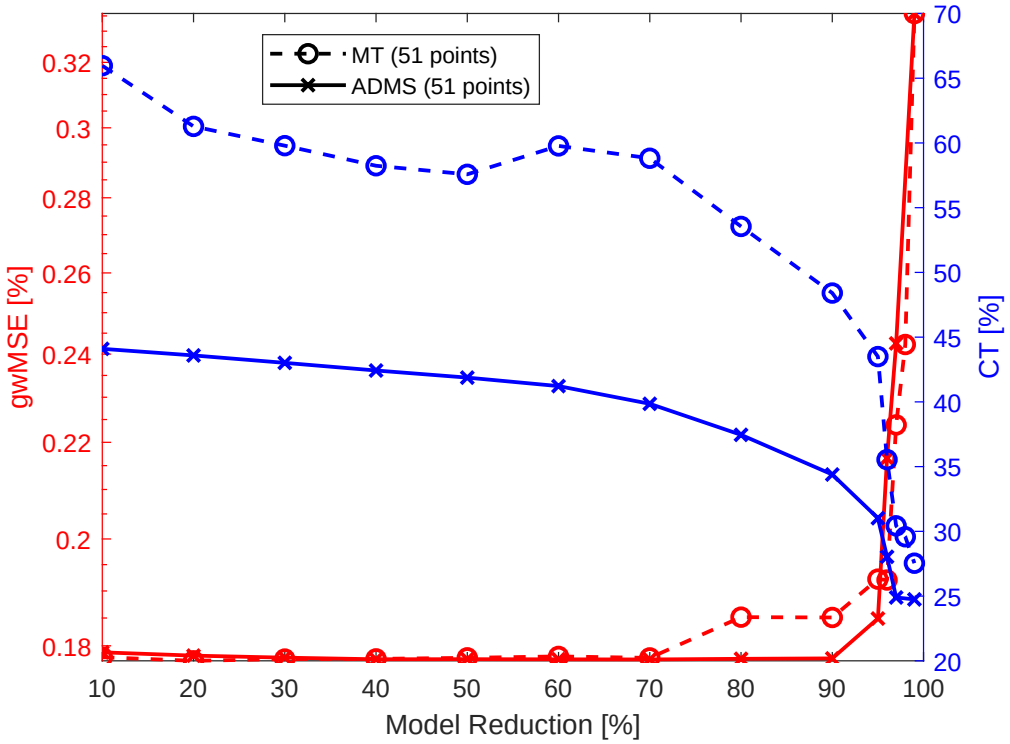

Fig. 6.41 Cubic Stiffness Beam with 51 linearisation points performance evaluation, percentage error (gwMSE, red) and computational time (CT, blue) as a function of the model reduction percentage.

It is interesting to observed how, with the same percentage error, the ADMS approach guarantees reduced computational time. This may be due to specificity in the implemented algorithms. Figure 6.42 shows the performance analysis of the ADMS approach by varying the number of linearisation points.

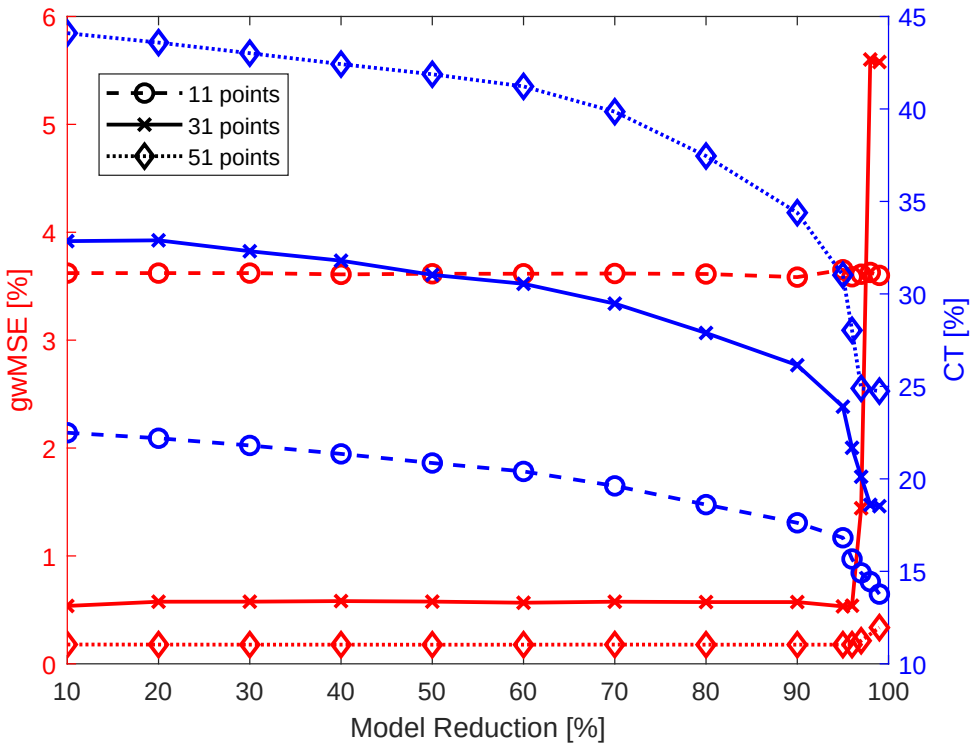

Fig. 6.42 Cubic Stiffness Beam, ADMS performance evaluation, percentage error (gwMSE, red) and computational time (CT, blue) as a function of the model reduction percentage.

As expected, the computational time increases with the number of linearisation points, while the percentage error decreases. The model reduction further decreases the computational time, maintaining a constant percentage error up to reductions greater than 90%.

6.3.2 Multiple Springs Beam

In the last example considered, the number of springs is increased, adding another spring, identical to the one used in Subsection 6.3.1 but in a different location, as indicated in Table 6.11.

Table 6.11 Multiple Springs Beam characteristics.

Name	Value
Non-linear Position, spring 1 (x)	$e_1 = 0.40\text{m}$
Non-linear Position, spring 2 (x)	$e_2 = 0.90\text{m}$
Force Position (x)	$f = 0.60\text{m}$
Force Amplitude	$F = 25\text{N}$
Force Pulsation	$\Omega = 60\frac{\text{rad}}{\text{s}}$ $(\approx 9.55\text{Hz})$
Stiffness Coefficients	$k_1 = 1000\frac{\text{N}}{\text{m}}$ $k_{3,UP} = 3 \times 10^7 \frac{\text{N}}{\text{m}^3}$ | $k_{3,DW} = 7.5 \times 10^7 \frac{\text{N}}{\text{m}^3}$

Figure 6.43 shows the non-linear system considered.

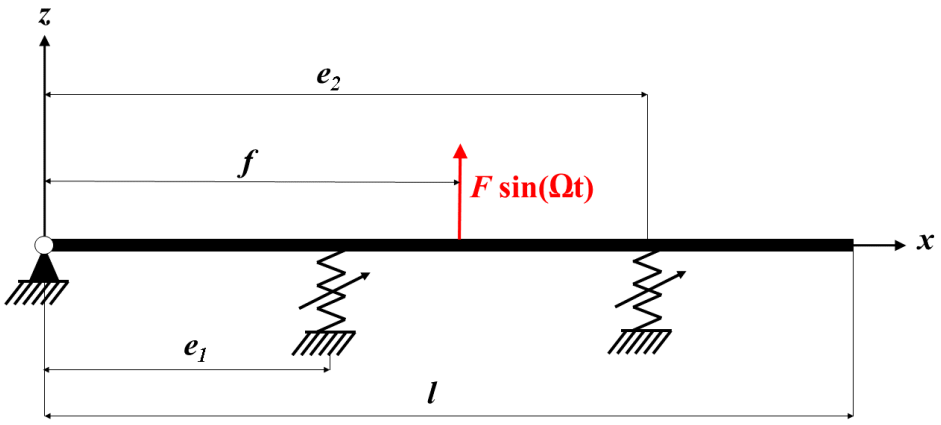

Fig. 6.43 Multiple Springs Beam, natural frequencies.

Natural frequencies depend on the elongation of the two springs, varying according to the combination of the displacements at the two spring connection points (Δx_1 and Δx_2), as shown in Figure 6.44.

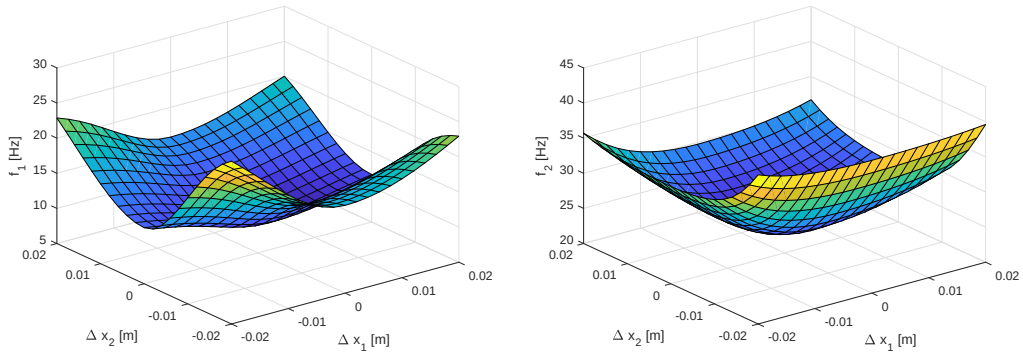

(a) First natural frequency f_1 (b) Second natural frequency f_2

Fig. 6.44 First two linearised natural frequencies as a function of spring 1 (Δx_1) and spring 2 (Δx_2) elongation.

Extremes of the first two natural frequencies are reported in Table 6.12, for 0, minimum and maximum displacements of each spring attachment point (in any combination).

Table 6.12 Multiple Springs Beam natural frequencies.

	Frequency [Hz] $(\Delta x_1, \Delta x_2)$			
Mode	$(0,0)$	$(min.min)$	(max,max)	
1	9.4	28.18	20.04	
2	23.76	41.23	31.69	
Mode	$(min,0)$	$(0,min)$	$(max,0)$	$(0,max)$
1	12.92	17.49	11.76	15.76
2	33.85	38.91	28.05	29.73

Modeshapes vary accordingly, as shown in Figure 6.45, in which the effects of the two springs are considered separately. Both Figure 6.45a and Figure 6.45b show the position of the spring considered.

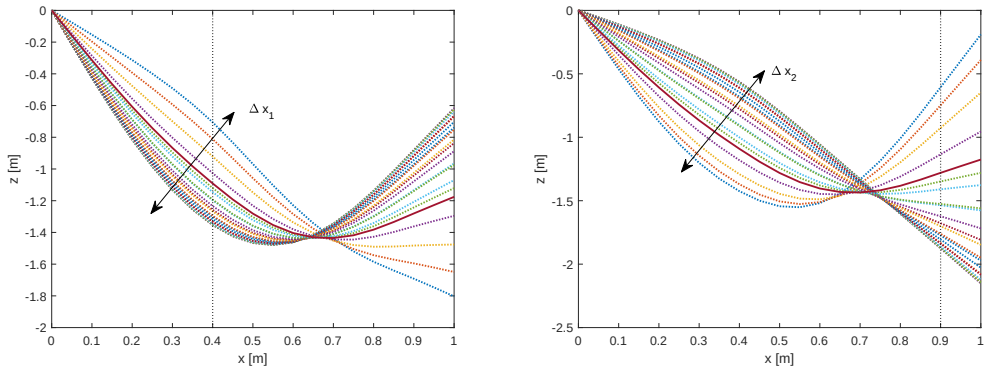

(a) Δx_1 effect (b) Δx_2 effect

Fig. 6.45 Multiple Springs Beam, modeshape variation (linear case in solid line).

As for the example proposed in Subsection 6.3.1, it is first necessary to define an adequate number of linearisation points to be used as reference. Figure 6.46 shows the free end displacement according to several non-reduced linearised models, showing similar results for more than 20 linearisation points.

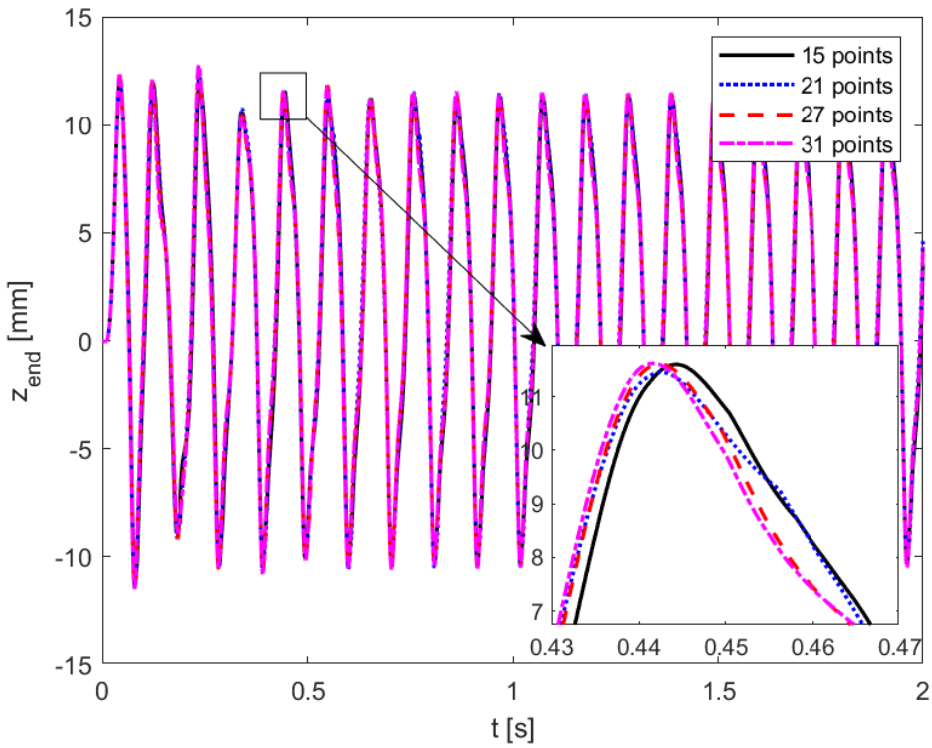

Fig. 6.46 Multiple Springs Beam, free end displacements for several non-reduced models.

To provide a more objective evaluation of the error due to the linearisation process, Figure 6.47 shows the percentage error and the associated computational time of the same non-reduced models. The reference used, for this and other evaluations, is the non-reduced model with 41 linearisation points.

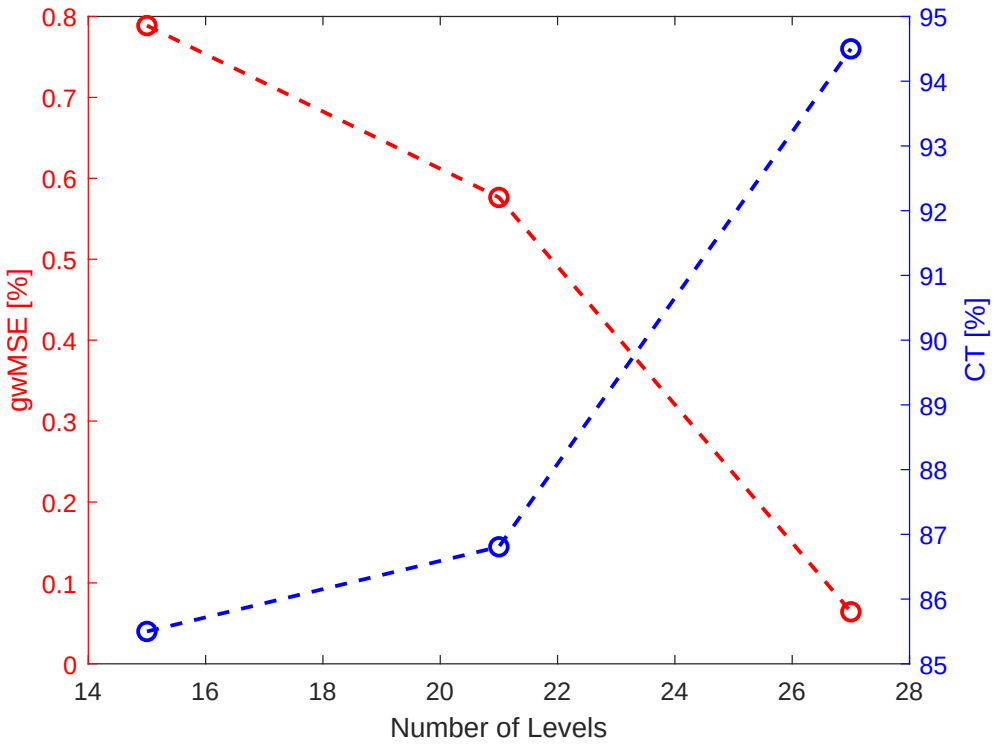

Fig. 6.47 Multiple Springs Beam, performance evaluation with 0% reduction (MT).

It is important to highlight that, as discussed in Subsection 4.3.2, the number of linear subsystems to be evaluated concurrently is equal to 2^p, with $p = 2$ in this example, so that 4 linear subsystems are integrated in each time span. The number of linear modal analyses to be performed is however lv^p, with lv as number of linearisation points. It is important to note that even if the reduce model generation needs to be performed only once, it is appropriate to maintain lv at a reasonable size. In general, the larger the number of parameters p, the lower the number of linearisation points lv, but it is possible to use the main idea of the TPWL approximation method to forecast the trajectory in the state space. By performing an inexpensive simulation first, with a low number of linearisation points, it is possible to largely reduce the number of linear subsystems to calculate, so that a new reduced model can be created, with a larger lv and improved accuracy, considering only a portion of all the possible linearised subsystems. Contrary to what proposed in TPWL, the exploratory simulation would be performed on a reduced model, resulting therefore inexpensive. Additionally, it is possible to enrich the reduced model by

adding linearisation points if needed, being each linearised subsystem independent by the others, since it uses its own reduction base.

Figure 6.48 shows the frequency content of the free end of the beam, considering the reference (41 linearisation points), highlighting how the response contains multiple harmonics due tothe system's non-linearities. A 10 second simulation was used to obtain a reasonable frequency resolution. The external force frequency is highlighted with a red circle.

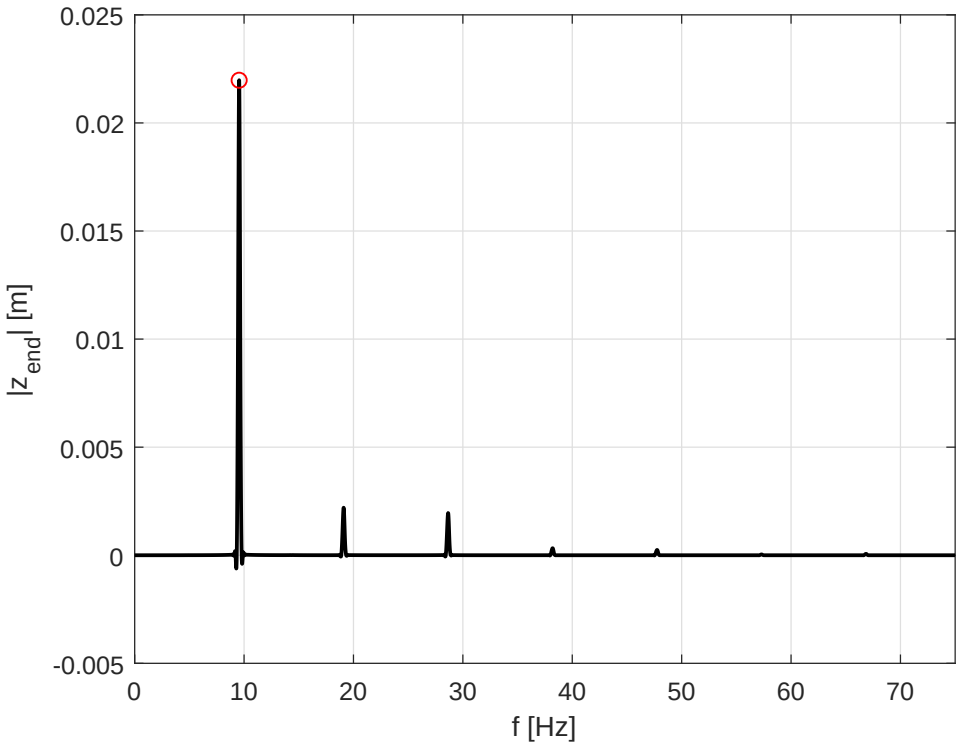

Fig. 6.48 Multiple Springs Beam, frequency content of the reference (free end displacement).

Figure 6.49 shows a comparison between the reference (solid black), MT 95% (dash dotted blue) and ADMS 95% (dashes red), highlighting a good, even if not perfect, approximation of the reference.

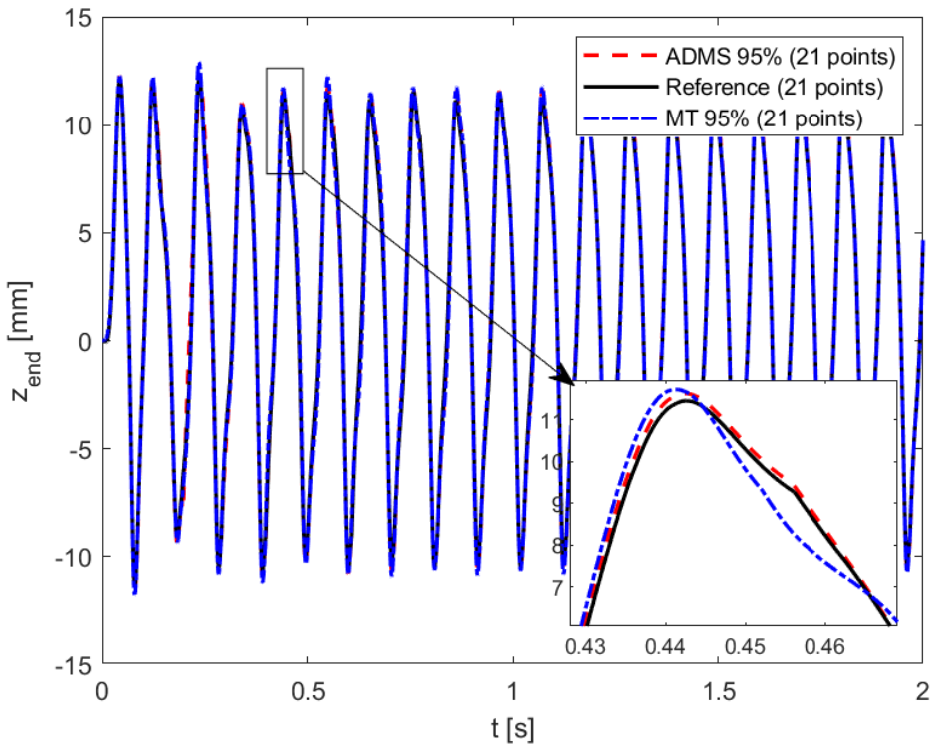

Fig. 6.49 Multiple Springs Beam, free end displacement, comparison between reference (solid black), MT 95% (dash dotted blue) and ADMS 95% (dashes red).

Figure 6.50 provides a more comprehensive evaluation of the global behaviour of the reduced model as a function of the reduction percentage, showing the percentage error (gwMSE, red) and computational time (CT, blue). The accuracy of the reduced model proves excellent even for severe reduction, with an appreciable saving in computational time.

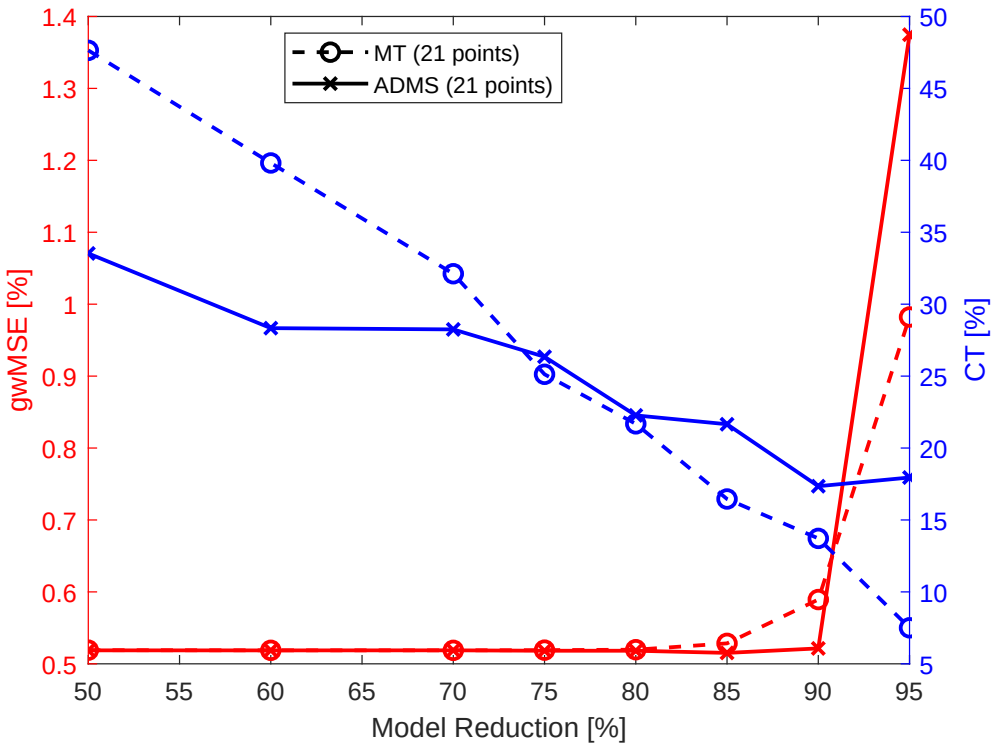

Fig. 6.50 Cubic Stiffness Beam with 21 linearisation points performance evaluation, percentage error (gwMSE, red) and computational time (CT, blue) as a function of the model reduction percentage.

In this example, MT and ADMS approaches provide similar results, as the modal truncation (MT) closely represents the best truncation available.

Chapter 7

Conclusions

In this thesis non-linear dynamic systems and the problem of their numerical simulation was addressed. Model reduction methods able to reduce the computational time while maintaining an acceptable level of accuracy were sought. The goal was to investigate and formulate methodologies allowing the use of virtual prototypes in the prototyping phase of the product development cycle. This in turn translates to a faster and/or more accurate design, leading to a reduced time to market and in more optimized products. In order to rely on the results obtained by means of the virtual prototype, it is necessary that the model used to describe the product is accurate enough, leading in most of the cases to complex non-linear models like the one studied in this thesis. Model reduction methods for this class of systems is however still an open research point, despite several proposed approaches.

In the development of the model reduction method proposed the focus was on the use of modal properties of mechanical systems; in particular, the tool of linear modal analysis was used to build a subspace on which the dynamic of the system was projected. The purpose was therefore to retain the non-linear behaviour while using a tool proper of linear analysis. Another key assumption used in the development of the novel method proposed was the evaluation of the whole system, with the objective of laying the foundations for a tool to be effectively used in a virtual prototyping environment, part of the design and development process.

A double approach was then followed, pursuing the implementation of a method which used fixed and linear modeshapes coupled with non-linear equations of motion

and the development of another method, which used variable linear modeshapes with linear equations of motion.

The first method, described in Chapter 3, used the assumption of cubic equations of motion in modal coordinates to retain system's non-linearities. Such an assumption proved to be appropriate for the class of systems considered, which was the one of geometrically non-linear structures. A beam model representing this category, by means of the von Kármán non-linearity was developed and tested in Section 3.1, and showed the ability to describe geometrically non-linear behaviours. The method of modal coefficients was then implemented in Section 3.2, deriving and providing all the necessary equations. A static assessment of the reduced model, compared with the full non-linear one, was provided in Subsection 3.3.1, and showed convergence between the full and the reduced non-linear models for a small amount of modes. From a dynamic point of view a comparison with experimental data was proposed in Subsection 3.3.2, showing a good approximation and identifying possible reasons of the non-perfect correspondence.

The second method, named Multi-Phi, represented the attempt of obtaining linear equations of motion while describing non-linear systems, with the use of a linearisation procedure. This first stage of the Multi-Phi method was described in Chapter 4, together with details about the switch between linear subsystems of their interaction. This part of the thesis dealt with the description of a non-linear system by means of a linear time variant one and of its approximation via a convolution of linear time invariant models.
The reduction of this linearised model was considered in Chapter 5, in which several criteria in the modes to retain and those to neglect were developed. Alongside a classic modal truncation approach, a criterion based on energetic considerations was proposed and implemented by means of 3 practical algorithm (AMS, ADMS, vADMS). In this chapter, moreover, performance evaluation indicators were introduced, in order to assess the effectiveness and efficiency of the reduction method.

In Chapter 6 the Multi-Phi method was applied to several numerical examples, analysing performance and characteristics. Despite the simplicity of the examples proposed (and the nature of the tools used in the implementation), the base idea has proved to be founded, showing an effective reduction of the computational burden with a reasonable accuracy.

Several conclusions can be drawn based on the results obtained. A first remark concerns the computational time, which was observed to be caused by several factors, summarized in the following categories:

- number of DoFs simulated
- number of linear subsystems concurrently used (CL only)
- number of level switches
- condition number of the matrices

The influence of the model reduction on the number of DoFs is straightforward, even though the vADMS method proved to be more difficultly to predict. The main effect of the model reduction is obtained in this point, but other factors significantly influence the performance.

If the continuous levels approach (CL) is used, the number of parameters used in detecting the system state influences the reduction of the computational time, since it increases the number of linear subsystems to be concurrently evaluated. This can be considered as one of the most critical points of the Multi-Phi method, if it is not possible to identify a very limited number of parameters able to describe the system non-linearity.

The number of switch events has an influence on the total computational time, as a fixed computational cost is associated with each of them. This is particularly important for ADMS and vADMS approaches, which retain all the computed modes, despite using only a fraction of them in the time integration. All modes are however used to describe the system's configuration at the switch event, so that the higher the number of switches, the lower the computational time saved.

A final point which may influence the computational time is related to the condition number of the matrices used in the time integration. It is proportional to the difference between the first and the last eigenvalues, so that it depends on the entity of the reduction (the higher the reduction, the lower the condition number) and on the approach used. MT, in fact, always cut the higher frequency modes, while the other approaches could retain the first and the last ones, maintaining the same condition number. Higher condition numbers reduce the accuracy of matrix operations and require smaller time steps due to the high dynamic involved.

Comparing the proposed approaches, vADMS was proven to be particularly effective when applied to systems with very different modeshapes, for which the energy distribution varied significantly. On the contrary, for non-linear systems with gradually varying modeshapes (such the CL examples) having a variable number of modes considered did not prove beneficial, especially given the computational costs associated. In this situation the MT approach has proved to be effective, despite being the least elaborate.

The AMS approach was not used in the proposed example, despite being tested. It resulted to be difficult to forecast which modes would not be important in the system description, especially in contact examples. In these cases, a large number of modes were *activated* during the level switches as a consequence of the modeshape differences and not by the external forces. This approach served however as starting point for ADMS and vADMS.

At the conclusion of this thesis, several open points can be addressed. Firstly, in order to fully understand the efficiency of the proposed method, it is necessary to provide a more meaningful evaluation of all its characteristics. It is for example assumed that additional computational time could be saved as a consequence of using linear uncoupled equation of motion, but it is necessary to use or develop simulation tools able to fully exploit this characteristic, which could result extremely beneficial. The algorithm used should then be perfected, especially for the switch events and their detection, which has proven to be a critical point in the current implementation. Lastly, given the simplicity of the examples proposed, it is important to extend to more complex as well as real-world examples, possibly comparing the method performance with commercial software. The use of MATLAB resulted adequate for the implementation of the main idea, but it had limitations in offering a realistic comparison with other more perfected methods or simply with more complex and large examples.

References

[1] G. Ferrari, S. Le Guisquet, P. Balasubramanian, M. Amabili, B. Painter, and K. Karazis. Identification of non-linear parameters of a nuclear fuel rod. In *ASME 2017 International Mechanical Engineering Congress and Exposition*, pages V04AT05A041–V04AT05A041. American Society of Mechanical Engineers, 2017.

[2] O. C. Zienkiewicz and R. L. Taylor. *The finite element method for solid and structural mechanics*. Butterworth-heinemann, 2005.

[3] O. C. Zienkiewicz. *The Finite Element Method in Structural and Continum Mechanics: Numerical Solution of Problems in Structural and Continuum Mechanics*. McGraw-Hill, 1967.

[4] Rayleigh. *The theory of sound, vols. I and II*. Dover Publications, New York, 1945.

[5] M. Géradin and D. Rixen. *Mechanical vibrations Theory and Application to Structural Dynamics*. Wiley, New York, 1997.

[6] A. K. Noor and J. M. Peters. Reduced basis technique for nonlinear analysis of structures. *Aiaa journal*, 18(4):455–462, 1980.

[7] A. K. Noor. Recent advances in reduction methods for nonlinear problems. *Computers & Structures*, 13(1-3):31–44, 1981.

[8] P. M. A. Slaats, J. De Jongh, and A. A. H.J Sauren. Model reduction tools for nonlinear structural dynamics. *Computers & structures*, 54(6):1155–1171, 1995.

[9] L. D. Flippen. A theory of condensation model reduction. *Computers & mathematics with applications*, 27(2):9–40, 1994.

[10] J. R. Phillips. Model reduction of time-varying linear systems using approximate multipoint krylov-subspace projectors. In *Computer-Aided Design, 1998. ICCAD 98. Digest of Technical Papers. 1998 IEEE/ACM International Conference on*, pages 96–102. IEEE, 1998.

[11] R. Kappagantu and B. F. Feeny. An" optimal" modal reduction of a system with frictional excitation. *Journal of Sound and Vibration*, 224(5):863–877, 1999.

[12] M. P. Mignolet, A. G. Radu, and X. Gao. Validation of reduced order modeling for the prediction of the response and fatigue life of panels subjected to thermo-acoustic effects. In *Proceedings of the 8th International Conference on Recent Advances in Structural Dynamics*, pages 14–16, 2003.

[13] A. Radu, B. Yang, K. Kim, and M. P. Mignolet. Prediction of the dynamic response and fatigue life of panels subjected to thermo-acoustic loading. In *Proceedings of the 45th Structures, Structural Dynamics, and Materials Conference*, pages 19–22, 2004.

[14] C. Touzé and M. Amabili. Nonlinear normal modes for damped geometrically nonlinear systems: application to reduced-order modelling of harmonically forced structures. *Journal of sound and vibration*, 298(4):958–981, 2006.

[15] M. P. Mignolet and C. Soize. Stochastic reduced order models for uncertain geometrically nonlinear dynamical systems. *Computer Methods in Applied Mechanics and Engineering*, 197(45):3951–3963, 2008.

[16] J. Degroote, J. Vierendeels, and K. Willcox. Interpolation among reduced-order matrices to obtain parameterized models for design, optimization and probabilistic analysis. *International Journal for Numerical Methods in Fluids*, 63(2):207–230, 2010.

[17] G. H. K. Heirman, T. Tamarozzi, and W. Desmet. Static modes switching for more efficient flexible multibody simulation. *International Journal for Numerical Methods in Engineering*, 87(11):1025–1045, 2011.

[18] T. Tamarozzi, G. H. K. Heirman, and W. Desmet. Static modes switching: on-line variable static augmentation for efficient flexible multibody simulation. *Proceedings of ASME IDETC/CIE*, 2011.

[19] T. Tamarozzi, P. Ziegler, P. Eberhard, and W. Desmet. Static modes switching in gear contact simulation. *Mechanism and Machine Theory*, 63:89–106, 2013.

[20] R. Sternfels and C. J. Earls. Reduced-order model tracking and interpolation to solve pde-based bayesian inverse problems. *Inverse Problems*, 29(7):075014, 2013.

[21] C. Farhat, P. Avery, T. Chapman, and J. Cortial. Dimensional reduction of non-linear finite element dynamic models with finite rotations and energy-based mesh sampling and weighting for computational efficiency. *International Journal for Numerical Methods in Engineering*, 98(9):625–662, 2014.

[22] M. Mohammadali and H. Ahmadian. Efficient model order reduction for dynamic systems with local nonlinearities. *Journal of Sound and Vibration*, 333(6):1754–1766, 2014.

[23] M. Rösner, R. Lammering, and R. Friedrich. Dynamic modeling and model order reduction of compliant mechanisms. *Precision Engineering*, 42:85–92, 2015.

[24] J. Shen and J. Lam. Improved results on h inf model reduction for continuous-time linear systems over finite frequency ranges. *Automatica*, 53:79–84, 2015.

[25] M. Amabili. Reduced-order models for nonlinear vibrations, based on natural modes: the case of the circular cylindrical shell. *Phil. Trans. R. Soc. A*, 371(1993), 2013.

[26] M. P. Mignolet, A. Przekop, S. A. Rizzi, and S. M. Spottswood. A review of indirect/non-intrusive reduced order modeling of nonlinear geometric structures. *Journal of Sound and Vibration*, 332(10):2437–2460, 2013.

[27] B. Besselink, U. Tabak, A. Lutowska, N. van de Wouw, H. Nijmeijer, D. J. Rixen, M.E. Hochstenbach, and W. H. A. Schilders. A comparison of model reduction techniques from structural dynamics, numerical mathematics and systems and control. *Journal of Sound and Vibration*, 332(19):4403–4422, 2013.

[28] T. Aizad, O. Maganga, M. Sumisławska, and K. J. Burnham. *A comparative Study of Model-Based and Data-Based Model Order Reduction Techniques for Nonlinear Systems*, pages 83–88. Springer, 2015.

[29] T. Aizad, M. Sumisławska, O. Maganga, O. Agbaje, N. Phillip, and K. J. Burnham. Investigation of model order reduction techniques: A supercapacitor case study. In *Advances in Systems Science*, pages 795–804. Springer, 2014.

[30] P. Benner, S. Gugercin, and K. Willcox. A survey of projection-based model reduction methods for parametric dynamical systems. *SIAM review*, 57(4):483–531, 2015.

[31] W. Schilders. Introduction to model order reduction. *Model order reduction: theory, research aspects and applications*, pages 3–32, 2008.

[32] D. Rixen. High order static correction modes for component mode synthesis. In *Fifth World Congress on Computational Mechanics, Vienna, Austria, July*, pages 7–12, 2002.

[33] D. C. Kammer, M. S. Allen, and R. L. Mayes. Formulation of an experimental substructure model using a craig–bampton based transmission simulator. *Journal of Sound and Vibration*, 359:179–194, 2015.

[34] R. Craig. A review of time-domain and frequency-domain component mode synthesis method. 1985.

[35] L. Nechak, H. F. Raynaud, and C. Kulcsár. Model order reduction of random parameter-dependent linear systems. *Automatica*, 55:95–107, 2015.

[36] G. Wang, V. Sreeram, and W. Q. Liu. A new frequency-weighted balanced truncation method and an error bound. *IEEE Transactions on Automatic Control*, 44(9):1734–1737, 1999.

[37] M. G. Safonov and R. Y. Chiang. A schur method for balanced-truncation model reduction. *IEEE Transactions on Automatic Control*, 34(7):729–733, 1989.

[38] K. Glover. All optimal hankel-norm approximations of linear multivariable systems and theirl_∞-error bounds. *International journal of control*, 39(6):1115–1193, 1984.

[39] G. Kerschen, J. C. Golinval, A. F. Vakakis, and L. A. Bergman. The method of proper orthogonal decomposition for dynamical characterization and order reduction of mechanical systems: an overview. *Nonlinear dynamics*, 41(1):147–169, 2005.

[40] G. Berkooz, P. Holmes, and J. L. Lumley. The proper orthogonal decomposition in the analysis of turbulent flows. *Annual review of fluid mechanics*, 25(1):539–575, 1993.

[41] D. D. Kosambi. Statistics in function space. 7:76–88, 1943.

[42] K. Karhunen. *Über lineare Methoden in der Wahrscheinlichkeitsrechnung*, volume 37. Universitat Helsinki, 1947.

[43] M. Loéve. *Fonctions Aléatoires du Second Ordre*. Gauthier-Villars, Paris, 1948.

[44] V. S. Pougachev. General theory of the correlations of random functions. *Izvestiya Akademii Nauk USSR*, 17:401–402, 1953.

[45] A. M. Obukhov. Statistical description of continuous fields. *Transactions of the Geophysical International Academy Nauk USSR*, 24:3–42, 1954.

[46] S. Watanabe. Karhunen-loeve expansion and factor analysis. In *Transactions of the 4th Prague Conference on Information Theory, Statistical Decision Functions, and Random Processes, Prague, 1965*, 1965.

[47] A. I. Mees, P. E. Rapp, and L. S. Jennings. Singular-value decomposition and embedding dimension. *Physical Review A*, 36(1):340, 1987.

[48] B. Ravindra. Comments on "on the physical interpretation of proper orthogonal modes in vibrations". *Journal of Sound and Vibration*, 219:189–192, 1999.

[49] J. L. Lumley. Stochastic tools in turbulenceacademic press. *New York*, 1970.

[50] P. Holmes, J. L. Lumley, and G. Berkooz. Turbulence, coherent structures, dynamical systems and symmetry, 1996.

[51] M. A. Davies and F. C. Moon. *Solitons, chaos, and modal interactions in periodic structures*. World Scientific, Singapore, 1997.

[52] M. F. A. Azeez and A. F. Vakakis. Numerical and experimental analysis of a continuous overhung rotor undergoing vibro-impacts. *International journal of non-linear mechanics*, 34(3):415–435, 1999.

[53] A. Steindl and H. Troger. Methods for dimension reduction and their application in nonlinear dynamics. *International Journal of Solids and Structures*, 38(10):2131–2147, 2001.

[54] Y. C. Liang, H. P. Lee, S. P. Lim, W. Z. Lin, K. H. Lee, and C. G. Wu. Proper orthogonal decomposition and its applications—part i: Theory. *Journal of Sound and vibration*, 252(3):527–544, 2002.

[55] Y. C. Liang, W. Z. Lin, H. P. Lee, S. P. Lim, K. H. Lee, and H. Sun. Proper orthogonal decomposition and its applications–part ii: Model reduction for mems dynamical analysis. *Journal of Sound and Vibration*, 256(3):515–532, 2002.

[56] M. Amabili, A. Sarkar, and M. P. Paıdoussis. Reduced-order models for nonlinear vibrations of cylindrical shells via the proper orthogonal decomposition method. *Journal of Fluids and Structures*, 18(2):227–250, 2003.

[57] Y. M. Marzouk and H. N. Najm. Dimensionality reduction and polynomial chaos acceleration of bayesian inference in inverse problems. *Journal of Computational Physics*, 228(6):1862–1902, 2009.

[58] O. Ciftci. Model order reduction. Master's thesis, Auburn University, 2014.

[59] R. J. Guyan. Aiaa journal 3, 380. *Reduction of stiffness and mass matrices*, 1965.

[60] Z. Q. Qu. *Model order reduction techniques with applications in finite element analysis*. Springer Science & Business Media, 2013.

[61] R. Craig and M. Bampton. Coupling of substructures for dynamic analyses. *AIAA journal*, 6(7):1313–1319, 1968.

[62] A. C. Antoulas. *Approximation of large-scale dynamical systems*. SIAM, 2005.

[63] V. M. Adamyan, D. Z. Arov, and M. G. Krein. Analytic properties of schmidt pairs for a hankel operator and the generalized schur–takagi problem. *Matematicheskii Sbornik*, 128(1):34–75, 1971.

[64] V. M. Adamjan, D. Z. Arov, and M. G. Krein. Infinite hankel block matrices and related extension problems. *American Mathematical Society Translations*, 111:133–156, 1978.

[65] A. C. Antoulas and D. C. Sorensen. Approximation of large-scale dynamical systems: An overview. *International Journal of Applied Mathematics and Computer Science*, 11:1093–1121, 2001.

[66] C. Lanczos. *An iteration method for the solution of the eigenvalue problem of linear differential and integral operators*. United States Governm. Press Office Los Angeles, CA, 1950.

[67] W. E. Arnoldi. The principle of minimized iterations in the solution of the matrix eigenvalue problem. *Quarterly of applied mathematics*, 9(1):17–29, 1951.

[68] P. Feldmann and R. W. Freund. Efficient linear circuit analysis by padé approximation via the lanczos process. *IEEE Transactions on Computer-Aided Design of Integrated Circuits and Systems*, 14(5):639–649, 1995.

[69] Z. Bai, P. Feldmann, and R. W. Freund. Stable and passive reduced-order models based on partial padé approximation via the lanczos process. *Numerical Analysis Manuscript*, 97(3):10, 1997.

[70] R. W. Freund. Reduced-order modeling techniques based on krylov subspaces and their use in circuit simulation. In *Applied and computational control, signals, and circuits*, pages 435–498. Springer, 1999.

[71] R. W. Freund. Krylov-subspace methods for reduced-order modeling in circuit simulation. *Journal of Computational and Applied Mathematics*, 123(1):395–421, 2000.

[72] E. J. Grimme. *Krylov projection methods for model reduction*. PhD thesis, University of Illinois at Urbana-Champaign Urbana-Champaign, IL, 1997.

[73] Z. Bai. Krylov subspace techniques for reduced-order modeling of large-scale dynamical systems. *Applied numerical mathematics*, 43(1-2):9–44, 2002.

[74] G. Kerschen, M. Peeters, J. Golinval, and A. F. Vakakis. Nonlinear normal modes, part i: A useful framework for the structural dynamicist. *Mechanical Systems and Signal Processing*, 23(1):170–194, 2009.

[75] R. M. Rosenberg and C. P. Atkinson. On the natural modes and their stability in nonlinear two-degree-of-freedom systems. *Journal of Applied Mechanics*, 26(377-385):2, 1959.

[76] R. M. Rosenberg. Normal modes of nonlinear dual-mode systems. *Journal of Applied Mechanics*, 27(2):263–268, 1960.

[77] R. M. Rosenberg. On normal vibrations of a general class of nonlinear dual-mode systems. *Journal of Applied Mechanics*, 28(2):275–283, 1961.

[78] R. M. Rosenberg. The normal modes of nonlinear n-degree-of-freedom systems. *Journal of applied Mechanics*, 29(1):7–14, 1962.

[79] R. M. Rosenberg. On nonlinear vibrations of systems with many degrees of freedom. *Advances in applied mechanics*, 9:155–242, 1966.

[80] Y. V. Mikhlin. The joining of local expansions in the theory of non-linear oscillations. *Journal of Applied Mathematics and Mechanics*, 49(5):567–571, 1985.

[81] L. I. Manevich, Y. V. Mikhlin, and V. N. Pilipchuk. The method of normal oscillation for essentially nonlinear systems, 1989.

[82] A. F. Vakakis. *Analysis and identification of linear and nonlinear normal modes in vibrating systems*. PhD thesis, California Institute of Technology, 1991.

[83] L. Jezequel and C. H. Lamarque. Analysis of non-linear dynamical systems by the normal form theory. *Journal of sound and vibration*, 149(3):429–459, 1991.

[84] S. W. Shaw and C. Pierre. Non-linear normal modes and invariant manifolds. *Journal of sound and Vibration*, 150(1):170–173, 1991.

[85] Y. V. Mikhlin. Matching of local expansions in the theory of non-linear vibrations. *Journal of Sound and Vibration*, 182(4):577–588, 1995.

[86] A. A. Muravyov, T. L. Turner, J. H. Robinson, and S. A. Rizzi. A new stochastic equivalent linearization implementation for prediction of geometrically nonlinear vibrations. 1999.

[87] A. A. Muravyov. Determination of nonlinear stiffness coefficients for finite element models with application to the random vibration problem. 1999.

[88] A. A. Muravyov and S. A. Rizzi. Determination of nonlinear stiffness with application to random vibration of geometrically nonlinear structures. *Computers & Structures*, 81(15):1513–1523, 2003.

[89] M. I. McEwan, J. R. Wright, J. E. Cooper, and A. Y. T. Leung. A combined modal/finite element analysis technique for nonlinear beam dynamic response under harmonic excitation. In *NASA CONFERENCE PUBLICATION*, pages 13–22. NASA, 1999.

[90] A. Lazarus, O. Thomas, and J. F. Deü. Finite element reduced order models for nonlinear vibrations of piezoelectric layered beams with applications to nems. *Finite Elements in Analysis and Design*, 49(1):35–51, 2012.

[91] M. Rewienski and J. White. A trajectory piecewise-linear approach to model order reduction and fast simulation of nonlinear circuits and micromachined devices. In *Computer Aided Design, 2001. ICCAD 2001. IEEE/ACM International Conference on*, pages 252–257. IEEE, 2001.

[92] P. Julian, A. Desages, and O. Agamennoni. High-level canonical piecewise linear representation using a simplicial partition. *IEEE Transactions on Circuits and Systems I: Fundamental Theory and Applications*, 46(4):463–480, 1999.

[93] A. Rantzer and M. Johansson. Piecewise linear quadratic optimal control. *IEEE transactions on automatic control*, 45(4):629–637, 2000.

[94] M. Rewienski and J. White. Improving trajectory piecewise-linear approach to nonlinear model order reduction for micromachined devices using an aggregated projection basis. In *Proceedings of the 5th International Conference on Modeling and Simulation of Microsystems*, pages 128–131, 2002.

[95] M. Rewienski and J. White. A trajectory piecewise-linear approach to model order reduction and fast simulation of nonlinear circuits and micromachined devices. *IEEE Transactions on computer-aided design of integrated circuits and systems*, 22(2):155–170, 2003.

[96] M. Rewieński and J. White. Model order reduction for nonlinear dynamical systems based on trajectory piecewise-linear approximations. *Linear Algebra and its Applications*, 415(2):426–454, 2006.

[97] D. Vasilyev, M. Rewienski, and J. White. A tbr-based trajectory piecewise-linear algorithm for generating accurate low-order models for nonlinear analog circuits and mems. In *Proceedings of the 40th annual Design Automation Conference*, pages 490–495. ACM, 2003.

[98] M. Storace and O. De Feo. Piecewise-linear approximation of nonlinear dynamical systems. *IEEE Transactions on Circuits and Systems I: Regular Papers*, 51(4):830–842, 2004.

[99] Z. Yacine, A. Benfdila, and S. Djennoune. Model order reduction of nonlinear systems via the trajectory piecewise linear approach application to transmission lines circuit. In *8th WSEAS International Conference on Applied Informatics and Communications (AIC'08) Rhodes, Greece*, pages 369–375, 2008.

[100] P. Khodabakhshi and J. N. Reddy. A unified beam theory with strain gradient effect and the von kármán nonlinearity. *ZAMM-Journal of Applied Mathematics and Mechanics/Zeitschrift für Angewandte Mathematik und Mechanik*, 97(1):70–91, 2017.

[101] S. Stoykov. *Nonlinear vibrations of 3D beams*. PhD thesis, Universidade do Porto (Portugal), 2012.

[102] R. E. Bank, W. M. Coughran, W. Fichtner, E. H. Grosse, D. J. Rose, and R. K. Smith. Transient simulation of silicon devices and circuits. *IEEE Transactions on Computer-Aided Design of Integrated Circuits and Systems*, 4(4):436–451, 1985.

[103] M. E. Hosea and L. F. Shampine. Analysis and implementation of tr-bdf2. *Applied Numerical Mathematics*, 20(1-2):21–37, 1996.

[104] E. L. Lehmann and G. Casella. *Theory of point estimation*. Wadsworth & Brooks/Cole Advanced Books & Software, 1991.

[105] M. Loève. *Probability theory*. Springer-Verlag, New York, 1977.